Universitat Rovira i Virgili

Departament de Química Física i Inorgànica

Improvement of the properties of zeolites for application in the nitrogen and oxygen separation process and in acid catalysis

Memòria de tesi doctoral

Isabel Salla Cabau

Tarragona, Octubre 2005

La Dra. Pilar Salagre Carnero i la Dra. Yolanda Cesteros Fernández, professores titulars del Departament de Química Física i Inorgànica de la Universitat Rovira i Virgili.

CERTIFICA:

Que la memòria de tesi doctoral "Improvement of the properties of zeolites for application in the nitrogen and oxygen separation process and in acid catalysis", que presenta Isabel Salla Cabau per a optar al grau de Doctor per la Universitat Rovira i Virgili, ha estat realitzada sota la nostra direcció en el Departament de Química Física i Inorgànica de la Universitat Rovira i Virgili.

Tarragona, Juliol 2005.

Dra. Pilar Salagre Carnero

Dra. Yolanda Cesteros Fernández

Després de tot el que ha suposat la realització d'aquesta tesi doctoral, m'agradaria expressar el meu agraïment a totes les persones que m'han ajudat tant durant aquest període, però especialment:

A les meves directores de tesi Dra. Pilar Salagre i Dra. Yolanda Cesteros, per la immillorable direcció d'aquest treball i pel gran recolzament i suport mostrat tant a nivell professional com a nivell personal.

També voldria agrair a la resta del grup de Catàlisi Heterogènia, pel bon ambient de treball i de grup, així com per les diverses discussions de química de les quals hem pogut gaudir.

Als companys de Catàlisi Homogènia, per les bones estones compartides al laboratori i seminari.

Al grup del Laboratorio di Catalisi e Chimica delle Superfici de la Univestità degli Studi di Genova, per l'agradable acollida en el seu laboratori.

Als meus amics, dels quals he rebut comprensió i suport en tot moment.

I finalment, a la meva família, per la confiança dipositada en mi i perquè sempre han estat al meu costat.

Gràcies a tots.

The present thesis studies several processes that take place on such aluminosilicate materials as mordenite, zeolite A, and zeolites X and Y. The thesis is presented in six chapters. Chapter one is a general introduction to zeolites: their composition, structure, properties and uses, and, in particular, the state of the art of the processes studied here, which are the separation of N_2 and O_2 from air and the acid isomerisation of styrene oxide to phenylacetaldehyde. The objective of the thesis is presented in accordance with the state of the art and the present and future trends in zeolites.

The second chapter, the experimental part, makes a detailed description of the zeolites used in this thesis, and the characterisation techniques, apparatus and conditions used. It also briefly describes the adsorption and catalytic procedures.

The third, fourth and fifth chapters present the results of the various studies, most of which involve zeolites. All these studies have been published, are in press or have been submitted to journals related to the field and, therefore, these parts will be presented as articles.

Chapter three deals with the nitrogen and oxygen adsorption. Mordenites and A zeolites have been used for this purpose.

Once the mordenites used in the separation experiments had been characterised, we believed that these modified mordenites could be used in acid-catalysed reaction. Chapter four presents the results of several mordenites in the styrene oxide isomeration in liquid phase using conventional and microwave heating.

Chapter five discusses the FTIR spectroscopy characterization, made by adsorbing different probe molecules on zeolites and studying the interactions adsorbate-adsorbent. These studies allow us to better understand our systems.

Finally, the last chapter draws the general conclusions of the present thesis.

Chapter 1

Introduction and Scope

1.1. General introduction to zeolites

A molecular sieve is a material that has selective adsorption properties and can separate components of a mixture by differentiating in molecular size and shape.[1] Molecular sieves include clays, porous glasses, microporous charcoals, active carbons, etc, but one of the most used and studied groups of molecular sieves are zeolites.

Zeolites are crystalline aluminosilicates with fully cross-linked open framework structures made up of corner-sharing SiO_4 and AlO_4 tetrahedra, named primary structural units. The name "zeolite" comes from the Greek words *zeo* (to boil) and *lithos* (stone); and was used for the first time in 1756 by the Swedish mineralogist Cronstedt.[2]

In inorganic chemistry, aluminosilicates are materials composed of Si^{4+} and Al^{3+}. They are formed when some of the Si^{4+} in silicates are replaced by Al^{3+}. For each Si^{4+} ion replaced by an Al^{3+}, the charge is balanced by other positive ions such as Na^+, K^+ or Ca^{2+} ions.

The structural formula of a zeolite is based on the crystallographic unit cell, represented by:

$$(M^{n+})_{x/n}\,[(AlO_2)_x(SiO_2)_y]\cdot wH_2O$$

where M represents the exchangeable cation of valence n and M is generally a Group I or II cation, although other metal, non-metal and organic cations can also balance the negative charge created by the presence of Al in the structure. The Si/Al ratio of the zeolite is indicated by y/x, and w represents the water contained inside the discrete size cages and/or channels of zeolites.

In addition to Si^{4+} and Al^{3+}, other elements can also be present in the zeolitic framework. They do not need to be isoelectronic with Si^{4+} or Al^{3+}, but must be able to occupy framework sites.

Zeolites can be divided into natural zeolites like Chabazite, Faujasite or Mordenite, and synthetic zeolites like zeolite A, X and Y or ZSM-5. Natural zeolites have the advantatge of their low economic cost while the second group, although they are more expensive, avoid the problem of impurities and changes in chemical composition, and thus enable their properties to be controlled better.

The structure of zeolites is based on an extensive three-dimensional framework in which the tetrahedral sites are linked by oxygen atoms. The result is a uniform microporous structure, which can be formed of channels and/or cavities.

In the zeolite structure, primary individual structural units are assembled into secondary building units called SBU's (Figure 1), by means of which the topology of all known molecular sieve framework types can be described.[3] The final framework structure consists of assemblages of secondary units in space, the union of which gives rise to bigger pentasil (a) or sodalitic (b) like-structural

units (Figure 1). Finally, the expansion of these units in the three space directions generates the different zeolitic structures. Therefore, zeolites can be classified according to the framework symmetry as ZSM, FAU, MFI, etc following the rules described by the International Zeolite Association (IZA).

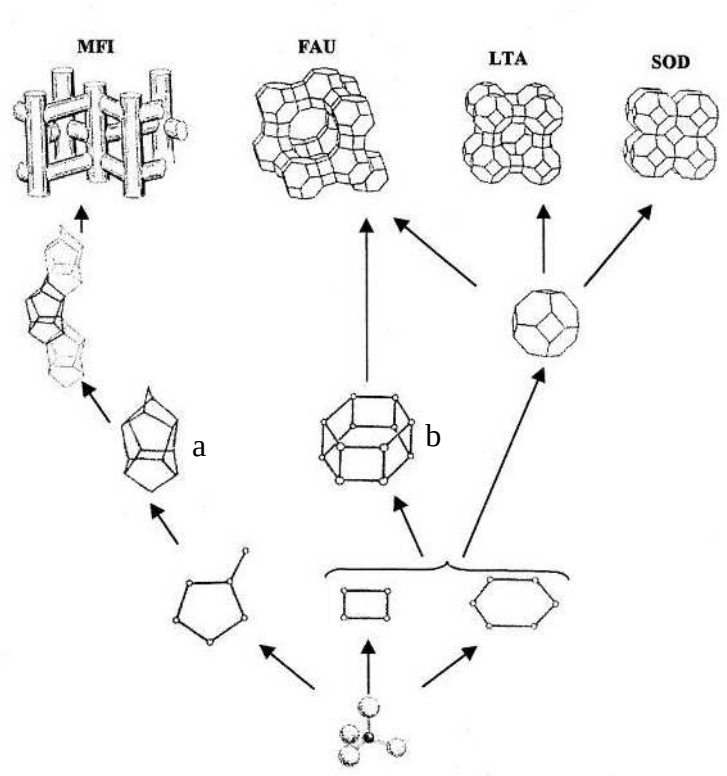

Figure 1. Structural genetics of zeolitic materials based in tetahedra TO_4 (T = Si o Al).

One of the fundamental characteristics of zeolites is the Si/Al ratio, because several properties such as thermal stability, acidity, and hydrophobic/hydrophilic character are related to it. According to the so-called Loewenstein rule,[4] Al-O-Al linkages in zeolitic frameworks are forbidden. As a result, all aluminate tetrahedra must be linked to four silicate tetrahedra, but a silicate tetrahedron may have five different possible environments: Si(0Al,4Si), Si(1Al,3Si), Si(2Al,2Si), Si(3Al,1Si) and Si(4Al,0Si).

1.2. Properties and uses of zeolites

The properties of zeolites depend mainly on their cavity and/or channel-based structure, and on their Si/Al ratio. Zeolites with low Si/Al ratios have strongly polar anionic frameworks. Low Si/Al ratios are characteristic of sodalitic-type zeolites, with a hydrophilic character, while high Si/Al ratios are more comon in more hydrophobic structures, type pentasil.

The cavities and/or channels that are such a feature of the porous structure of zeolites generate a high internal surface area. In some cases, this surface area can be even higher than one thousand square meters per gram.

Another important property is related to the compensating charge cations. The exchangeable cations, which are necessary to compensate the negative charge of the framework created by the isomorphous substitution of Si^{4+} for Al^{3+}, origine strong local electrostatic fields. These cations are largely responsible for most of their properties. Thus, protonic exchanged zeolites are considered to be strong acid catalysts[5,6] while alkali and alkaline earth metal exchanged zeolites can act as basic catalysts.[7-9] These cations can also be largely responsible for the

separation of some binary mixtures[10] or resin cation exchange processes for water softening.[11]

In general, these materials present high thermal stabilities, which depend basically on their Si/Al composition. Thus, the thermal stability increases from about 700ºC in low silica zeolites to 1300ºC in silica molecular sieves.

Taking into account all these attractive properties, molecular sieves in general, and zeolites in particular, have found widespread industrial applications as highly selective adsorbents, ion exchangers and, most importantly, catalysts of exceptionally high activity and selectivity in a wide range of reactions.[12] Separation processes are another of these applications, one example of which is the separation of N_2 and O_2 from air, by exploiting the different polarities of the two molecules.[12] The amount of adsorbed gas or liquid depends on the pressure, the temperature and the nature of the adsorbate as well as on the kind of molecular sieve, since variations in the chemical composition of the sieve also affect adsorption.

However, in industry, the most important application of zeolites is as acid catalysts. Zeolites combine high acidity with shape selectivity, high surface area and high thermal stability and so they have been used to catalyse a variety of hydrocarbon reactions, such as cracking, hydrocracking, alkylation and isomerisation. In acid catalysis, the activity of zeolites is determined by the Brönsted and Lewis sites, mainly brought about by the presence of aluminium in the zeolite framework.

1.3. The N_2 and O_2 separation process

A separation process can be defined as a process in which a product mixture can be separated into two or more streams that are richer in one of the products.[13] According to the second law of thermodynamics, this process is not thermodynamically favourable, and consequently, requires an energetic cost.

There are a considerable number of separation processes on both the industrial and the laboratory level.[13]

In the case of gas mixtures, nowadays two industrial processes are applied as a function of the nature of the gas mixture. The first is a cryogenic distillation consisting of liquefaction followed by distillation. The second process is separation by selective adsorption over an asdorbent of one or more components of the mixture in order to give a gas stream that is richer in the lesser adsorbed components.

The first process has the advantages of simplicity and scalability and it also yields high-purity products. But its main drawback is that it is an energy-intesive process. On the other hand, the adsorption processes have the advantages of low energetic cost and the possibility of regenerating the adsorbent but they are less scalable and the purity of the products obtained is lower.

For a long time, distillation played a dominant role in separation technology. However, nowadays both processes are applied in industry and, in general, the choice of whether to use adsorption processes will depend on the nature of the mixture components, on technical considerations and on economic factors.[14]

Gas separation by adsorption processes are based on the different strengths of interaction on a given sorbent for the constituents in the mixture.

Table 1 lists some industrial processes based on adsorption and the adsorbents used.

Table 1. Some processes based on adsorption phenomena

Gas separation	*Adsorbent used*
Normal paraffins/iso-paraffins, aromatics	Zeolite
N_2/O_2	Zeolite
O_2/N_2	Carbon molecular sieves
CO, CH_4, CO_2, N_2, Ar, NH_3/ H_2	Zeolites, activated carbon
Acetone/ vent streams	Activated carbon
C_2H_4/ vent streams	Activated carbon
Gas purification	*Adsorbent used*
H_2O/ olefin-containing cracked gas, natural gas, air, synthesis gas, etc.	Silica, alumina, zeolite
CO_2/C_2H_4, natural gas, etc.	Zeolite
Organics/ vent streams	Activated carbon
Sulfur compounds/ natural gas, hydrogen, liquified petroleum gas(LPG), etc.	Zeolite
Solvents/air	Activated carbon
Odors/air	Activated carbon
NO_x/N_2	Zeolite
SO_2/vent streams	Zeolite
Hg/chlor-alkali cell gas effluent	Zeolite

The production of high purity N_2 and O_2 from air components is one of the main separation processes applied in industry nowadays.

N_2 and O_2 separation from an air mixture has been applied since the beginnings of the 20th century using cryogenic distillation.[15] At the end of the 1970s adsorption was first applied to this separation process. Distillation is still dominant in the chemical and petrochemical industries in spite of its higher economic cost, and separation by adsorption processes represents only 20% of the total N_2 and O_2 industrial separation processes at low and medium scale.

Because adsorption methods have developed quickly during the last three decades, various methods have been implemented on the industrial level: Vacuum Swing Adsorption (VSA),[16] Fractionated Vacuum Swing Adsorption (FVSA),[17] Pressure Swing Adsorption (PSA)[18] and Temperature Swing Adsorption (TSA), although the PSA process with carbon molecular sieves as adsorbent is the most frequently used.

Since then, the PSA process has been improved,[19,20] up to the point that it is now more economic than cryogenic distillation for productions lower than 30 metric tonnes per day.[14] It is expected that new PSA processes using new adsorbents will continue to be developed in the near future. The trends are to use rapid PSA cycles for bulk gas separation and to develop novel adsorbed designs, like radial or rotatory beds.[21]

Throughout the world, oxygen is mainly used for steel making, ethylene oxide production and coal gasification. Substantial quantities of oxygen or oxygen-enriched air are also used to treat municipal waste.

The use of N_2 as an inert gas for blanketing started gaining ground in the 1950s and it was given fresh impetus when it started to be used for purging the tanks and vessels that store hydrocarbons and corrosive liquids in chemical industries. Similarly, in metal industries nitrogen blanketing is used to prevent metal oxidation during smelting. Another growing application for nitrogen is for maintaining dust-free and inert atmospheres in the electronic industry.

Selecting the appropriate sorbent is a key factor in obtaining a good separation. Some of the properties to be considered when choosing an adsorbent are: a) its adsorptive capacity, b) the adsorption selectivity to the desired component c) the heat of adsorption of the molecules on the adsorbent and d) the life of the adsorbent.[22] As can be seen in Table 1, zeolites and carbon molecular sieves (CMS) can be used as adsorbents in the N_2 and O_2 separation process. The basis of the separation is different in the two cases.

For CMS, the separation is kinetic, governed by the different diffusion rates of N_2 and O_2 molecules inside the CMS, because O_2 molecules (3.46 Å) are smaller than N_2 molecules (3.64 Å).[23]

The diffusion time constants expressed for oxygen and nitrogen in carbon molecular sieves, as calculated from sorption uptake, are reported to be 1.7 10^{-4} s^{-1} and 7.6 10^{-6} s^{-1}, respectivelyfor. This difference explains why the adsorption rate of oxygen is faster (Figure 2) even though both gases have similar adsorption capacities on CMS (Figure 3).

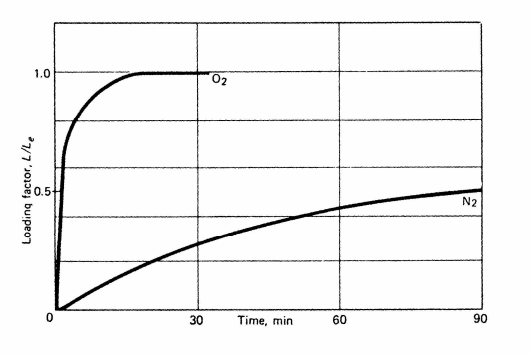

Figure 2. N_2 and O_2 adsorption rate on CMS

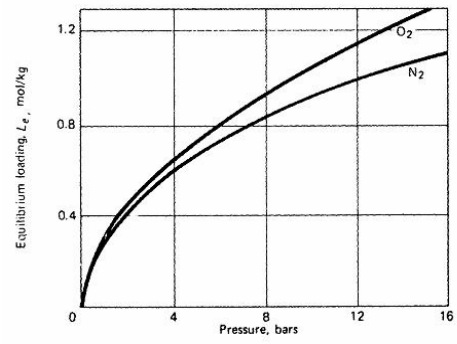

Figure 3. N_2 and O_2 adsorption isotherms on a CMS at room temperature

Several studies have described in detail hydrocarbon deposition in the mouth of sieves, as a step for obtaining a mouth diameter of 5Å. This enables the difference in rate diffusion between nitrogen and oxygen molecules to be increased, thus giving a good selectivity in the entrance of gases into the sieve.[24-26]

On zeolitic adsorbents, however, N_2 and O_2 separation is governed by the different adsorption strengths of the two gas molecules at equilibrium with the adsorbent.

With alkali and alkali earth zeolites, the interaction between the quadrupolar moment of molecules and the extraframework zeolite cations is electrostatic. Considering that the N_2 quadrupole moment (0.31 $Å^3$) is three times higher than that of O_2 (0.1 $Å^3$), the electrostatic interaction of N_2 molecules with cations will be stronger than with O_2 molecules.[27,28]

The first patent was taken out in 1964 when McKee used X zeolite with Si/Al ratios compressed between 1.25 and 1.5 to separate N_2 and O_2.[29] Several studies showed the influence of extraframework cations on the N_2 and O_2 adsorptive properties in zeolite X,[29,30] and they pointed out the importance of the cation type on the adsorbent-adsorbate interaction (Table 2).

Table 2. Separation factor (α) depending on the cation.

Adsorbent	Exchange degree (%)	Separation factor (α)*
LiX	86	7.6
NaX	100	4.9
KX	100	2.2
RbX	56	3.5
CsX	50	1.5
Mg-X	56	2.4
Ca-X	96	3.5
Sr-X	96	3.6

* $\alpha = ([\text{adsorbed } N_2]/[\text{adsorbed } O_2] \times [O_2 \text{ gas}]/[N_2 \text{ gas}])$

Therefore, the authors concluded that in the same periodic group and for a given zeolitic structure, both adsorption selectivity and capacity follow the tendency $Li^+ \geq Na^+ \geq K^+ \geq Rb^+ \geq Cs^+$ (i. e. when the radius decreases, the electrostatic interaction between the cation and the gas molecules increases).

Later, Coe et al. in studies also made on zeolite X showed how the exchange degree influenced its N_2 and O_2 adsorption properties, in such a way that the N_2 and O_2 adsorption selectivity increases exponentially when the cation exchange degree increases in the most interacting cation.[31]

Other publications of this period showed the same tendency for other zeolitic structures like chabazite[32] and zeolite A.[33]

As well as alkali and alkali-earth zeolites, a block of zeolite-based adsorbents that contain silver cations as extraframework cations has emerged more recently. In this case the interaction is a π-complexation bond between the sorbent and the sorbate. Thus, authors such as Yang et al. used the principle that silver-containing zeolites can separate olefins from paraffins to separate N_2 and O_2, since the electronic properties of this pair are similar to those of the olefin/paraffin pair.[34,35] This kind of interaction consists of two contributions: a) the usual electron density donation from the antibonding π-orbitals of N_2 and O_2 molecules to the empty s-orbitals of silver cation Ag^+ and b) a backdonation electron density to the antibonding π-orbitals of the molecule to be bonded (N_2 and O_2).

The second contribution basically determines the separation selectivity, since the antibonding π-orbitals of the N_2 molecules are empty whereas they are partially occupied in the O_2 molecules, which does not favour the back-donation interaction.

The total substitution of earth and alkaline earth cations for Ag^+ cations in type X, LSX and Y zeolites leads to higher adsorption selectivites but also to higher

adsorption heats (parabolic isotherms), which are undesirable for the desorption process (Figure 4). Therefore, the introduction of fewer Ag^+ cations equilibrates the adsorption selectivity and the adsorption heat, and means that the adsorption properties are better than those of the corresponding zeolite without silver.[34,35]

In this kind of silver zeolite adsorbents, a very important factor that must be controlled is the activation temperature, since the formation of Ag_m^{n+} clusters is an autoreduction process that involves framework oxygens and silver cations. The presence of these Ag_m^{n+} clusters modifies the adsorption properties of zeolites, and improves their adsorption properties when they are activated under proper conditions.[35] However, when the temperature is increased too much, the size of these clusters also increases, which means that the number of active centres decreases, and the N_2 adsorbed volume and the N_2/O_2 adsorption selectivity also decrease.

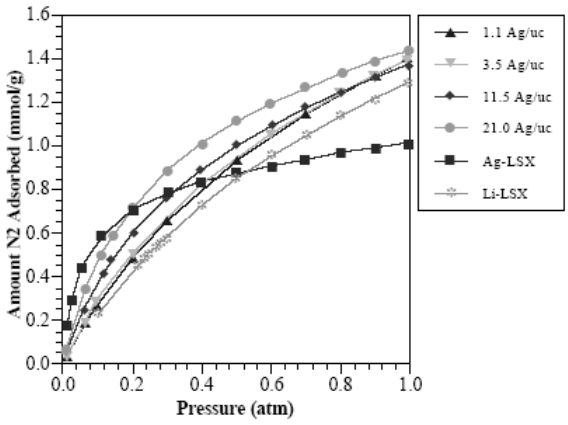

Figure 4. Adsorbed volume depending on the Ag^+ content in LSX zeolite

Parameters other than the nature of the extraframework cations can also influence the N_2 and O_2 adsorption properties: for example, the cation location, the charge on the cation and the presence of water molecules.

As far as the cation location in the zeolite structure is concerned,[36] for example, zeolite X has several possible positions, known as sites I, I', II, II' and III (see Figure 5). Thus, for cations with a high charge density, the preferred positions are sites I and I'. These positions are located in the six rings and hinder the access of the gas molecules, while positions II and III are more accessible for N_2 and O_2. Thus, the N_2 and O_2 adsorption properties will depend on where the cations are located.

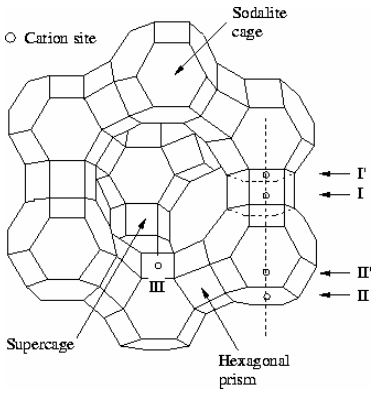

Figure 5. Cation location on an X zeolite

Several FTIR studies of low temperature N_2 adsorption[37] and H_2 adsorption[38] on alkali zeolites show the different adsorption properties of cations located in different positions on an X zeolite.

Theoretical studies have also been made using DFT (Density Functional Theory) calculations and they reveal the shielding effect that the framework oxygen atoms have on the zeolitic extraframework cations. The results show a decrease in the net cation charge, which therefore disfavours the interaction cation-adsorbate.[39-41]

The last parameter found in the literature that influences the adsorption properties derives from the fact that zeolites with low Si/Al ratios have high affinity for polar molecules (for example, water molecules). The presence of water molecules inside the zeolite cavities seriously affects the adsorption properties as can be seen in the figure below (Figure 6).[42]

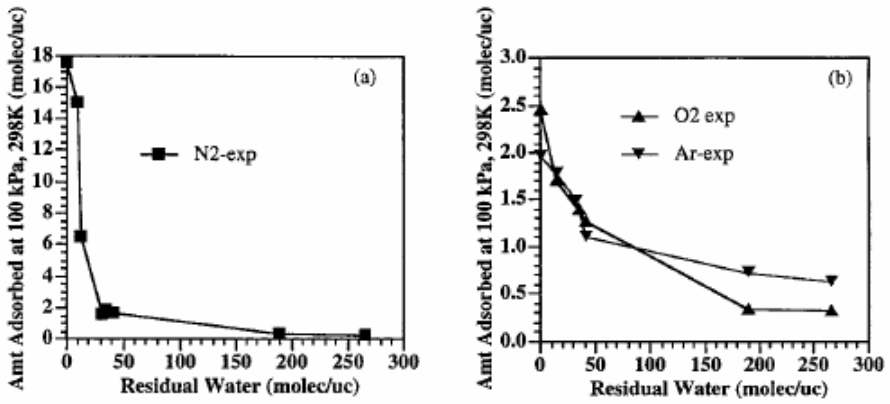

Figure 6. Theoretical and experimental amounts of adsorbed N_2 and O_2 on LiX at 100KPa and 298 K with respect to the amount of residual water

The presence of water is also a drawback in the sense that it favours the hydroxylation of cations (scheme 1), especially those with a higher positive charge.[31]. This hydrolisis quickly deactivates the sites for the adsorption

process because, for example, $Ca(OH)^+$ species are inactive for nitrogen adsorption.

$$M^{n+} + xH_2O \rightarrow M(OH)_e^{(n-e)+} \qquad \textbf{(Scheme 1)}$$

So far, then, all the examples have shown the use of zeolites as nitrogen adsorbents. However, the literature describes some cases in which zeolites are used as oxygen adsorbents like the CMS adsorbents described above. In some cases, depending on the cations used, zeolites are transformed in size discriminators. Several examples of this are zeolite A with Fe^{2+} cations,[43] Na-K-A zeolite,[44,45] and more recently, Na-Ce-A zeolite.[46] The separation is based on the different diffusion rates of the adsorbates on the molecular sieve, since the presence of cations in certain positions can convert zeolites into molecular sieves that can discriminate between the N_2 and O_2 size.

Another new, but more unusual, class of oxygen selective adsorbents are those based on inorganic metal complexes, which are able to reversibly bind oxygen in solution or solid state (see scheme 2).[47,48]

$$n\ M(L) + O_2 \leftrightarrow [M(L)]_n\ (O_2) \qquad \textbf{(Scheme 2)}$$

where n = 1 or 2

There are several metal complexes of such transition metals as Co^{II}, Fe^{II}, Mn^{II}, Cr^{II} and Cu^{II}, which are able to reversibly bind oxygen. However Co^{II} complexes are the ones that have been investigated most, because they can have an oxidation potential in a range that makes possible to donate some

electrons to oxygen molecules but not to such an extent that the metal is irreversibly oxidised.[49]

The reversible uptake of oxygen by cobalt complexes in solution has been extensively studied.[50,51] However, the synthesis of these complexes in the porous cavities of microporous solids of a zeolite and their use for air separation is an area of more recent interest.[52] Therefore, further efforts are needed in order to improve the thermal stability of Co^{II} complexes in a zeolite matrix.

1.4. Acid catalysis

Nowadays acid catalysis is one of the most important fields in catalysis on both the industrial and the laboratory scale. In fact a wide variety of solid-acid catalysts are available.[53]

Acidity in heterogeneous catalysis can be of two types: Brönsted acidity and Lewis acidity. For aluminosilicates, Brönsted acid sites are generated when the negative charge in the lattice is compensated by a proton. In general terms, a Brönsted acid site is considered to be able to protonate reactant molecules X according to the following scheme:

$$M\text{-}OH + X \leftrightarrow MO^- + XH^+ \qquad \textbf{(Scheme 3)}$$

In aluminosilicates, OH groups can be divided into: a) structural or bridging groups [SiO(H)Al], b) terminal silanol groups [SiOH] and c) aluminium hydroxy groups (AlOH). The first group are considered the strongest Brönsted acid sites, whereas the second group are usually generated on the external surface or by the presence of structural defects, and the last group are basically generated by the presence of an aluminium extraframework phase. The main factors that affect acid strength are the Si/Al ratio and the nature of other M^{3+} species that can be present instead of Al^{3+}. Thus, the acidity increases in the same way as the sequence $Al^{3+} > Ga^{3+} > Fe^{3+} >> B^{3+}$. There are several methods for achieving stronger acid sites in zeolites or more stable acid zeolites: steam procedures with mineral acids, which can extract M^{3+} atoms from the surface;[54-57] the preparation of organic-functionalized zeolites[58]; or the addition of cations such as La^{3+} easily hydrolizable to form $[La_2(OH)_2]^{4+}$ or $La(OH)^{2+}$.[59]

On the other hand, Lewis acid sites are generated by the presence of cationic species, which are deficient in the number of electrons. In the case of zeolites, the Lewis acidity is associated to the extraframework cations and to the aluminum species dislodged from the framework.

There are many more solid acid catalysts than basic and acid-basic catalysts because they have played an important role in the progress of the petroleum and petrochemical industry in the last 40 years.

Of the 127 industrial catalytic processes described by Tanabe, 15 are catalogued as industrial isomerization processes.[60]

One of the aims of catalysis nowadays is to find zeolite-based catalysts with very strong acid sites that enable some processes to be carried out at lower reaction temperatures or with smaller catalyst amounts.

1.4.1. Isomerisation of styrene oxide to phenylacetaldehyde

An extremely valuable method for introducing an aldehyde or ketone group into organic fine chemicals is to epoxidize olefins and subsequently to rearrange the oxiranes in the presence of acidic catalysts. Epoxide reactivity has been widely studied, because they are versatile intermediates in organic chemistry.[61,62] Homogeneous catalysts such as phosphoric acid, BF_3, $FeCl_3$, $ZnBr_2$ and $SnCl_y$, as well as heterogeneous catalysts such as SiO_2, Al_2O_3, ZnO, WO_3, supported metals and various precipitated phosphates have been applied as isomerisation catalysts.

The isomerisation of styrene oxide to β-phenylacetaldehyde (scheme 4) is an acid catalysed reaction, which is used at industrial scale in fine chemistry to produce fragrances (this aldehide gives a narcissus-like smell in floral perfumes), pharmaceuticals, insecticides, fungicides and herbicides.[63] Furthermore, phenylacetaldehyde is a valuable intermediate for producing more stable acetals with a honey aroma (glycolacetate), a sweet leaf odour (diethylacetate) or a tangy aroma (diphenylacetate).[64]

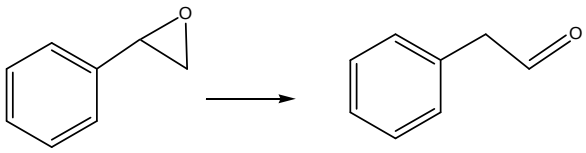

Scheme 4. Isomerisation of styrene oxide to phenylacetaldehyde

Several solid catalysts have been used to study the rearrangement of various styrene oxides under gas and liquid conditions.[65,66] The main products of the

styrene oxide isomerisation are the corresponding aldehyde and ketone depending on the properties of the catalyst.[67] This reaction can be catalysed by Brönsted acids (addition of a proton to the epoxide oxygen), by Lewis acids (coordination of the epoxide oxygen to a multivalent cation) and by bases,[68] although the first are much more active (see scheme 5).[64] On the whole, increasing the acidity increases the transformation of these oxides and favours the formation of the aldehyde.[69]

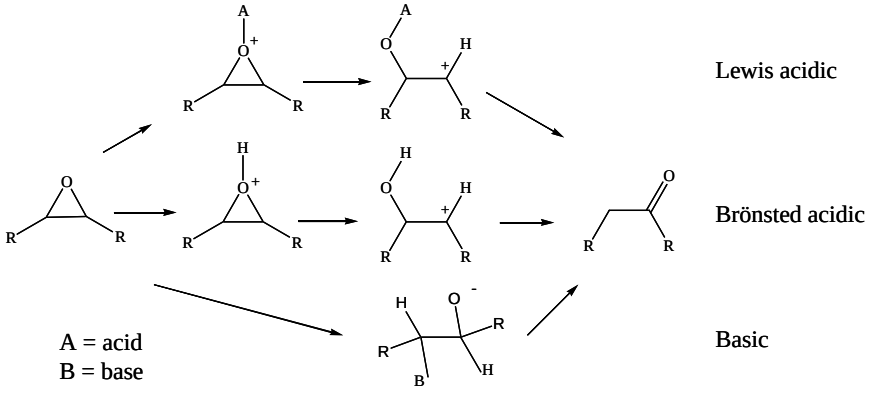

Scheme 5. Acid/base catalysed epoxide rearrangement to carbonyl compounds

In the styrene oxide isomerisation reaction to phenylacetaldehyde, conventional catalysts often result in the formation of a mixture of ketones and aldehydes, and also by-products such as aldol condensation products, diols and dioethers. The high-weight molecules formed by aldol condensation are the first step in the formation of 1,3,5-triphenylbenzene and coke, which causes a fast deactivation of the catalysts, and limits their lifetime.[68]

The homogeneous catalysts described above are used in industry although they are not as a rule regenerable, and generate voluminous and often corrosive

waste streams. On the other hand, heterogeneous catalysts like TiO_2, P_2O_5/SiO_2, γ-alumina, B_2O_3/SiO_2 and bentonite have been used for this reaction. One of their advantages is that they can be used in gas-phase reactions and therefore continuous processes can be created with relatively little technical effort. However, they do have some drawbacks: incomplete conversion, formation of mixtures of ketones and aldehydes and the formation of aldol condensation products. The formation of these condensation products is the first step in the formation of coke and therefore limits the lifetime of these catalysts. Styrene oxide can also be rearranged in liquid-phase reactions using a titanium-silicalite catalyst (TS-1) with high conversion and high phenylacetaldehyde selectivity.[70] More recently, zeolites have been used in their H-form for this reaction. This use is of increasing interest because they can stabilize the α-carbocation intermedium and therefore suppress the formation of by-products.[64] Zeolites favour the selectivity to the aldehyde because of their shape selectivity, and they supress reactions that form bulkier molecules (e.g. furans or aldol condensation products).[62] Therefore, zeolites such as ZSM-5 hinder the formation of this aldol condensation because of the steric constraints of the framework. MFI zeolites, which have mild acidity, have also been considered to be good catalysts for this reaction.[71]

Nevertheless, these catalytic results depend on the solvent used. Smith et al.[72] pointed out that, in the liquid-phase, rearranging styrene oxides over zeolites in their H-form gives poor results with protic solvents such methanol, but yields to phenylacetaldehyde are higher when chlorinated aprotic solvents are used.

Therefore, the efficient supression of side-products makes the zeolite-based catalytic system environmentally benign and economically superior when the appropriated conditions are used.

1.5. Scope of this thesis

One of the main objectives of this thesis is to design new zeolite-based adsorbents with properties favouring N_2 and O_2 separation. Once we had reviewed the bibliographic section, we saw that for a good separation, adsorbents needed to have a high number of cations, high accessibility to the adsorbates and minimum shielding of the cations. We also saw that in the presence Ag^+ cations and Ag_m^{n+} clusters, the N_2 and O_2 separation can improve. Therefore, we propose to use systems that allow us to improve the adsorption process from the point of view of the adsorbent. Our proposals are:

- to use Mordenite as the main material to achieve this first objective. Mordenite was chosen because of its high framework robustness, relatively high number of cations (low Si/Al ratio), its aparently high accessibility to the active sites and poor gas diffusion problems. These characteristics mean that it is likely to improve the adsorption properties and therefore lead to a better nitrogen and oxygen separation than the systems found in the literature. Also, other faujasite and sodalite type zeolites have been used through the thesis for comparison.
- to study the adsorption properties of several alkali-cation exchanged mordenites, with such cations as Li^+ and Na^+, which have a low q/r ratio.
- to introduce a certain number of fluorine atoms into the mordenite structure framework in order to achive adsorbent systems in which cations are less shielded.
- to obtain systems with Ag_m^{n+} clusters inside mordenite channels and to study their nitrogen and oxygen adsorption properties.

- to characterize all these materials with appropriate and commonly used characterization techniques, in an attempt to relate the characterization results to their adsorption behaviour, to understand this process better and, therefore, to make improvements.

The second main objective of this thesis is to apply some of these mordenite-based systems as catalysts in acid-catalysed isomerisation reactions. The synthesis and/or modification of zeolites with stronger acid sites is one of the goals of catalysis at the moment.[73] Specifically, we propose:

- to test the catalytic activity of NaMOR, HMOR and those mordenites modified with fluorine in an acid catalysed styrene oxide isomeration reaction, since the presence of highly electronegative atoms, like fluorine atoms, in the structure should favour the obtention of stronger Brönsted acid sites.
- to use microwave heating instead of conventional heating for this reaction. The main advantages of this technique are that reaction rates can be accelerated, yields can be improved, and reaction pathways can be selectively activated or suppressed.

Finally, in order to better understand the behaviour and nature of active sites of our adsorption and/or catalytic systems, we propose to use FTIR spectroscopy through the adsorption/desorption behaviour of several molecules with different electronic properties and sizes (e. g. various nitriles and CO).

1.6. References

[1] McBain, J. W. *The Sorption of Gases and Vapors by Solids*, Rutledge and Sons: London, 1932, chapter 5, p. 17.

[2] Cronstedt, A. F. *Ron och beskriting om en obekant bärg ant, som kallas zeolites*. In Kongl. Vetenskaps, Acad. Handl. Stocholm., 1756, Vol. 17, p. 120.

[3] Smart, L. Zeolites and related structures. In *Solid State Chemistry: An Introduction*, Moore, E. Ed.; Champman and Hall: London, 1995; p. 238.

[4] Loewenstein, W. *Am. Mineral.* **1954**, 39, 92.

[5] Corma, A. *Chem. Rev.* **1997**, 97, 2373.

[6] Martens, J. A.; Jacobs, P.A. Introduction to Acid Catalysis with Zeolites in Hydrocarbon Reactions. In *Introduction to Zeolite Science and Practice,* Van Bekkum, H.; Flanigen, E. M.; Jacobs, P. A.; Jansen, J. C. Eds., Elsevier: Amsterdam, NL, 2001, chapter 14, p. 633.

[7] Weitkamp, J.; Hunger, M.; Rymsa, U. *Micropor. Mesopor. Mater.* **2001**, 48, 255.

[8] Davis, R. J. *J. Catal.* **2003**, 216, 396.

[9] Martra, G.; Ocule, R.; Marchese, L.; Centi, G.; Coluccia, S. *Catal. Today* **2002**, 73, 83.

[10] Yang, R. T. *Adsorbents: Fundamentals and Applications,* John Wiley and Sons: New Jersey, 2003, chapter 7, p. 157.

[11] Towsend, R. P.; Coker E. N. Ion exchange in zeolites. In *Introduction to zeolite science and practice,* van Bekkum, H.; Flanigen, E. M.; Jacobs, P. A.; Jansen, J. C. Eds.; Elsevier: Amsterdam, NL, 2001., chapter 11, p. 467.

[12] Breck, D. W. *Zeolite Molecular Sieves: Structure, Chemistry and Use*, John Wiley: London, 1974.

[13] King, C. J. *Separation Processes,* Brown, J. V.; Eichberg, M.; Eds., Mc Graw-Hill Chemical Engineering Series: New York, 1981.

[14] Yang, R. T. *Gas Separation by Adsorption Processes*, Butterworth: Boston, 1987 reprinted by Imperial College Press, London and World Scientific Publishing Co.: River Edge, N. J., 1997.

[15] Isalski, W. H. *Separation of Gases,* Clarendon Pr.: Oxford, 1989.

[16] Sicar, S.; Zondlo, J. W. *U.S. Patent* 4012429, 1977.

[17] Sicar, S. *U.S. Patent* 5084075, 1992.

[18] Knoblauch, K.; Heimbach, H.; Harder, B. *U.S. Patent* 4548799, 1985.

[19] Kim, J. N; Chue, K. T.; Cho, S. H. *Sep. Sci. Technol.* **1995**, 30(3), 347.

[20] Rege, S. U.; Yang, R. T. *Ind. Eng. Chem. Res.* **1997**, 36, 5358.

[21] Sicar, S. *Adsorpt. Sci. Techn.* **2001**, 19 (5), 347.

[22] Ruthven, D. M., *Principles of adsorption and adsorption processes*, John Wiley and Sons: New York, 1984, chapter 1, p. 1.

[23] Coe, C. G. Structural Effects on the Adsorptive Properties of Molecular Sieves for Air Separation. In *Access in Nanoporous Materials, Procedings of a Symposium on Access in Nanoporous Materials*. East Lansing, Michigan, 1995, p. 213.

[24] Cabrera, A. L.; Amor, J. N. *U.S. Patent* 5071450, 1991.

[25] Gaffey, T. R.; Farris, T. S.; Cabrera, A. L.; Amor, J. N. U.S. Patent 5098880, 1992.

[26] Amor, J. N.; Braymer, T. A.; Farris, T. S.; Gaffey, T. R. U.S. Patent 5086033, 1992.

[27] Drain, L.E. *Trans. Faraday Soc.* **1953**, 49, 650.

[28] Kington, G. L.; Macleod, A.C. *Trans. Faraday Soc.* **1959**, 55, 1799.

[29] McKee, D. W.; Buffalo, N.Y. *U.S. Patent 3140932*, 1964.

[30] McKee, D. W.; Buffalo, N.Y. *U.S.Patent 3140933*, 1964.

[31] Coe, C. G.; Kuznicki, S. M. *U.S. Patent 4481018*, 1984.

[32] Coe, C.G.; Gaffney, T. R.; Srinivasan, R. S. *U.S. Patent 4925460*, 1990.

[33] Chao, C. C.; Sherman, J. D.; Mullhaupt, J. T.; Bolinger, C. M. *U.S. Patent 5174979*, 1992.

[34] Yang, R. T.; Chen, Y. D.; Peck, J.D.; Chen, N. *Ind. Eng. Chem. Res.* **1996**, 35, 3093.

[35] Hutson, N. D.; Reisener, B. A.; Yang, R. T.; Toby, B. H. *Chem. Mater.* **2000**, 12, 3020.

[36] Jasra, R. V.; Choudary, N. V.; Bhat, S. G. T. *Ind. Eng. Chem. Res.* **1996**, 35, 4221.

[37] Smudde, G. H.; Slager, J. R.; Coe, C. G.; McDougall, J. E.; Weigel, S. J. *Appl. Spectrosc.* **1995**, 49 (12), 1747.

[38] Kazansky, V. B.; Bülow, M.; Tichomirova, E. *Adsorption* **2001**, 7, 291.

[39] Pápai, I.; Goursot, A.; Fajula, F.; Plee, D.; Weber, J. *J. Phys. Chem.* **1995**, 99, 12925.

[40] Goursot, A.; Vasilyev, V.; Arbuznikov, A. *J. Phys. Chem. B* **1997**, 101, 6420.

[41] Jale, S. R.; Bülow, M.; Fitch, F.R.; Perelman, N.; Shen, D. *J. Phys. Chem. B* **2000**, 104, 5272.

[42] Hutson, N. D.; Zajic, S. C.; Yang, R. T. *Ind. Eng. Chem. Res.* **2000**, 39, 1775.

[43] Izumi, J. *EP Patent 40935*, 1981.

[44] Oka, N.; Izumi, J.; Suzuki, M. *Adsorption* **2000**, 6, 149.

[45] Izumi, J.; Suzuki, M. *Adsorption* **2001**, 7, 27.

[46] Jayaraman, A.; Yang, R. T.; Cho, S. H.; Bhat, T. S. G.; Choudary, V. N. *Adsorption* **2002**, 8, 271.

[47] Jones, R. D.; Summerville, D. A.; Basolo, F. *Chem. Rev.* **1979**, 79, 139.

[48] Li, G. Q.; Govind, R. *Ind. Eng. Chem. Res.* **1994**, 33, 755.

[49] Vogt, J. R.; Lester, H.; Faigenbaum, H. M.; Wiberley, S. E. *Chem. Rev.* **1963**, 63, 269.

[50] Howe, R. F.; Lundsford, J. H. *J. Phys Chem.* **1975**, 79, 1836.

[51] Taylor, R. J.; Drago, R. S.; George, G. E. *J. Am. Chem. Soc.* **1989**, 111, 6610.

[52] Hutson, N. D.; Yang, R. T. *Ind. Eng. Chem. Res.* **2000**, 39, 2252.

[53] Campanati, M.; Vaccari, A. Solid-acid Catalysts-General. In *Fine Chemicals through Heterogeneous Catalysis,* Sheldon, R. A.; Van Bekkum, H. Eds.; Wiley-VCH: Germay, 2001, p. 61.

[54] J. Scherzer, ACS Symp Ser. 48, 157, 1984.

[55] Lukyanov, D. B. *Zeolites* **1991**, 11, 325.

[56] Van Bokhoven, J. A.; Tromp, M.; Koningsberger, D. C.; Miller, J. T.; Pieterse, J. A. Z.; Lercher, J. A.; Williams, B. A.; Kung, H. H. *J. Catal.* **2001**, 202, 129.

[57] Peixoto, D. P. B.; Cabral de Menezes, S. M.; Pais da Silva, M. I. *Mater.Lett.* **2003**, 57, 3933.

[58] Jones, C. W.; Tsuji, K.; Davis, M. E. *Nature* **1998** 393, 52.

[59] Carvajal, R.; Chu, P. J.; Lunsford, J. H. *J.Catal.* **1990**, 125, 123.

[60] Tanabe, K.; Hölderich, W. F. *Appl. Catal. A- Gen.* **1999**, 181, 399.

[61] Ruiz-Hitzky, E.; Casal, B.; *J. Catal.* **1985**, 92, 291

[62] Neri, C.; Buonomo, F. *US Patent* 4609765, 1986.

[63] Hölderich, W. H.; Barsnick, U.; Rearrangement of Epoxides. In *Fine Chemicals through Heterogeneous Catalysis*, Sheldon, S. A; Van Bekkum, H.; Eds.; Wiley-VCH: Germany, 2001, p. 217.

[64] Hoelderich, W. F.; Laufer, M. C. Zeolites and "Non Zeolitic" Molecular Sieves in the Synthesis of Fragances and Flavours. In *Zeolites for Cleaner Technologies*, Guisnet, M.; Gilson, J. P.; Eds.; Imperial College Press: London, Catalytic Science Series, Vol 3, 2002, p. 301.

[65] Hölderich, W.H. *US Patent* 4990684, 1989.

[66] Taramasso, M.; Pergo, G.; Notari, B. *US Patent* 4410501, 1983.

[67] Arata, K.; Tanabe, K. *Catal. Rev. Sci. Eng.* **1983**, 25, 365.

[68] Kochkar, H.; Clacens, J. M.; Figueras, F. *Catal. Lett.* **2002**, 78, 91

[69]. Molnár, I. Bucsi, M. Bartók, G. Resofski, G. Gáti, *J. Catal.* **1991**, 129, 303.

[70] Serrano, D. P.; Ugina, M. A.; Ovejero, G.; Grieken, R.V.; Camacho, M. *Microp. Mater.* **1995**, 4, 273.

[71] Hölderich, W. F.; Goetz, N.; *Proceedings from the 9th international zeolite conference, Montreal, 1992*; Ballmoos, R. V.; Higgins, J. B.; Treacy, M. M. J. Eds.; Butterworth-Heinemann: USA, 1993, p. 309.

[72] Smith, K.; Al-Shamali, M.; *Proceedings from the 12th International Conference on Zeolites, Baltimore, 1999*; Treacy, M. M. J.; Marcus, B. K.; Bisher M. E.; Higgins, J. B; Eds.; Material Research Society: USA, 1999, vol. 3, p. 228.

[73] Corma, A. *J. Catal.* **2003**, 216, 298.

Chapter 2

Experimental Section

2.1. Sample description and preparation

In this thesis, various zeolitic materials have been used. Mordenite was the main focus of the work, while the other zeolites (zeolite A and Faujasite (zeolite X and zeolite Y)) were used for comparison. All the samples used are summarized in Table 1.

Table 1. Summary of all samples used.

Mordenite	Na-Mordenite H-Mordenite Li-Mordenite K-Mordenite Cs-Mordenite Li/Ag-Mordenite Ag-Mordenite Na- Mordenite1%F Li- Mordenite1%F Li/Ag- Mordenite1%F H-Mordenite1%F Na- Mordenite10%F H- Mordenite10%F
Zeolite A	Na/Ag(0.01M)-A Na/Ag(1M)-A
Zeolites X and Y	NaX NaY

In order to understand how zeolites behave in the different processes studied, a structural description of each zeolite is presented below.

2.1.1 Sample description

2.1.1.1. Mordenite

Mordenite is basically a natural mineral, but it can also be synthesized.[1] In the Mordenite framework type, units of four 5-rings are joined to one another via common edges to form chains. Mirror images of these chains are connected via oxygen bridges to form corrugated sheets. These sheets, displaced by half a translation in c, are then connected to one another to form 12-and-8-rings along the corrugations. The lining of the 12-ring channels contains 8-rings, but the 8-ring openings in the adjacent 12-ring channels are displaced, so there is only very limited access from one channel to the next. Consequently the channel system is effectively one dimensional.

Figure 1 shows the Periodic Building Unit (PBU), which is composed of T12 units. Neighbouring PBUs, related by a lateral shift of ½ *b* axes, are connected along the *a* axes.

Cations can be located in different parts of the zeolite channels, which have different roles in the adsorption and catalytic processes. The figure below shows the position of the cationic sites in the mordenite structure according to several studies.[2,3] It seems that half of the Na^+ ions are located in the midle of the compressed channels (site I), while the other half of the total Na^+ cations are located mainly at sites IV and VI (Figure 2).

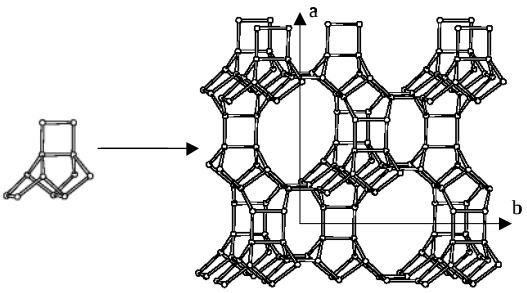

Figure 1. Mordenite's PBU, formed of T12 units (left) and the cell content seen along [001] in perspective view (right).

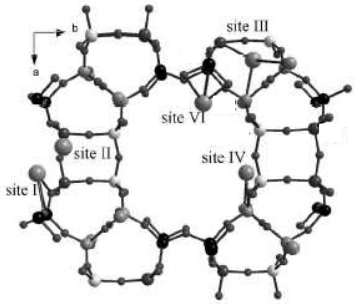

Figure 2. Representation of extra-framework cation sites I, II, III, IV and VI in mordenite

The structure of mordenite is characterized by relatively high silica content, which gives it high thermal stability. Mordenite is also formed of 5-membered rings, which are thought to enhance the acid strength of the material.[4,5] It is the combination of these properties that makes it suitable for such industrial processes as cracking and isomerisation of hydrocarbons,[6] and separation processes.[7] Actually, Tanabe and Hölderich reported that mordenite is used as a catalyst in seven industrial processes.[8]

2.1.1.2. Zeolite A

This zeolite is also known as LTA and is one of the most commonly used zeolites mainly in cation-exchange (as water softener) and in adsorption.

The LTA framework type is related to a sodalite structure. The Periodic Buiding Unit is the so-called sodalite cage or β-cage (Figure 3). In this case, the sodalite cages in a primitive cubic arrangement are joined via double 4-rings rather than single ones (as in the sodalite structure). This creates an α-cage in the center of the unit cell, and a 3-dimensional, 8-ring channel system. Alternatively, the framework can be described as a primitive cubic arrangement of α-cages joined through single 8-rings (producing a sodalite supercage in the center). This is one of the more open zeolite framework types with a framework density of only 12.9 T-atoms per 1000Å^3.

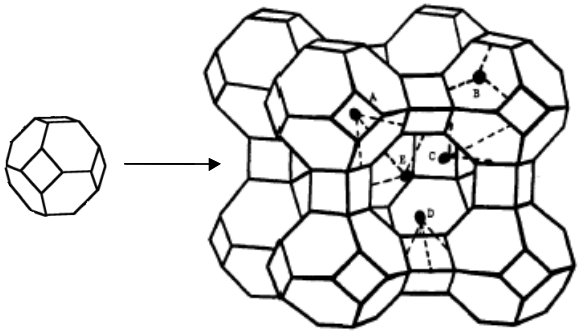

Figure 3. The sodalite cage, T24 unit (left) and unit cell content in perspective view (right)

In this zeolite, with a Si/Al ratio of 1, cations can be located in 4 O-rings (α-cage), in 6 O-rings (α-cage) and in 8 O-rings (β-cages). In the activated sodium

form (i.e. for monovalent cations), eight Na^+ cations are in 6O-rings, three in 8 O-rings and and one in 4 O-rings, while in the calcium form (i.e. for divalent cations) all cations are located in the 6 O-rings.

This zeolite is mainly used as a water softener since it can easily exchange its sodium ions for calcium and magnesium ions.[9]

2.1.1.3. Faujasite

Faujasite is a natural zeolite, while zeolites X and Y are synthetic. Zeolite X is characterized by lower Si/Al ratios (between 1 and 1.5) than zeolite Y (between 1.5 and 3).

Also in this case, the PBU is the β-sodalite cage. The cages are arranged in the same way as the carbon atoms in the diamond, and are joined to one another via double 6-rings. This creates the so-called supercage with four, tetrahedrically-oriented, 12-ring pore openings, and a 3-dimensional channel system (Figure 4).

The combination of large void volume, a 12-ring pore opening and a 3-dimensional channel system makes them ideal for many catalytic applications such as catalytic cracking and hydrocracking, and also separation processes.[10]

For faujasite-type zeolites, the location of cations is well known.[11,12] Thus, in zeolite X with a Si/Al ratio of 1, there are 96 monovalent cations (M^+) per unit cell, $S_{I'}$ and S_{II} are fully occupied by 32 M^+ cations each, and the remaining 32 M^+ are equally distributed between sites S_{III} and $S_{III'}$.

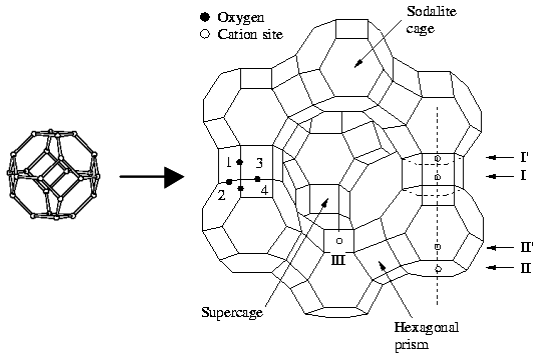

Figure 4. PBU in FAU structure (left) and sodalite cage (right)

2.1.2. Sample preparation

Mordenite, zeolite A and zeolites X and Y were used as starting materials.

Mordenite was purchased from Zeolyst in its sodium form (named as M or MOR through the text). Its chemical composition was SiO_2/Al_2O_3 with a mole ratio of 13 and a Na_2O weight % of 6.6.

Zeolite A was purchased from Prolabo as hydrated binderless pellets with a chemical composition of 1 Na_2O : 1 Al_2O_3 : 2 ± 0.1 SiO_2 : xH_2O.

Zeolite NaY, with a Si/Al ratio of 2.56 was synthesized at the Institute of Industrial Chemistry of Warsaw University while NaX zeolite with a Si/Al ratio of 1.31 was synthesized at the Institute of Chemical Technology of the Jagellonian University in Krakow.

These zeolites were chemically modified so that their properties would be better for the different applications. These chemical modifications are described below:

2.1.2.1. Cationic exchange

The exchange was done with:

a. Alkaline metal salts. High concentrations (2.2 M) of LiCl, KCl and CsCl salts were used. The cation exchange process was repeated several times depending on the cationic exchange properties of the zeolite used. Using this procedure we obtained LiMOR, KMOR and CsMOR and LiA samples.

b. Transition metal salts. In this case, the cationic exchange was done using 0.01 and 1 M concentrations of $AgNO_3$ solution. With this procedure, Na/Ag(1M)-A, Na/Ag(0.01M)-A and Na/AgMOR samples were obtained. The number in brackets, in this case, refers to the concentration of $AgNO_3$ used in the cation exchange.

c. NH_4Cl solution. Cation exchange with NH_4^+ is generally used when the protonic form of a zeolite is required. From the alkaline form, in which the zeolite is generally found, we obtain the NH_4^+-zeolite by exchange, which becomes H-zeolite after calcining at high temperatures. HMOR (or also called HM in some cases) was obtained in this way.

2.1.2.2. Anionic exchange

This exchange was carried out in accordance with the procedure described elsewhere.[13,14] In order to introduce fluorine atoms into the zeolite structure, different concentrations of NH_4F were used. All the fluorine in solution was assumed to have been involved in the attack and NH_4F concentrations were calculated in order to achieve a specific % of F per gram of zeolite. The treatment was made at room temperature and with the protonic form of the zeolite (H-zeolite). Two mordenite-based samples were obtained using this procedure, HM1F and HM10F: the former containing a maximum of 1% in

weight of F atoms per 100 g of zeolite, and the second one containing no more than 10% of F atoms.

Then NaM1F, LiM1F, LiAgM10F and NaM10F were obtained from HM1F and HM10F samples after cation exchanging their ammonium form with NaCl, LiCl and $AgNO_3$ salts, as described above. The ammonium form was obtained by cation exchang of HM1F and HM10F samples with NH_4Cl.

2.1.2.3. Formation of clusters by applying temperature

Different temperatures (between 623 K and 723 K) were applied under vacuum to silver containing zeolites (Ag-A and AgMOR) prepared by cationic exchange with $AgNO_3$ solution as described above, in an attempt to form silver clusters (Ag_m^{n+}) within the zeolite structure. Throughout the procedure, the samples were protected from light in order to prevent silver cations from being reduced to silver atoms.

2.2. Sample characterization

Typical characterization methods were used to characterize the various samples. Basically, most of them are related to surface characterization.

2.2.1. Determination of surface area by N_2 physisorption

N_2 physisorption is one of the oldest techniques in surface characterization. Continued addition of nitrogen gas molecules at 77 K after the monolayer formation leads to the gradual stacking of multiple layers (or multilayers) on top

of each other. As the equilibrium adsorbate pressures approach saturation, the pores become completely filled with adsorbate.

On the basis of the well-known Brunauer, Emmett and Teller (B.E.T.) theory, one can estimate the sample's surface area from the monolayer volume (V_m):

$$V/V_m = c(p/p_o)/[(1-p/p_o)(1-(1-c))(p/p_o)]$$

where V is the volume of gas (STP conditions) adsorbed, V_m is the volume of the gas (STP conditions) adsorbed in the monolayer and p_o is the vapour pressure above the macroscopically thick layer of the pure liquid on the surface. The quantity c approximates to $\exp -(\Delta H_d - H_{vap})/RT$, in which the ΔH_d is the enthalpy of adsorption on the first adsorbed layer and H_{vap} is the heat of vaporisation.

For these measurements we used a Micromeritics ASAP 2000 apparatus. Samples were first activated in vacuum at temperatures between 573 and 623 K.

2.2.2. X-ray diffraction (XRD)

X-ray diffraction is widely used to identify bulk phases and to estimate particle sizes.[15] X-rays have wavelengths in the Å range, which are sufficiently energetic to penetrate solids and well suited to probe their internal structure.

This technique allows us to derive lattice spacings, d, by measuring the 2θ angles under which constructively interfering X-rays, with wave lengh, λ, leave the crystal using the known Bragg Brentano relation:

$$n\lambda = 2 d \sin\theta$$

Additionally, the Scherrer formula relates crystal size to line width:

$$\langle L \rangle = K\lambda / \beta \cos \theta$$

where β is the peak width, corrected respect to the instrumental error, and K is a constant. The linear dimension $\langle L \rangle$ is the volume average thickness of the crystallites, measured normal to the reflecting planes.

In recent years, besides conventional XRD mesurements, high-temperature X-ray diffraction has been increasingly used because it makes possible to directly observe the evolution of structure as a function of the heat treatment.

Conventional powder X-ray diffraction patterns of the samples were obtained with a Siemens D5000 diffractometer (Bragg-Brentano parafocusing geometry and vertical θ-θ goniometer) fitted with a curved graphite diffracted-beam monochromator, incident and diffracted-beam Soller slits, a 0.006º receiving slit and scintillation counter as a detector. The data were collected from 2θ values between 5º and 75º with an angular step of 0.05º at 3s per step and sample rotation. $Cu_{K\alpha}$ (1.542 Å) radiation was obtained from a copper X-ray tube operated at 40kV and 30mA.

High temperature XRD measurements were obtained using a temperature chamber equipped with an Anton-Paar HTK10 platinum ribbon heating stage and connected to a vacuum pump. A Braun position sensitive detector (PSD) was used and the measuring time per degree was 6 sec. A static argon-atmosphere was used throughout the measurement.

The crystalline phases were identified using the Joint Committee on Powder Diffraction Standards (JCPDS) files. From the diffraction patterns, the deconvolutions, cell parameters and cell volumes were calculated using a matching profile with TOPAS 2.1 software (Bruker AXS), in which the instrument error is corrected.

2.2.3. Magic angle spinning nuclear magnetic resonance (MAS NMR)

Since nuclear magnetic resonance (NMR) was discovered, it has emerged as one of the most powerful tools in research for characterising structure, since the observation of the transition frequency measured in the NMR spectrum for an atomic nucleus is a very sensitive probe of its environment.

Since high resolution solid-state NMR was first applied to zeolites in 1979,[16] many authors have worked in this field and contributed to the results and literature available.[17-20]

High-resolution solid NMR spectra can be achieved when line broadening phenomena due to dipolar coupling, chemical shift anisotropy and quadrupolar interaction are removed or reduced. This can be done by Dipolar Decoupling (DD), Multiple Pulse Sequences (MPS), and Magic Angle Spinning (MAS). This last technique, discovered by Andrew et al.[21] and Lowe,[22] is now the one that is most commonly used because line broadenings due to dipolar interactions and chemical shift anisotropy can be reduced to their isotropic values by rotating the sample quickly about an axis inclined at the angle =54º44' (magic angle spinning). MAS NMR can reduce, but not fully remove, quadrupolar line broadenings, for which other techniques are required.

In order to achieve optimum line narrowing and a sufficient signal-to-noise ratio in the solid state NMR spectra, the experimental procedures described above may be used in combination. However, in zeolites, none or only a few hydrogen atoms are present, so Cross Polarization is not an effective technique, and dipolar proton decoupling is not always necessary. Thus, application of MAS is sufficient to remove the chemical shift anisotropy and any small dipolar interaction, and to narrow quadrupolar broadened lines.

All three basic atomic nuclei of framework zeolites can be detected by NMR measurements by its naturally isotopes ^{29}Si, ^{27}Al and ^{17}O. Most elements acting as charge-balancing cations in zeolites also have isotopes that are suitable for NMR experiments (^{7}Li, ^{23}Na, ^{133}Cs, ^{139}La, and ^{205}Tl). Finally, high-resolution solid-state ^{1}H NMR plays an important role in investigating zeolites.

In our case, in order to obtain ^{29}Si NMR and^{27}Al NMR, the MAS technique is mostly sufficient to obtain highly resolved spectra of zeolites. The local environment of the SiO_4 tetrahedra can be derived from the chemical data shift, since it will depend on whether there are 0, 1, 2, 3 or 4 silicon atoms in the four surrounding tetrahedral sites. For Si(0Al,4Si) chemical shifts are expected to be between –105 and –120 ppm; for Si(1Al,3Si) between –95 and 105 ppm; for Si(2Al,2Si) between –90 and –100 ppm; for Si(3Al,1Si) between –90 and –95 ppm; and for Si(4Al,0Si) between –80 and –90 ppm. ^{27}Al NMR spectra of zeolites, however, are generally simpler since, according to Lowenstein's rule, only one environment is possible: $Al(OSi)_4$. Consequently a single narrow peak is observed in the ^{27}Al MAS NMR spectra of zeolites with a typical chemical shift of about 60 ppm (from aqueous $Al(NO_3)_3$ solution) and a non framework aluminium, which is typically an octahedral AlO_6 coordination gives rise to signals at about 0 ppm.[23]

For ^{1}H NMR, the MAS technique was also used. The Brönsted acidic strength depends on the polarisation of the OH bond and therefore on the electronic environment of H, which is determined by its screening constant. Bonardet et al. [23] suggested to use OH chemical-shift as a measure of the Bronsted acidity while other authors use probe molecules.[24] In our case, we use the ^{1}H NMR chemical shift in order to detect changes in Brönsted acidity.

Spectra were obtained at a frequency of 400 MHz by spinning at 5 kHz. The pulse duration was 2 μs and the delay time was 5 seconds. The chemical shift references for aluminum and silicium were high purity octahedral hexahydrated

aluminum chloride $AlCl_3 \cdot 6H_2O$ and silicon nitride Si_3N_4, respectively. In the case of ^1H MAS NMR, TMSP (trimethyl silyl-3-propionic acid 4-2,2,3,3 sodium salt) was used as a reference. All spectra were obtained on a Mercury 400 MHz apparatus.

2.2.4. Fourier transform infra red spectroscopy (FTIR)

The IR technique is one of the oldest instrumental techniques used to study the surface in heterogeneous catalysis including zeolites. Nowadays it is one of the most commonly used surface characterization tools basically because of its low cost and simplicity.

Infrared spectroscopy is extremely valuable for investigating powder samples. It gives direct information about the surface or about the adsorbed species. Mid- and far IR spectra of zeolites are generally used for investigating their framework and cation properties, respectively. However, it gives rather poor information about the acidity of surface hydroxyl groups, which are of great importance for the surface properties.[25] These problems are solved by using probe molecules, which interact with the surface and the alteration of the spectral features as a result of adsorption can provide indirect information about properties, location, and concentration of the surface sites among other things. Several factors must be taken into account when probe molecules are chosen.[26] For example, adsorption complexes should be stable enough to allow characterization; the probe molecules should have spectral parameters that are sensitive to the state of the sites on which they are adsorbed; the informative absorption bands on the surface should be in regions in which the sample is transparent; and the extinction coefficients of their informative bands must be high, otherwise the molecules should not cause any chemical modifications of the surface and be small enough to prevent steric hindrance.

In our case, the experiments were performed on a FTIR Nicolet apparatus in the range 4000-400 cm^{-1}, and the spectra were registered after one hundred scans in transmission mode with a resolution of 4 cm^{-1}. The detector used was KBr deuterated tryglycine sulphate detector (DGTS).

The IR cell (Figure 5) used allows their use on sorption and reaction studies in high vacuum conditions, in which sample handling (activation, adsorption, reaction, and desorption) can be performed in situ.

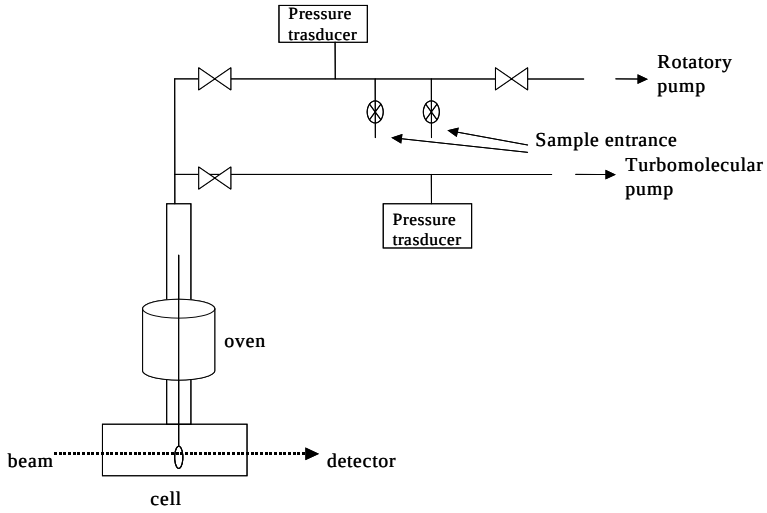

Figure 5. Scheme of an adsorption/desorption in situ IR cell.

Several probe molecules were used in the adsorption/desorption experiments. For example, various nitriles such as acetonitrile (AN), propionitrile (PrN), isobutylonitrile (IBN), pivalonitrile (PN), benzonitrile (BN) and o-toluonitrile (o-TN). These nitriles had different acidity-basicity properties and steric hindrance, which made it possible to characterize the strength and position of the acidic or basic sites in zeolites.[27-30]

Carbon monoxide (CO) was also used as a probe molecule because of its non-reactive adsorption. In this case the oxidation and the coordination states of the metal ions can be determined by the spectral behaviour, stability, and other characteristics of the carbonyls formed.[31] However, low temperature CO adsorption has increasingly been applied to determine the acid strength of the surface hydroxyl groups.[32-34]

Several Far-IR spectra were also taken on a Nicolet Magna 750 in the region 600-50 cm^{-1} using a Polietilene DTGS as a detector.

2.2.5. Ultraviolet-visible spectroscopy (UV-Vis)

UV/VIS spectroscopy is a non-destructive technique for determining the chemical species of a material. A light beam of a certain wavelength range interacts with the sample and the intensity of the transmitted or reflected signal is recorded as a function of the wavelength. Because of the interaction with the sample, at certain frequencies the light is absorbed resulting in absorption peaks in the spectrum. The absorption frequencies are specific for certain chemical compounds and associated with electron transitions in the material. The chemical composition of the sample can therefore be determined by analysing the spectrum using standards that allow quantitative measurement.

The basis of this theory is the Lamber-Beer law:

$$A=ebc$$

where A is absorbance, e is the molar absorbtivity (L mol^{-1} cm^{-1}), b is the path length of the sample (cm) and c is the concentration of the compound in solution (L^{-1}).

In our case, a Shimadzu UV-2101 UPC Diffuse Reflectance UV/Vis apparatus with integrating sphere was used. Spectra were recorded at room temperature in the range 200 nm to 800 nm.

2.2.6. Temperature programmed desorption (TPD)

Temperature programmed desorption relates some characteristic properties of a sample to its temperature in the course of a temperature-programmed heating. In TPD studies a solid that has previously been equilibrated with an adsorbing gas in well-defined conditions is submited to a programme temperature rise and the amount of gas desorbed is continuously monitored.

In our case the apparatus used is a TPD/R/O 1100 Thermo Finnigan equipped with a temperature-programmable oven, a thermal conductivity detector (TCD) and a PFEIFFER GSD 301 02 mass spectrometry detector.

For the pre-treatment, samples were activated in situ by flowing Ar at increasing temperature. Afterwards, the corresponding probe molecule gas was adsorbed at 313 K and desorbed by flowing He 20 cm^3/min. The conditions used for each sample are specified in the corresponding section. The gases used for sample characterization were NH_3 in He, CO_2 and acetonitrile (CH_3CN).

In some cases, a more exhaustive characterisation was necessary, for which the following techniques were used.

2.2.7. X-ray fluorescence (XRF) spectroscopy

An electron microscope offers additional possibilities for analysing the sample. Emitted X-rays are characteristic of an element and make possible to determine the chemical composition of a particular part of a sample.

In our case, X-ray fluorescence was used to determine the atomic distribution maps and the Si/Al ratio of several samples. Experiments were performed on a scanning electron microscope, JEOL JSM6400, operating at accelerating voltage of 15 kV and work distances of 15 mm. All samples were covered with a graphite layer. Accumulating time for mapping experiments was around 120 seconds.

2.2.8. Elementary analysis

Atomic absorption spectroscopy (AAS) and induced coupled plasma (ICP), both based on the Planck equation, are considered to be two of the best techniques for zeolite elementary analysis.

The elementary analysis of zeolites for their major and minor components requires a sample preparation approach that will dissolve a wide variety of elements without volatilisation or precipitation losses. One of the most commonly used procedures is to perform a sample digestion in cold hydrofluoric acid. Due to the ability of HF to attack glass containers, the whole pre-treatment process was performed on polypropilene vessels.

The method to be used depends on the sample, the matrix sample, the desired analysis accuracy and also on the time and funds available.

We used ICP for Al, K, and Ca determination and AAS for Li and Na determination.

2.2.9. Cation exchange capacity (CEC)

Cation exchange capacity gives information about the number of exchangeable cations, which can be replaced more or less easily with other cations without affecting the aluminosilicate framework. The magnitude of such cation

exchange in a given zeolite is known as its cation-exchange capacity (CEC) and is commonly measured in terms of moles or equivalents of exchangeable cations per gram of zeolite.

Several methods have been described in the literature for CEC determination. In our case, the CEC of several mordenite samples was determined in a similar way to that proposed by Bergaya et al.[35] First, mordenite samples were exchanged with an aqueous solution of $CuSO_4$ for 6 h at room temperature. Then, the samples were centrifuged and washed with distilled water several times. The amount of Cu^{2+} exchanged was determined by UV-visible spectroscopy at 809 nm. The CEC in meq/100g of zeolite was calculated as the difference in Cu^{2+} concentration between the starting solution and the final solution obtained after the cationic exchange.

2.3. Adsorption and catalytic experiments

2.3.1. Adsorption experiments

In order to test the adsorption properties of the adsorbants, we measured the adsorption isotherms of the isolated adsorbates, which are high purity N_2 and O_2. The adsorption properties measured were:

1. Sorption capacity of each gas (N_2 and O_2), expressed as the volume in cm^3 of gas adsorbed per gram of sample before activation.
2. Sorption N_2/O_2 selectivity, which was calculated as the ratio between the volume of N_2 adsorbed and the O_2 adsorbed volume at a given pressure.

Adsorption isotherms were measured using a static volumetric system Micromeritics ASAP-2010. The gases used were high purity (99.999%) N_2 and O_2. Both gases were supplied by Carburos Metálicos.

Experiments were made using 0.20-0.30 g. of sample. The sample was contained in a quartz cup. Due to the fact that small amounts of molecular water inside the framework of the aluminosilicates seriously affect their adsorption capacity,[36] samples were activated with temperature in vacuum using a turbomolecular vacuum pump to a pressure lower than 1μmHg before the adsorption measurements were made. Adsorption isotherms were measured at 298 K in the pressure range 0.05 and 760 mmHg.

2.3.2. Catalytic experiments

As stated above, the aim of these catalytic tests was to check the acidity of some samples after specific modifications had been made.

The reaction studied was the acid catalysed isomerisation of styrene oxide (SO) to give the corresponding phenylacetaldehyde (PA).

Isomerisation reactions were carried out in liquid phase using batch reactors heated by conventional methods and also by microwaves.

The experiments using batch reactors with conventional heating were carried out in an oil bath and using a contact thermometer.

The experiments heated using microwaves were performed in a Milestone ETHOS-TOUCH CONTROL equipped with a temperature controller at a work frequency of 2.45 GHz and using closed vessels. The main advantages of using this technology are the faster preparation rate and the high yields and purity of the products obtained. However, microwaves have not been practically used in catalysis until now. The closed vessels provide a clean

environment for the sample during processing and prevent the loss of volatile species, even when the materials are processed at temperatures well above the normal boiling point of the mixture.

The catalytic experiments were performed using 0.04 g of catalyst, 25 ml of solvent (n-hexane or methanol) and 0.3 ml of reactant (SO or PA). PA was used as a reactant for purposes of comparison, as we will see in the results and discussion section. In all cases, catalysts and solvents were first activated using the appropriate procedures.

The reaction products were analysed by gas chromatography (GC) on a Shimadzu GC-2010 instrument equipped with a 30 m capillary column RTX-5 coated with phenylmethylsilicon and a FID detector.

Conversion was defined by the following equations:

$$[[\text{area PA/area SO}]_{\text{after reaction}}-[\text{area PA/area SO}]_{\text{before reaction}}]\ g\ cat^{-1}$$

$$[[\text{area MPE/area SO}]_{\text{after reaction}}]\ g\ cat^{-1}.$$

where PA means phenylacetaldehyde; SO, styrene oxide and MPE, 2-methoxy-2-phenylethanol.

2.4. References

[1] Barrer, R. M. *J. Chem. Soc.* **1948**, 2158.

[2] Maurin, G.; Bell, R. G.; Devautour, S.; Henn, F.; Giuntini, J. C. *J. Phys. Chem. B* **2004**, 108, 3739.

[3] Devautour, S.; Abdoulaye, A.; Giuntini, J. C.; Henn, F. *J. Phys. Chem. B* **2001**, 105, 9297.

[4] Nagy, J. B.; Bodart, P.; Hannus, I.; Kiricsi, I. *Synthesis, characterization and use of zeolitic microporous materials*, DecaGen Ltd: Szeged (Hungary), 1998.

[5] Van Bokhoven, J. A.; Tromp, M.; Koningsberger, D. C.; Miller, J. T.; Pieterse, J. A. Z.; Lercher, J. A.; Williams, B. A.; Kung, H. H. *J. Catal.* **2001**, 202, 129

[6] Moreau, F.; Ayrault, P.; Gnep, N. S.; Lacombe, S.; Merlen, E.; Guisnet, M. *Microp. Mesop. Mat.* **2002**, *51*, 211.

[7] Méthivier, A.; Separation of Paraxylene by Adsorption. In *Zeolites for cleaner technologies* Guisnet M.; Gilson, J. P.; Eds.; Imperial College Press: London, Catalytic Science Series, Vol 3, 2002, p. 209.

[8] Tanabe, K.; Hölderich, W. F. *Appl. Catal. A- Gen.*, **1999**, 181, 399.

[9] Rees, L. V. C.; Ion Exchange and Detergent Building. In *Zeolites as Catalysts, Sorbents and Detergents Builders* Karge, H. G.; Weitkamp, J. Eds.; Elsevier: Amsterdam, 1989.

[10] Coe, C. G. Structural Effects on the Adsorptive Properties of Molecular Sieves for Air Separation. In *Access in Nanoporous Materials, Procedings of a Symposium on Access in Nanoporous Materials*. East Lansing, Michigan, 1995, p. 213.

[11] Breck, D. W. *Zeolite Molecular Sieves: Structure, Chemistry and Use*, John Wiley: London, 1974, p. 97.

[12] Plévert, J.; DiRenzo, F.; Fajula, F.; Chiari, G. *J. Phys. Chem. B* **1997**, 101, 10340.

[13] Kowalak, S.; Khodakov, A. Y.; Kustov, L. M.; Kazanky, V. B. *J. Chem. Soc. Faraday Trans.* **1995**, 91, 385.

[14] Becker, K. A.; Kowalak, S. *J. Chem.Soc., Faraday Trans I* **1985**, 81, 1161.

[15] Cohen, J. B.; Schwartz, L. H. *Diffraction from Materials*, Academic Press, New York, 1977.

[16] Engelhardt, G.; Kunath, D.; Mägi, M.; Samson, A.; Tarmak, M.; Lippmaa, E. *Preprints of the Workshop "Adsorption of Hydrocarbons in Zeolites"*, Berlin-Adlershorf, 1979.

[17] Engelhardt, G.; Michel, D. *High –Resolution Solid-State NMR of Silicates and Zeolites*, John Wiley and Sons: Chichester, 1987.

[18] Stöcker, M. Review on recent NMR Results. In *Advanced Zeolite Science and Applications* Jansen, J. C.; Stöcker, M.; Karge, H. G.; Weitkamp, J. Eds.; Elsevier: Amsterdam, 1994 , vol 85, p. 429.

[19] Srikanth, K.; Schurko, R. W.; Hung, I.; Ramamoorthy, A. *Mater. Sci. Tech-Lond.* **2003**, 19 (9), 1191.

[20] Pruski, M.; Amoureux, J. P.; Fernandez, C. Progress in high resolution solid state NMR of quadrupolar nuclei. Applications to porous materials and catalysts. In *Magnetic Resonance in Colloid and Interface Science*, Resing H. A.; Wade, C. G. Eds.; ACS Symposium Series: San Francisco, 1976, vol. 76, p. 107.

[21] Andrew, E. R.; Bradbury, A.; Eades, R.G. *Nature*, **1958**, 182, 1659.

[22] Lowe, I. J. *Phys. Rev. Lett.* **1959**, 2, 285

[23] Bonardet, J. L.; de Menorval, L. C.; Fraissard, J Some applications of high resolution NMR to the study of gas-solid interactions. I. Chemical shift of

nuclei at solid surfaces. II. Chemisorption of hydrogen on oxide-supported platinum. In *Magnetic Resonance in Colloid and Interface Science*, Resing H. A.; Wade, C. G. Eds.; ACS Symposium Series: San Francisco, 1976, vol. 76, p. 248.

[24] Semmer-Herlédan, V.; Heeribout, L.; Batamack, P.; Dorémieux-Morin, C.; Fraissard, J.; Gola, A.; Benazzi, E. *Microp. Mesop. Mat.* **2000**, 34, 157-169.

[25] Busca, G. *Phys. Chem. Chem. Phys.* **1999**, 1, 723.

[26] Hadjiivanov, K. I.; Vayssilov, G. N., Adv. Catal. **2002**, 47, 309.

[27] Bevilacqua, M.; Busca, G. *Catal. Commun.* **2002**, 3, 497.

[28] Bevilacqua, M.; Gutièrrez Alejandre, A.; Resini, C.; Casagrande, M.; Ramírez, J.; Busca, G. *Phys. Chem. Chem. Phys.* **2002**, 4, 4575.

[29] Bordiga, S.; Turnes Palomino, G.; Pazè, C.; Zecchina, A. *Microp. Mesop. Mat.* **2000**, 34, 67.

[30] Lavalley, J. C. *Catal. Today* **1996**, 27, 377.

[31] Bordiga, S.; Lamberti, C.; Geobaldo, F., Zecchina, A.; Turnes Palomino, G; Otero Areán, C. Langmuir **1995**, 11, 527.

[32] Mauche, M.; Janin, A.; Lavalley, J. C.; Benazzi, F. *Zeolites* **1995**, 15, 507.

[33] Cairon, O.; Chevereau, T.; Lavalley, J. C. *J. Chem. Soc. Faraday Trans.* **1998**, 94, 3039.

[34] Marie, O.; Massiani, P.; Thibault-Starzyk, F. *J. Phys. Chem. B* **2004**, 108, 5073.

[35] Bergaya, F.; Vayer, M. *Appl. Clay Sci.* **1997**, 12, 275.

[36] Hutson, N. D.; Zajic, S. C.; Yang, R. T. *Ind. Eng. Chem. Res.* **2000**, 39, 1775.

Chapter 3

Nitrogen and Oxygen Separation

After revising the literature on nitrogen and oxygen separation, we decided to use mordenite, the porous structure of which consists of one-dimensional channels, to separate the nitrogen and the oxygen (Chapter 3.1). We selected this zeolite because the cations are aparently in easily accessible positions for N_2 and O_2 molecules. Then, we studied the adsorption properties on various cation exchanged (Na^+, Li^+, Ag^+) mordenites with different electronic properties.

In this chapter we also study how to decrease the shielding that framework walls produce on the cations. The shielding decreases the charge location on the cation and indeed disfavours the conditions for quadrupolar interaction between cations and N_2 and O_2 molecules. We therefore studied the introduction of F atoms into the zeolitic structure and the shielding effect in different cations for the N_2 and O_2 adsorption.

We also studied the incorporation of silver cations into the zeolite structure and their activation in conditions that favour the nitrogen/oxygen separation in zeolite X. After seeing the potential of mordenite as an adsorbent for nitrogen and oxygen separation, in the second part of this chapter (chapter 3.2), we attempted to form Ag_m^{n+} clusters inside the mordenite structure in order to study their adsorption properties. However, and probably because the Si/Al ratio was higher than that of zeolite X, we were not able to form these clusters

in the mordenite channels. So we performed the nitrogen and oxygen adsorption experiments on silver-exchanged zeolite A, with a Si/Al ratio around 1.

The formation of silver clusters inside zeolite A has been extensively studied; however, its adsorption properties have hardly been tested. Therefore, we formed these clusters on zeolite A and studied their nitrogen and oxygen adsorption properties as a function of the temperature used for their formation.

3.1. Study of the influence of several mordenite modifications on its N_2 and O_2 adsorption properties*

Abstract

Na-Mordenite zeolite was cation-exchanged to obtain Li, Li/Ag and Ag-Mordenite, and treated with NH_4F to obtain Na, Li, Li/Ag-MordeniteF (1%) and Na-MordeniteF (10%). Samples were characterized by XRD, nitrogen physisorption, ^{27}Al and ^{29}Si MAS NMR, FT-IR spectroscopy and X-ray fluorescence. Special attention was given to the presence of F^- ions in the mordenite structure. Equilibrium adsorption isotherms of high purity components N_2 and O_2 were measured at 298 K. For the cation-exchanged mordenite samples, the adsorbed nitrogen volume is slightly higher than that obtained in other zeolites such as zeolite X with lower Si/Al ratio. This reveals the significant influence of the cations accessibility to the gas molecules in these adsorption processes. N_2 adsorption capacity increases in the order $Na^+ < Ag^+ < Li^+$ whereas the N_2/O_2 adsorption selectivity varies in the way $Na^+ < Li^+ < Ag^+$ for the cation-exchanged mordenite samples. In samples prepared by fluorinated treatment, the effect is different depending on the extraframework cation present. When Na^+ and Li^+ cations are present, F atoms make a decrease of the shielding caused by the walls to the cations charge resulting in an increase on the adsorption selectivity, especially at low pressures, with a slight decrease in the number of active sites. However, the effect of F to Ag^+ cations is mainly an electronegative effect, making the interaction adsorbate-adsorbent less favorable.

* Journal of Physical Chemistry B **2004**, 108 (17), 5359-5364.

3.1.1. Introduction

Separation of nitrogen and oxygen by adsorption processes has become in the latest 30 years an alternative method instead of cryogenic distillation because of the large energetic cost of the later.[1,2]

Adsorption of nitrogen and oxygen in zeolites is thermodynamically controlled and it depends on the strength of interaction between the quadrupolar moment of N_2 and O_2 molecules with extraframework cations located inside the structure.[3,4,5] The quadrupolar moment of the nitrogen is three times that of oxygen. It is well known that this separation is strongly influenced by the composition and structure of the zeolites.[6] Thus, zeolites with high aluminum content (Si/Al=1), basically A and X, have been mainly used for air separation because of their high cations content, which are responsible for the coulombic interaction.

Some of these zeolites have been already modified by cationic exchange with alkaline and alkaline earth metals to improve the nitrogen and oxygen separation.[7-11] The factors affecting the interaction are mainly effective charge, polarizing power and radius of the cation. Interestingly, when Ag^+ cations interact with N_2 and O_2 molecules the bonding is a result of two contributions: the donation of the π-bond electrons to the empty s-orbital of Ag^+ and the backdonation of the d-orbital electrons of Ag^+ to the empty antibonding π-orbitals of the N_2 and O_2 molecules.[12] Because of the electron configuration of N_2 and O_2, the interaction of Ag^+ cations with N_2 becomes more favorable than with O_2.

N_2 and O_2 interactions with zeolites of low Si/Al ratio, such as zeolite X and LSX, have been highly studied by IR spectroscopy and also quantum chemically using methods based on the density functional theory.[8,13-19] These studies show that despite their high number of extraframework cations, not all sites are

equally accessible for the interaction with N_2 and O_2 molecules.[18-19] The 3D porous structure of these zeolites is based in cavities, and only cations located in determined positions are susceptible to interact with N_2 and O_2 molecules. Then, it appears interesting to choice zeolites with porous structures with lower dimensionality where cations could be more accessible to the molecules.

Theoretical results show that extraframework cations need to have a charge of + n.0 (were n= 1, 2,...) to compensate the framework's negative charge. Theoretical calculus point that the effective charge on the cations might be reduced due to a certain shielding by partial hydration and/or by the influence of framework oxygen atoms on them.[18] Introduction of elements with less polarizability in the structure, such as fluorine, should result in an increase on the total effective charge of the extraframework cations, and, consequently, an increase of the interaction between cations and the quadrupolar moment of N_2 and O_2 molecules could be expected.

The insertion of fluorine atoms in different zeolite and clay-type structures has been widely studied.[20-25] Several authors reported changes in the structure and catalytic properties of mordenite after activation by solutions of HF, KF, NH_4F and F_2, and considerable higher catalytic activity in some reactions catalyzed by acids.[23,24]

Fluorination under mild conditions (e.g. with NH_4F solutions) could involve a certain dealumination, as reported by several authors. However, there are different proposals about the location of fluorine after treatment. Some authors have discussed two possible ways for the fluoride treatment:

$$\text{zeoliteOH} + F^- (aq) \rightarrow \text{zeoliteF} + OH^- (aq) \qquad \text{(eq. 1)}$$

$$\text{zeoliteOH} + F^- (aq) \rightarrow AlF_xOH_y \text{ zeolite} \rightarrow AlF_3 (aq) + \text{zeolite}^- \qquad \text{(eq. 2)}$$

Thus, Kowalak et al.[23,24] reported the incorporation of fluorine in the framework (eq. 1) whereas Breck et al.[25] and, subsequently, Panov et al.[20]

proposed the formation of extraframework aluminium fluoride species (eq. 2). Examining the fluorination conditions used in these studies, it seems clear that the way (eq. 2) is more favoured when using high fluorine concentrations (> 3% w/w) as well as calcining at high temperatures (> 450ºC).

No studies of fluorinated zeolites are reported for separation processes. In this work, we propose to study the N_2 and O_2 adsorption properties of mordenite. This material is the natural zeolite with the lowest Si/Al ratio (6.5 in our sample). It has a 2D structure, which, actually, works as a one dimensional channel system formed by 12-ring and 8-ring channels, leading probably to a better accessibility of the extraframework cations to the molecules of adsorbate. Besides, we want to increase the charge location of different cations (Na^+, Li^+ and Ag^+) by introducing less polarizing atoms of fluorine in the framework channels of the mordenite in order to improve its adsorption properties.

3.1.2. Experimental Section

3.1.2.1. Starting Materials

Commercial Na-Mordenite (Si/Al = 6.5, CBV 10A Lot No. 1822-50), designated as NaM, was used as starting material. It was supplied by Zeolist as hydrated powder. Its chemical composition was SiO_2/Al_2O_3 mole ratio 13 and a Na_2O weight % of 6.6. Lithium chloride (LiCl, 99 % min, Prolabo), sodium chloride (NaCl, 99 % min, Prolabo), silver nitrate ($AgNO_3$, 99.8 % min, Prolabo), ammonium chloride (NH_4Cl, 99% min, Prolabo), ammonium fluoride (NH_4F, high purity, Probus) and ammonia solution (NH_3, 28%, Prolabo) were used in the preparation of the ion-exchange solutions.

3.1.2.2. Samples preparation

The treatments used to prepare the different samples are shown in Table 1.

Table 1. Sample preparation procedures

Sample	Starting sample	Treatment
NaM		None
LiM	NaM	Three exchanges with LiCl 2.2 M for 12 hours. Vacuum filtered, washed with distilled water and dried in a furnace at 383 K overnight.
AgM	NaM	One exchange with $AgNO_3$ 1M for 12 hours protected from light. Vacuum filtered, washed and dried in a furnace at 383 K overnight.
Li/AgM	LiM	One exchange with $AgNO_3$ 0.01M for 6 hours protected from light. Vacuum filtered, washed and dried in the furnace at 383 K overnight.
NaM_xF (x= 1,10)	NaM	Repeated NH_4^+ exchange with NH_4Cl 2.2 M and calcined at 673 K for 12 hours.
	HM	In tefflon flasks by exchanging 1g of H-Mordenite with 50 mL of NH_4F 8.8 mM and 0.105 M respectively (x =1, 10). After impregnation the samples were vacuum filtered and washed with distilled water.[a]
	HMxF	Bubbling a flow of NH_3/Ar through it.
	NH_4MF_x	Cation exchanged several times with NaCl 2.2 M. Vacuum filtered and washed with distilled water until be free of chlorides, and dried in a furnace at 383 K overnight.
LiM1F	NaM1F	Several exchanges with LiCl 2.2 M. Vacuum filtered, washed and dried in the furnace at 383 K overnight.
LiAgM1F	LiM1F	One exchange with $AgNO_3$ 0.01M 6 hours protected from light. Vacuum filtered, washed and dried in the furnace at 383 K overnight.

[a] Concentrations and volumes of NH_4F were calculated in the way that the % w/w of F introduced per gram of zeolite was 1 and 10.

3.1.2.3. Characterization techniques

N_2 adsorption isotherms. Nitrogen adsorption isotherms at 77K and BET surface areas were obtained using a Micromeritics ASAP 2000 surface analyzer with a value of 0,164 nm^2 for the cross section of the nitrogen molecule. Specific surface areas were obtained from the BET equation.

Powder X-ray diffraction. Powder X-ray diffraction patterns of the samples were obtained with a Siemens D5000 diffractometer (Bragg-Brentano parafocusing geometry and vertical θ-θ goniometer) fitted with a curved graphite diffracted-beam monochromator, incident and diffracted-beam Soller slits, a 0.006º receiving slit and scintillation counter as a detector. The angular 2θ diffraction range was between 5º to 70º. The data were collected with an angular step of 0.05º at 3s per step and sample rotation. $Cu_{K\alpha}$ (1.542 Å) radiation was obtained from a copper X-ray tub operated at 40kV and 30mA. The cell parameters and cell volume values were calculated using a matching profile with TOPAS 2.0 software (Bruker AXS).

^{27}Al and ^{29}Si, MAS NMR spectra were obtained at a frequency of 400 MHz by spinning at 5 kHz. The pulse duration was 2 μs and the delay time was 5 seconds. High purity octahedral hexahydrated aluminum chloride $AlCl_3 \cdot 6H_2O$ in its solid state and silicon nitride Si_3N_4 were used as the chemical shift reference for aluminum and silicium, respectively.

DRIFTS Investigations. Infrared spectra were recorded using a FTIR Bruker Equinox 55 instrument in the frequency range of 400 to 4000 cm^{-1} with a spectral resolution of 4 cm^{-1}. A MCT detector was used. Samples mixed with KBr were placed on a DRIFT cell connected to a temperature controller. Spectra of the dehydrated samples were taken after activation at 673 K for a minimum of 4 hours under an Ar flow of 2 ml/s.

X-ray fluorescence. X-ray fluorescence was used to determine the atoms distribution maps and the Si/Al ratio of the fluorinated and non-fluorinated samples. Experiments were performed on a scanning electron microscope, JEOL JSM6400, operating at accelerating voltage of 15 kV and work distances of 15 mm. All samples were covered with a graphite layer. Accumulating time for mapping experiments was around 120 seconds.

Cation exchange capacity (CEC). Cation exchange capacity (CEC) of different samples was determined in a similar way of that proposed by Bergaya et al.[26] First, mordenite samples were exchanged with an aqueous solution of $CuSO_4$ for 6 h at room temperature. Then, the samples were centrifuged and washed with distilled water several times. The amount of Cu^{2+} exchanged was determined by UV-Visible spectroscopy at 809 nm. The CEC in meq/100g of zeolite was calculated as the difference in concentration between the starting solution and the final solution obtained after the exchange.

3.1.2.4. N_2 and O_2 adsorption measurements.

Adsorption isotherms were measured using a static volumetric system Micromeritics ASAP-2010. The gases used were high purity (99,999%) N_2 and O_2. Both gases were supplied by Carburos Metálicos.

Experiments were made using an amount of sample between 0,20 to 0,30 g. Sample was contained in a quartz cup and previously activated before the adsorption measurements at 623 K using a turbomolecular vacuum pump until a pressure lower than 1μmHg. It is known that small amounts of molecular water inside the framework of the aluminosilicates seriously affect the adsorption capacity of these materials.[27] Adsorption measurement isotherms were performed at 298 K in the range of pressures compressed between 0.05 and 760 mmHg.

3.1.3. Results and Discussion

3.1.3.1. Samples characterization

Nitrogen adsorption isotherms obtained at 77 K were classified of type I for all samples, which correspond to microporous materials, according to the BDDT classification.[28] The BET surface area of the starting sample was around 350 m^2/g. Sample modifications by cation exchange do not modify porosity and surface area results. In contrast, the fluorination of mordenite with NH_4F causes structural variations which results in a slightly increase of its meso-macro porosity (see Table 2), but it does not practically affect the isotherm shape. These results are in agreement with the dealumination detected by other techniques for these samples, as commented below.

Table 2. N_2 physisorption characterization of several samples

Sample	Surface area (m^2/g)	Microp. surface area (m^2/g)	Non-microp. surface area (m^2/g)	Microp./ Non-microp.
NaM	352	321	31	10.35
NaM1F	334	303	31	9.77
NaM10F	370	320	50	6.40

Figures 1 and 2 show the ^{27}Al and ^{29}Si MAS NMR spectra, respectively, for several samples. ^{27}Al NMR of the starting mordenite (NaM) and the low fluorinated mordenite (NaM1F) show that the aluminum is mainly tetrahedrically coordinated since only one peak at 50 ppm can be observed. However, for the highly fluorinated material (NaM10F), besides this tetrahedrical aluminum, a broad band around 0 ppm indicates the presence of some octahedrical aluminum. Therefore, fluorination in mild conditions does not cause an appreciable dealumination of the structure when the amount of

fluorine used is low (1 % w/w). This has also been suggested by Kowalak et al.[23] Otherwise, when the amount of fluorine is higher (10 % w/w) part of the tetrahedrically aluminum becomes octahedrically coordinated. This peak confirms the framework dealumination, which is responsible for the new mesoporosity observed from physisorption data.

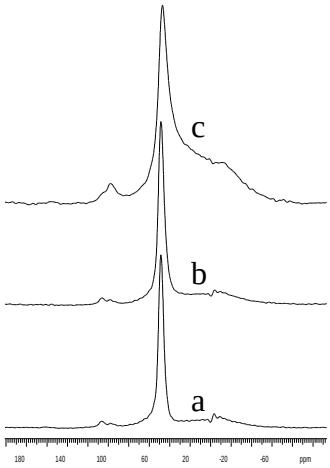

Figure 1. ^{27}Al MAS NMR spectra for (a) NaM, (b) NaMF1, (c) NaMF10 samples.

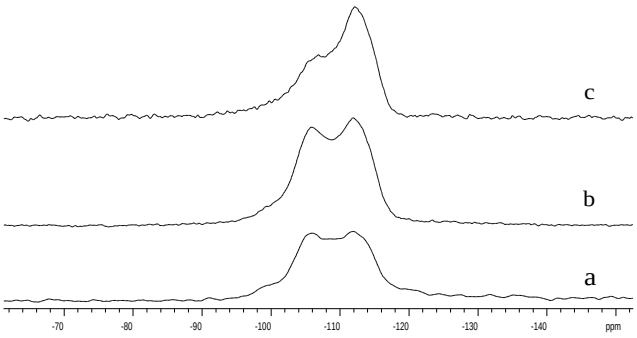

Figure 2. ^{29}Si MAS RMN of (a) NaM, (b) NaM1F and (c) NaM10F.

From the ^{29}Si NMR results (Figure 2), the starting mordenite and the low fluorinated mordenite show three bands at -115 ppm, –105 ppm, and –100 ppm (less intense) which correspond to the Si coordinated to 0 Al, 1 Al and 2 Al, respectively. ^{29}Si NMR spectra for NaM and NaM1F samples are very similar with a very slight decrease of the band at –105 ppm for NaM1F, which indicates a few dealumination not observed before by ^{27}Al NMR. For the NaM10Fsample, this band at –105 ppm tends to disappear, increasing the band at –115 ppm. From these results, we can suggest that the dealumination observed is mainly produced by the initial attack of fluorine to the SiOHAl groups of its acidic form (HM10F).

X-ray powder diffraction patterns of mordenite samples before and after fluorination were taken. The samples, which show similar cristallinity, were identified as mordenite. Additionally, no other phases were detected although the ^{27}Al MAS NMR spectra showed the presence of octahedral aluminum for the highly fluorinated sample (NaM10F), as reported above.

Nevertheless, some structural modifications have been detected as reflected in the variation of the cell parameters calculated from the diffraction patterns (see Table 3). The cell volume practically does not change for the NaM1F sample respect to the non-fluorinated sample (NaM) whereas there is a significant decrease in the cell volume value for the sample NaM10F. However, the cell parameters values do not change in the same direction since parameter *a* increases whereas parameters *b* and *c* decrease when increasing the fluorine treatment. These different tendencies are a consequence of several factors such as the incorporation of fluorine in the structure as well as the dealumination of samples but also the presence of extraframework aluminium in the channels of the mordenite. Therefore, we think that the decrease observed in the cell volume for sample NaM10F should be mainly due to both dealumination and incorporation of the fluorine in the structure.

Table 3. Cell parameters of NaM, NaM1F and NaM10F samples calculated by XRD.

Sample	a (Å)	b (Å)	c (Å)	Cell volume (Å^3)
NaM	18.103(4)	20.451(3)	7.514(1)	2782
NaM1F	18.113(4)	20.437(3)	7.512(1)	2781
NaM10F	18.181(4)	20.383(3)	7.490(1)	2775

In order to confirm this behavior, the IR spectra of HM, HM1F and HM10F samples were also taken. Figure 3 shows the FTIR spectra in the region compressed between 3800 and 3500 cm^{-1}. For the non-fluorinated sample (HM) two peaks are observed at 3740 and 3645 cm^{-1}. The first corresponding to SiOH terminal groups, and the second corresponding to SiOHAl groups although it cannot be discarded the presence of silanol groups related to structural defects.[29] After fluorination, some changes are observed in the FTIR spectra of that region, especially respect to the band at 3645 cm^{-1} since the band at 3740 cm^{-1} does not almost change for both samples. This makes us to think that the attack of fluorine practically does not affect the terminal silanol groups.

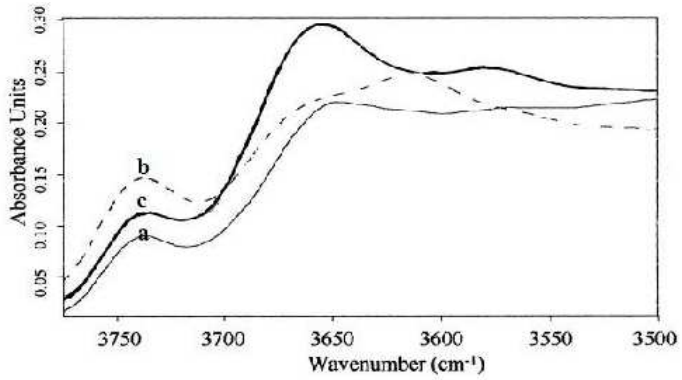

Figure 3. FTIR spectra of (a) HM, (b) HM1F and (c) HM10F samples.

For the HM1F sample, a new band appears at 3614 cm^{-1}. We think that this band corresponds to the same bridged groups of that of 3645 cm^{-1} observed for the non-fluorinated sample. It shifts to lower wavenumber probably due to the effect of the fluorine introduced inside the structure, which makes them more acidic. The shift observed is in agreement with the appearance of framework species (3), previously proposed by Kowalak et al.[23,24]

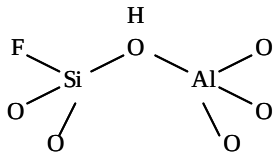

(3)

Also, a less intense band was observed for this sample around 3650 cm^{-1}, which should correspond to the original SiOHAl groups.

For the sample HM10F, more important changes are observed. The first is the appearance of a more intense band at 3655 cm^{-1}. From the results obtained by ^{27}Al MNR for this sample, and together with the data found in the literature,[24] this band can be attributed to AlOH non-framework groups formed as a consequence of the dealumination. Second, there is a band at 3580 cm^{-1} which could be explained in a similar way that the band observed at 3614 cm^{-1} for the HM1F sample. In this case, the higher red shift of the SiOHAl groups band could be due to the presence of stronger Brönsted sites, associated to a more extensive fluorination suffered by NaM10F, although the interaction of these groups with some Al-F species formed during dealumination in the intracrystalline space probably contributes to this shift.[30]

Moreover, the shift in the position for symmetric and asymmetric TO_4 tetrahedra bands in the mid-IR region (see Table 4), is almost the same for the non-fluorinated (NaM) and the low fluorinated (NaM1F) structures, but

shifting towards higher frequencies for the highly fluorinated sample (NaM10F), confirming the dealumination of the structure.

Table 4. IR Frequencies of fluorinated Mordenites, C.E.C. and Si/Al ratio determined by X-ray fluorescence

Sample	IR frequencies (cm^{-1})		C.E.C. (meq/100g)	Si/Al ratio
	ν_{as} (T-O)	ν_{s} (T-O)		
NaM	1064	630	240	7.0
NaMF1	1065	629	217	7.4
NaMF10	1072	637	52	8.2

Finally, to complete the characterization of samples, X-ray fluorescence element maps distribution (not shown here) of Si, Al and Na were also performed and Si/Al ratio was determined by X-ray fluorescence for some samples. Si, Al and Na maps distribution showed an homogeneous atomic distribution in all cases. Quantification results, expressed as Si/total Al (framework + extraframework) ratio (Table 4), indicate that in addition of what was observed by other techniques, there is an initial loss of aluminium during fluorination treatment, which is higher when a higher amount of NH_4F is used. The same tendency was observed in the C.E.C. values (Table 4). The more important decrease observed for the NaM10F sample is in agreement with the presence of extraframework $[Al(OH)_{3-x}]^{x+}$ groups, hardly exchangeable, which are responsible for the neutralization of the framework charge.

3.1.2.2. N_2 and O_2 adsorption measurements.

Nitrogen and oxygen adsorption isotherms are shown in Figures 4, 5 and 6 for different samples. The adsorption volume values are referred to the weight of sample before activation (cm^3/g). The N_2/O_2 selectivity results are listed on

Table 5. N_2/O_2 selectivity was calculated as the ratio between the volume of N_2 adsorbed and the volume of O_2 adsorbed at three given pressures (760, 345 and 50 mmHg).

From the results exhibited in Figure 4 and Table 5, for the non-fluorinated samples it can be observed that substitution of Na^+ cations by Li^+ cations leads to an increase on the adsorption volume and, besides, there is also an increase on the N_2/O_2 adsorption selectivity. This is attributed to the major charge/radium ratio of the Li^+, which favours the electrostatic interaction with the adsorbate molecules.[6]

Table 5. N_2/O_2 adsorption selectivity at 298 K at different pressures.

Sample	Selectivity [a]		
	760 mmHg	**345 mmHg**	**50 mmHg**
NaM	2.8	3.3	4.1
NaMF10	2.0	2.2	2.3
NaMF1	2.8	3.4	4.6
LiM	3.0	4.0	6.6
LiMF1	2.9	4.0	7.2
LiAgM	2.8	4.0	7.3
LiAgMF1	3.0	3.9	6.3
AgM	3.3	4.3	10.2

[a] N_2/O_2 adsorption selectivity was defined as the ratio of the volum adsorbed of N_2 and the volume adsorbed of O_2 at the given pressure

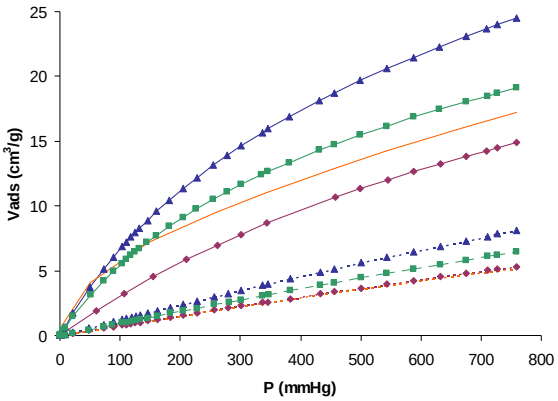

Figure 4. Equilibrium isotherms of N_2 (upper) and O_2 (lower) at 298 K on NaM (♦), LiM (▲),Li/AgM (■) and AgM (—).

Interestingly, the adsorption volumes obtained for these Na-Mordenite and Li-Mordenite samples are slightly higher than those reported in the literature[12] for NaX and LiX samples, respectively, with comparable selectivity values. This reveals the importance of the accessibility of the cations for the gas molecules and confirms our expectations about the use of a zeolite with less cation content but more accessible.

On the other hand, when Na^+ cations are substituted by Ag^+ cations in the mordenite, the isotherm shape becomes less linear (Figure 4). This has also been observed in other Ag-exchanged zeolites,[12] where the N_2/O_2 selectivity increases specially at low pressures. In contrast, we observe a less increase in the total volume adsorbed for the AgM sample respect to the reported for other Ag-exchanged zeolites. This can be attributed to the different degree of complexation interactions, since it is well known that these interactions are strongly influenced by the nature of the zeolite.[31,32]

The adsorption results obtained after the fluorination procedures are shown in Figures 5 and 6 and in Table 5. NaM1F and LiM1F show similar behavior respect to the volume adsorbed and adsorption selectivity results. The total volume adsorbed decreases in both cases after fluorination. This could be explained by a slightly decrease in the number of active sites, because some dealumination takes place when the amount of fluorine introduced is low, according to the Si/Al ratio and C.E.C. values (Table 4). Interestingly, these results also show an increase on selectivity preferentially at low pressures for both samples. This indicates a less shielding of cations when F atoms are incorporated inside the mordenite structure, because of the less polarizability character of fluorine although, probably, fluorination only affects to the more accessible surface.

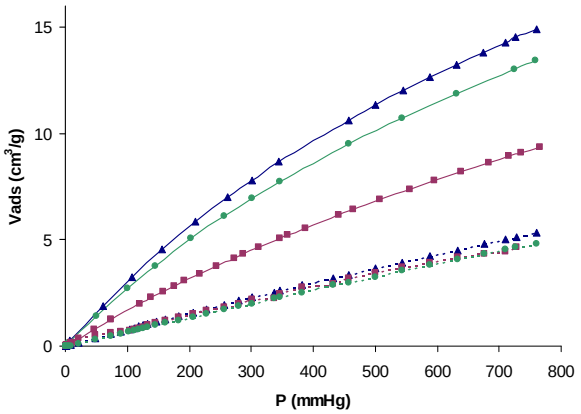

Figure 5. Equilibrium isotherms of N_2 (upper) and O_2 (lower) at 298 K on NaM (■), NaMF1 (●), Na MF10 (▲).

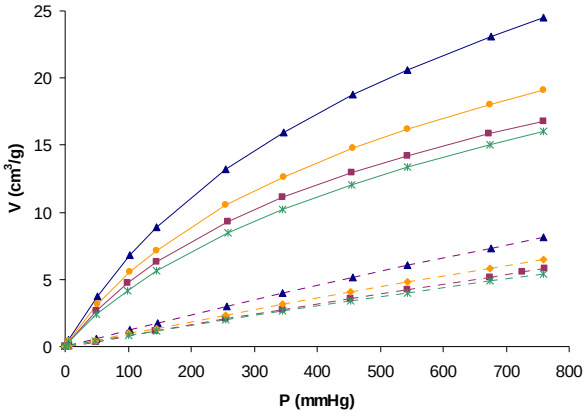

Figure 6. Equilibrium isotherms of N_2 (upper) and O_2 (lower) at 298 K on LiM (▲), LiM1F (■), LiAgM (●), LiAgM1F (×).

On the other hand, for the NaM10F sample, with more fluorine introduced, both volume adsorbed and adsorption selectivity decrease sharply due to the higher dealumination and the presence of hardly exchangeable $[Al(OH)_{3-x}]^{x+}$ groups, which should have scarcely capacity for quadrupolar interaction . This involves a considerable decrease in the number of active sites.

Otherwise, the introduction of small amounts of fluorine in the presence of Ag^+ cations (sample LiAgM1F) results in a decrease both on the volume adsorbed and on the N_2/O_2 selectivity. This can be explained by the effect of the high electronegativity and low polarizability of the fluorine atoms, which cause a decrease on the π-complexation interactions between the cations Ag^+ and the N_2 and O_2 molecules.

In a study reported by Yang et al.[33] about the adsorption of oxygen and nitrogen on silver halides revealed that the polarization effect can influence the 5s orbital energies of Ag. In fact, the difference of energy between the highest occupied molecular orbital (HOMO) of the adsorbate and the lowest

unoccupied molecular orbital (LUMO) of the adsorbent increases when the polarizability of the halide decreases and, consequently, the presence of fluorine probably contributes to obtain a weaker adsorbate-adsorbent interaction, although not important differences between N_2 and O_2 can be expected. However the electronegativity of fluorine atoms would "attract" the electronic density from the Ag and, consequently, this reduces the contribution of backdonation. This reduction affects more to nitrogen since its two π^*-antibonding orbitals are empty while those of oxygen are occupied by one electron each. This explains the decrease in the N_2/O_2 selectivity.

3.1.4. Conclusions

Mordenite, in spite of its Si/Al ratio of 6.5, can adsorb slightly higher volumes of N_2 than zeolites with lower Si/Al ratio, maintaining high N_2/O_2 selectivity. This behaviour can be explained because its 2-dimensional porous structure in channels makes easier the cation accessibility than in zeolites based on cavities. Therefore, this natural zeolite is a good alternative to the synthetic zeolite X for the N_2/O_2 separation process.

In samples prepared by cationic exchange, the volume of N_2 adsorbed increases in the way $Li^+ > Ag^+ > Na^+$ and the adsorption selectivity N_2/O_2 in the way $Ag^+ > Li^+ > Na^+$. For samples exchanged with Li^+ and Na^+ cations, linear isotherms typical of weak electrostatic interaction are observed whereas for Ag^+ samples parabolic isotherms are observed as a consequence of the π-complexation interactions.

The introduction of fluorine in the structure framework is found to have a positive effect on the N_2/O_2 adsorption selectivity. The fluorination with high amounts of NH_4F involves an important dealumination, while the fluorination

with low amounts does not practically cause dealumination of mordenite and some fluorine remains inside the structure modifying the electronic properties of some cations. This fluorine results in a less shielding of these cations by the framework structure, which leads to an increase on the N_2/O_2 selectivity adsorption at lower pressures, despite the loss of the number of active sites.

3.1.5. Acknowledgements

The authors are grateful for the financial support of the Fundación Domingo Martínez and to the Generalitat de Catalunya (2002FI 00667).

3.1.6. References

[1] Sicar, S. *Adsorpt. Sci. Technol.* **2001**, 19, 347.

[2] Kim, J. N.; Chue K. T.; Cho S. H. *Separ. Sci. Technol.* **1995**, 30(3), 347.

[3] Yang, R. T. *Gas separation by adsorption process*; Butterworth: Boston, USA, 1987 reprinted by Imperial College Press, London and World Scientific Publishing Co.: River Edge, NJ, 1997; pp 9-48.

[4] Armor, J. N. Molecular sieves for air separation. In *Materials chemistry: An Emerging Discipline*; Interrante, L. V.; Casper, L. A.; Ellis, A. B. Eds.; ACS: Washington, USA, 1995; pp 321-334.

[5] Ruthven, D. M. *Principles of adsorption and adsorption processes*; John Wiley & Sons, Inc.: New York, USA, 1984.

[6] Coe, C. G., *Acces in Nanoporous Materials*; Pinnavaia, J. B.; Thrope, M. F., Eds.; Plenum Press: New York, 1995.

[7] Coe, C. G.; Kirner, J. F.; Pierantozzi, R.; White, T. R. U.S. Patent 5152813, 1992.

[8] Pápai, I.; Goursot, A.; Fajula, F.; Plee, D.; Weber J. *J. Phys. Chem.* **1995**, 99, 12925.

[9] Rege, S. U.; Yang, R. T. *Ind. Eng. Chem Res.* **1997**, 36, 5358.

[10] Chousdary, V. N.; Jasra, R. V.; Bhat, T. S. Ind. Eng. Chem Res. **1993**, 32, 548.

[11] Chao, C. C. EP Patent 0297542A2, 1998.

[12] Yang, R. T.; Chen, Y. D.; Peck, J. D.; Chen, N. *Ind. Eng. Chem. Res.* **1996**, 35, 3093.

[13] Smudde, G. H.; Slager, T. L.; Coe, C. G.; MacDougall, J. E.; Weigel, S. J. *Appl. Spectrosc.* **1995**, 49 (12), 1747.

[14] Kazansky, V. B.; Bülow, M.; Tichomirova, E. *Adsorption* **2001**, 7, 291.

[15] Goursot, A.; Vasilyev, V.; Arbuznikov, A. *J. Phys. Chem. B* **1997**, 101, 6420.

[16] Shen, D.; Bülow, M.; Jale, S. R.; Fitch, F. R.; Ojo, A. F. *Micropor. Mesopor. Mat.* **2001**, 48, 211.

[17] Kazansky, V. B. *J. Mol. Catal. A: Chem.* **1999**, 141, 83.

[18] Jale, S. R.; Búlow, M.; Fitch, F. R.; Perelman, N.; Shen, D. *J. Phys. Chem. B* **2000**, 104, 5272.

[19] Jasra, R. V.; Choudary, N. V.; Bhat, S. G. T. *Ind. Eng. Chem. Res.* **1996**, 35, 4221.

[20] Panov, A. G.; Gruver, V.; Fripiat, J. *J. Catal.* **1997**, 168, 321.

[21] Sánchez, N. A.; Saniger, J. M.; d'Epinose de la Caillerie, J. B.; Blumenfeld, A. L.; Fripiat, J. *J. Catal.* **2001**, 201, 80.

[22] Belzunce, M. J.; Mendioroz S.; Haber, J. *Clay. Clay Miner.* **1998**, 46 (6), 603.

[23] Becker, K. A.; Kowalak, S. *J. Chem.Soc., Faraday Trans I* **1985**, 81, 1161.

[24] Kowalak, S.; Khodakov, A. Y.; Kustov, L. M.; Kazanky, V. B. *J. Chem. Soc. Faraday Trans.* **1995**, 91(2), 385.

[25] Breck, D. W.; Skeels, G. W. in *Proc. 6th Int. Congr. Catal. (The Chemical Society, London, 1977)*, vol 2, p. 645.

[26] Bergaya, F.; Vayer, M. *Appl. Clay Sci.* **1997**, 12, 275.

[27] Hutson, N. D.; Zajic, S. C.; Yang, R. T. *Ind. Eng. Chem. Res.* **2000**,39, 1775.

[28] Gregg, S. J.; Sing, K. S. W. *Adsorption, surface area and porosity*; Academic Press: London, UK, 1982.

[29] Jentys, A.; Lercher, J. A. Tecniques of zeolite characterization. In *Introduction to zeolite science and practice*; van Bekkum, H.; Flanigen, E. M.; Jacobs, P. A.; Jansen, J. C. Eds.; Elsevier: Amsterdam, NL, 2001. pp 345-386.

[30] Becker, K. A.; Kowalak, S. *J.Chem.Soc, Faraday Trans.I* **1986**, 82, 2157.

[31] Wu, Z.; Han, S.; Cho, S.; Kim, J.; Chue, K.; Yang, R. T. *Ind. Eng. Chem. Res*, **1997**, 36, 2749.

[32] Safark, D. J.; Eldridge, B. *Ind. Eng. Chem. Res.* **1998**,37, 2571.

[33] Chen N.; Yang, R. T. *Ind. Eng. Chem. Res.* **1996**, 35, 4020.

3.2. Influence of the Ag^+ location on the N_2 and O_2 adsorption properties of several Na/Ag-A zeolites

Abstract

Two silver A zeolites were prepared from Na-A zeolite by cation exchange using different Ag^+ concentration. The samples were activated at different temperatures under vacuum in order to study the evolution of their N_2 and O_2 adsorption properties. X-ray diffraction and UV-visible Diffuse Reflectance techniques were used for samples characterization. Adsorption and characterization results showed that the location of Ag^+ cations on/in the zeolite A structure plays an important role on its adsorption properties. Thus, when very low Ag^+ concentration was used for sample preparation, Ag^+ cations are mainly located on the external surface and during vacuum-temperature activation, silver metallic particles are formed, which partially block the entrance to the gas molecules, decreasing the N_2 and O_2 adsorption volumes with a slight decrease of the N_2/O_2 adsorption selectivity respect to Na-A. For the sample exchanged with higher Ag^+ concentration, Ag^+ cations are located inside the cavities of the zeolite. The different samples obtained by the application of temperature under vacuum show higher N_2 and O_2 adsorption volumes respect to the zeolite Na-A, due to their stronger interaction with the silver cations, showing the maximum N_2/O_2 selectivity and the highest N_2 adsorbed volume at 623 K. Surprisingly, when the activation temperature increases over that value, there is a decrease of the N_2 adsorbed volume while the O_2 adsorbed volume increases which could be associated to the migration-reduction of some Ag^+ cations with the temperature.

3.2.1. Introduction

Zeolites, since their first application reported by Barrer,[1] have been mainly used at industrial and laboratory level as catalysts, cation exchangers and selective adsorbents due to their shape selectivity and acidic properties.[2] However, for air separation, shape selectivity at room temperature is not the discriminating feature, since N_2 and O_2 have similar molecular size, but separation depends on the structure type of the zeolite and the number, type, degree of hydration, and location of the extraframework cations.[3,4] Thus, small structural modifications can induce strong modifications in their adsorption behaviour.[5]

Zeolite structures that contain Ag^+ cations as extraframework cations have been extensively used as adsorbents for paraffin/olefin separations on the basis of π-complexation,[6,7] and also, catalysts containing both Ag^o and Ag^+ are important in partial oxidation processes.[8] Silver cations can also interact with N_2 and O_2 molecules by π-complexation, where the bond has two contributions: the donation of π-bond electrons of the N_2 and O_2 molecules to the empty s-orbital of Ag^+, and the backdonation of the d-orbital electrons of Ag^+ (4d orbitals filled with 10 electrons) to the empty antibonding π orbitals of the molecules.[9] This second contribution is lower for O_2 molecules since the antibonding π orbitals are partially occupied on O_2 molecules.

According to the studies published by Yang et al., X and LSX zeolites containing Ag^+ showed N_2 and O_2 adsorption properties that could be related to the presence of silver clusters (Ag_m^{n+}) inside the zeolite, which seem to favor the interaction with the nitrogen molecules, increasing the N_2/O_2 adsorption selectivity.[9,10] The formation of these clusters has been investigated for different zeolites (zeolite A, X, Y and LSX) by several authors which reported that when dehydration takes place, by applying temperature and/or vacuum, two different phenomena could be observed: first, silver cations can interact with other near

silver cations, and second, Ag^+ cations can interact with framework oxygen giving an autorreductive process in suitable conditions, where the transition metal reduces and water or lattice oxygen oxidates.[11] The nuclearity and charge of the clusters formed is certainly dependent on the pretreatment conditions used.[12-17]

Although we can find in the literature many studies about the silver clusters formation within zeolite A, there are only few studies about the adsorption of N_2 and O_2 using this Ag^+ modified zeolite.[18,19] In these studies, an improvement of N_2 adsorption properties, respect to the zeolite Na-A, was observed when fully Ag^+-exchanged commercial zeolite A was activated at temperatures between 623 and 653 K. The good adsorption results published for this commercial zeolite show the interest of its use for the N_2/O_2 separation. However, it is not easy to explain this behavior. Sebastián et al.[18] pointed out that a strong interaction with Ag_m^{n+} species or with the wall charge generated in typical Ag^+ autoreductive processes together with the migration of Ag^+ cations from α to β cavities could explain those results. This let us to think that more studies are needed in order to try to understand that behavior.

The aim of this work is to study the influence of the silver species location on the N_2 and O_2 adsorption properties at room temperature of several silver A zeolites, prepared by treatment of NaA zeolite with two different $AgNO_3$ concentrations. In order to induce variations on the cation distribution in the zeolite structure, the samples were activated at different temperatures under vacuum.

3.2.2. Experimental Section

3.2.2.1. Starting materials

The starting material of this work is a commercial Na-A zeolite (Si/Al = 1) supplied by Prolabo as hydrated binderless pellets with chemical composition 1 Na_2O : 1 Al_2O_3 : 2 ± 0.1 SiO_2 : xH_2O. Silver nitrate ($AgNO_3$, > 99.8 %, Prolabo) was used for samples preparation.

3.2.2.2. Samples preparation

Commercial zeolite was treated in a mortar until a fine powder was obtained. Then, two samples were prepared by cation exchange with different $AgNO_3$ concentration. The one was prepared using higher concentration of silver cations than the other.

Samples Na/Ag(1M)-A and Na/Ag(0.01M)-A were prepared by exchanging at room temperature under stirring for 48 h, 2 g and 0.5 g of zeolite Na-A with 33 mL of $AgNO_3$ 1M and 0.01M, respectively. These experiments were carried out completely protected from light in order to avoid the reduction of Ag^+ cations to metallic silver. Afterwards, the samples were filtered and washed with abundant distilled water and finally dried at 383 K overnight.

3.2.2.3. Characterization techniques

Samples were characterized by powder X- ray diffraction, and UV-Visible Diffuse Reflectance.

Powder X-ray diffraction. (XRD). High Temperature XRD measurements were obtained with a Siemens D5000 diffractometer (Bragg-Brentano parafocusing

geometry and vertical θ-θ goniometer) equipped with an Anton-Paar HTK10 platinum ribbon heating stage. The angular 2θ diffraction range was between 5º and 70º and the measuring time per degree was 6 sec. Ni-filtered $Cu_{K\alpha}$ radiation (30 mA, 40 kV) and a Braun position sensitive detector (PSD) were used. The patterns were collected at 298, 573, 623, 673 and 723 K and at heating rate of 5 K/min. A static argon-atmosphere was used throughout the measurement. The crystalline phases were identified using the Joint Committee on Powder Diffraction Standards (JCPDS) files. The JCPDS files used were 75-2484 and 4-0783 for the zeolite and metallic Ag phases, respectively. From the diffraction patterns, the deconvolutions and cell parameter calculations for each phase ere made using the TOPAS 2.1 software by Brücker-AXS in which the instrument error is corrected.

UV-Visible Diffuse Reflectance. Experiments were performed on a Shimadzu UV-2101 UPC equipment. Spectra were recorded in the range 200 nm to 800 nm at room temperature.

N_2 and O_2 adsorption measurements. Adsorption isotherms were measured using a static volumetric system Micromeritics ASAP-2010. The gases used were high purity (99.999%) N_2 and O_2. Both gases were supplied by Carburos Metálicos.

Adsorption experiments were made using an amount of sample between 0.2 to 0.3 g. Sample was contained in a quartz cup and previously activated before the adsorption measurements at different temperatures (623 K, 673 K, 723 K (for 3 h), 723 K (for 8 h) and 723 K (for 15 h)) using a turbo molecular vacuum pump until a pressure lower than 1 μmHg since it is known that small amounts of molecular water inside the framework of the aluminosilicates seriously affect the adsorption capacity of these materials.[4] Adsorption measurement of pure N_2 and pure O_2 were performed separately at 298 K in the range of pressures compressed between 0.05 and 760 mmHg. The adsorption volume values are

referred to the weight of sample before activation (cm^3/g). N_2/O_2 selectivity was calculated as the ratio between the adsorbed volumes of each pure gas at 760 mmHg.

3.2.3. Results and Discussion

3.2.3.1. Samples characterization

Figure 1 shows the X-ray diffraction patterns of the Na/Ag(1M)-A and Na-A samples. The cristallinity of the zeolite does not vary significantly after exchange, as observed.

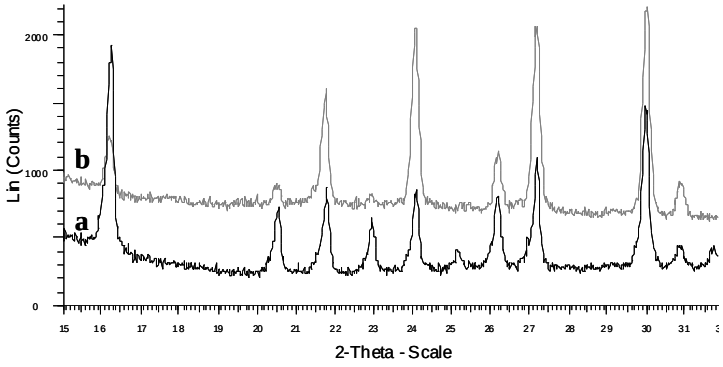

Figure 1. X-ray diffraction patterns of the samples a) Na/Ag(1M)A, and b) NaA.

Table 1 shows the different colors observed for the samples after the activation treatment depending on the conditions used. Sample Na/Ag(1M)-A shows a wider variety of colors than the sample Na/Ag(0.01M)-A.

Table 1. Colors observed after the activation treatment for both samples.

Sample / T^a (K)	573	623	673	723 (3h)	723 (8h)	723 (15h)
Na/Ag(1M)-A	Yellow	Orange	Redish	Redish	Brown	Dark-brown
Na/Ag(0.01M)-A	Greyish	Blackish	Metallic-black	Metallic-black	-	-

In order to follow the possible formation of different silver species, which could explain the different colors observed, several powder X-ray diffraction experiments were performed using a temperature chamber.

The X-ray diffraction patterns obtained for sample Na/Ag(0.01M)-A (Figure 2A) show the peaks corresponding to the zeolite Na-A. Additionally, a new peak seems to appear at 2θ equal to 38.1 at temperatures higher than 623 K, which corresponds to the (100) peak of metallic silver associated with the cubic crystallographic Fm3m group (indicated on the figure). The deconvolution of these diffractograms confirms the presence of metallic Ag particles. One example of XRD deconvolution is given in Figure 2B for the sample cooled at 298 K after the sample was activated at the different temperatures.

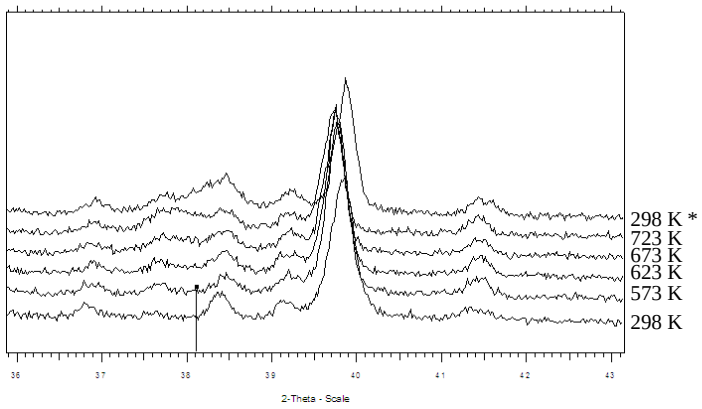

Figure 2A. XRD of Na/Ag(0.01M)-A sample at 298, 573, 623, 673, 723 and 298* K. The diffraction line at 2θ=38,1 corresponds to the (100) Ag Fm3m (JCPDS file). * this XRD pattern was taken after cooling at 298 K the sample previously activated at the different temperatures.

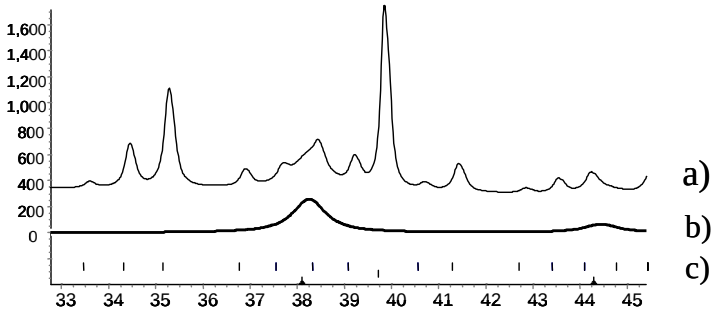

Figure 2B. Whole powder pattern decomposition a) XRD pattern of sample Na/Ag(0.01M)-A cooled at 298 K after the sample was activated at the different temperatures; b) Pattern obtained by subtracting the A zeolite JCPDS file to the pattern a); c) A zeolite diffraction lines (JCPDS file).

The structure of the zeolite Na-A corresponds to the cubic $Pm\bar{3}m$ group and its cell parameter is 11.9735 Å. Table 2 shows the cell parameters of the zeolite and Ag particles calculated from the XRD patterns of sample Na/Ag(0.01M)-A at the different temperatures. As we can see, the cell parameter of the zeolite almost does not change with the temperature. Only a small increase was observed at temperatures higher than 298 K due to the unit cell expansion, which could indicate a low Ag^+ cations exchange degree. However, the adsorption of some Ag^+ on the external surface could explain the presence of metallic particles. Ag^+ cations on the surface can easily migrate and form bigger aggregations giving to the formation of the detected metallic silver particles, whose cristallinity and size increases by increasing the temperature. This is in agreement with the black color observed for this sample at temperatures higher than 623 K (Table 1).

Table 2. Zeolite and Ag cell parameters for the activated Na/Ag(0.01M)-A samples.

Sample	T[a] (K)	Cell parameter (zeolite, Å)	Cell parameter (Ag, Å)
Na/Ag(0.01M)-A	298	11.9705(1)	-
	573	11.9760(3)	-
	623	11.9799(2)	4.1155(1)
	673	11.9844(1)	4.1182(5)
	723	11.9875(4)	4.1249(3)
	298*	11.9670(1)	4.0876(1)

* This sample was cooled at 298 K after it was activated at the different temperatures

The behaviour observed for this Na/Ag(0.01M)-A sample is quite different with respect to other previously reported when exchanging a pure synthesized zeolite A at low silver loading.[14,16,20] In those publications, the authors only observe cationic exchange phenomena. The fact that we use to prepare sample

Na/Ag(0.01M)-A a very low $AgNO_3$ concentration together with the use of a commercial zeolite A (which can contain impurities traces) could explain a certain adsorption of Ag species on the external surface.

On the other hand, no peak due to metallic silver was detected by X-ray diffraction for the Na/Ag(1M)-A sample at any temperature. This is in agreement with the color variation observed for this sample. Also, the cell parameter of that zeolite increases up to 12.3572 Å. This increase is indicative that, in this case, Ag^+ cations are located in the internal positions, and consequently, the unit cell expands maintaining the same symmetry when the Na^+ cations are replaced by the bigger Ag^+. Despite the different colors observed, which could be related to the presence of different Ag_m^{n+} species, it was not possible to detect them by this technique.

In order to characterize those Ag_m^{n+} species, UV-Visible spectra of Na/Ag(1M)-A sample treated at different temperatures were also taken and the spectra were compared with others described on the literature. In this kind of AgA materials, some typical bands, due to charge transferences from the oxygen of the zeolite walls to silver cations, can be observed for this kind of samples in the range compressed between 400 and 600 nm depending on the cation coordination:[15,20] a) the absorption band at 420 nm, caused by the presence of Ag^+ cations in a 6 or 8 O-rings sites; b) the absorption band at 475 nm, only visible when the Ag^+ cations occupy the 4-ring oxygen sites, responsible for the yellow colour; and c) the absorption band at 530 nm when a Ag^+ cation located in a 4-ring oxygen has a second Ag^+ as a neighbor, responsible for the red color.

Table 3 indicates the UV-visible bands for the Na/Ag(1M)-A samples. Observing these data, the sample treated at 298 K shows an intense band at 404 nm, which can be attributed to the type-a) transition. This sample also shows a band at 470 nm associated to the type-b) transition. The samples treated at 573

K and 673 K show also two bands associated to the type a) and b) transitions. However, a progressive increase of the band corresponding to the transition type b) at expenses of the band associated to the transition type a) was observed when increasing temperature. This indicates some migration of silver cations from 6 or 8 O-rings sites to 4 O-ring sites when higher temperatures are used. Finally, for the samples treated at 723 K for different times (3 h, 8 h and 15 h) major changes can be observed. The first and the second spectra show an intense band around 475 nm whereas the band around 420 nm appears just like a small shoulder, indicating a very low amount of silver cations in 6 and 8 O-rings sites for these samples. Otherwise, the UV-Vis spectrum of the third sample, treated at 723 K for 15 h, is completely different. A new band appears at 554 nm, which can be associated to the presence of Ag_m^{n+} species. Although this band could not be observed for the other samples activated at higher temperatures than 673 K, these Ag_m^{n+} species should be present, in small amounts, as suggests the color observed for these samples.

Tabla 3. Absorption wavenumber in nm of the different transitions observed on the UV-Vis region for the Na/Ag(1M)-A sample.

Temperature (K)	a) transition	b) transition	c) transition
298	404	470	-
573	411	463	-
673	417	466	-
723(3h)	420*	477	-
723 (8h)	412*	472	-
723 (15h)	-	-	554

*shoulder

3.2.3.2. N_2 and O_2 adsorption measurements.

The N_2 and O_2 adsorption results are shown in Figures 3 and 4 for the samples Na/Ag(0.01M)-A and Na/Ag(1M)-A, respectively. For the Na/Ag(0.01M)-A sample, all the isotherms (N_2 and O_2) obtained show a linear tendency and lower gas adsorbed volumes than the Na-A zeolite. Otherwise, for the Na/Ag(1M)-A samples, O_2 isotherms show also a linear tendency, while for N_2 isotherms a more parabolic tendency can be observed in comparison with the Na-A sample. This parabolic tendency has been related to the strong π-complexation interactions of the silver cations with the N_2 molecules.[9] In this case, the adsorbed volumes of both gases are higher for the Na/Ag(1M)-A samples than for the Na-A zeolite.

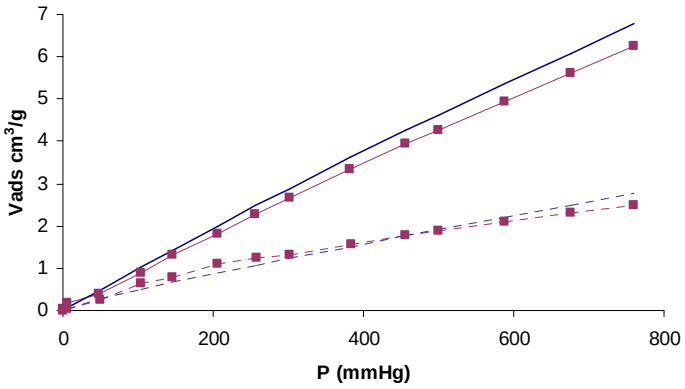

Figure 3. Equilibrium isotherms of N_2 (—) and O_2 (---) at 298 K on the samples Na/Ag(0.01M)-A (■) and Na-A (no symbol) activated at 673 K.

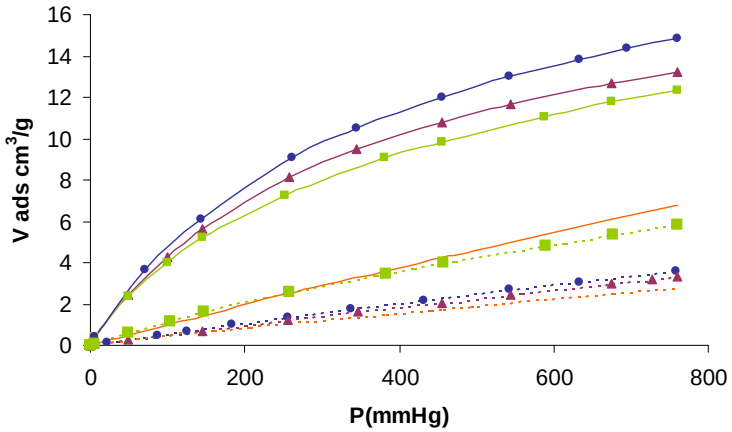

Figure 4. Equilibrium isotherms of N_2 (▬) and O_2 (---) at 298 K on Na/Ag(1M)A activated at different temperatures: 623K (●), 673K (▲), 723 K (■) comparing with Na-A zeolite (no symbol).

Regarding sample Na/Ag(0.01M)-A, we observe that when it is activated, in order to eliminate all the water located inside the cavities, it becomes blackish from 623 K (Table 1). Thus, the observed decrease of the N_2 and O_2 adsorbed volumes together with the slight decrease of the N_2/O_2 adsorption selectivity respect to the Na-A sample (Figure 3) can be associated to the formation of silver metallic particles on the zeolite external surface, which become more crystalline at higher temperatures, according to the XRD characterization results. The presence of these particles hinders the access of the gas molecules, since they partially block the entrance of the cavities, and consequently, the number of adsorbed molecules decreases. The linearity observed for these isotherms is also in agreement with the XRD results that showed very low amounts of Ag^+ inside the cavities for this sample, since the zeolite cell parameter almost does not change respect to the Na-A zeolite (Table 2). This explains the slight decrease of N_2/O_2 selectivity values observed for sample

Na/Ag(0.01M)-A with respect to the Na-A sample (Figure 3) since silver cations do not participate on the interaction with the gas molecules.

On the other hand, for the Na/Ag(1M)-A samples, the volume of adsorbed N_2 and O_2 is always higher than for the Na-A sample independently of the different activation temperature used (Figure 4). This can be mainly explained in terms of the higher $\Delta H_{adsorption}$ of N_2 and O_2 values obtained for silver zeolites than for sodium zeolites.[9]

Interestingly, as we can see numerically in Table 4, this sample presents the maximum adsorbed volume of N_2 at 623 K, which starts to decrease when temperatures higher than 673 K are used in the activation process. Respect to the adsorbed O_2 volume, it is always lower than the N_2 adsorbed volume at all activation temperatures tested. On the other hand, it is surprising that the volume of adsorbed O_2 decreases from 623 K to 673 K, whereas for activation temperatures higher than 673 K, the total O_2 adsorbed volume increases. In outline, N_2/O_2 adsorption selectivity decreases when higher temperatures than 623 K are used in the activation process.

Table 4. N_2 and O_2 adsorbed volumes (in cm^3/g) and N_2/O_2 adsorption selectivity at 760 mmHg for the Na/Ag(1M)-A sample activated at different temperatures.

Temp (K)	Vads N_2	Vads O_2	N_2/O_2 Selectivity
623	14.83	3.59	4.13
673	13.55	3.35	3.95
723 (3 h)	12.35	5.84	2.11

We think that in order to understand this behavior, the cation location in the zeolite plays an important role. In a fully silver exchanged zeolite A, eight cations are located at 6 O-rings, one cation is located at 4 O-ring, and three

silver cations at 8 O-rings, which are mainly related with the diffusion trough the channels.[14] By applying temperature, the cations located in the 8 O-rings probably move towards inside the framework and possibly toward the β-cages (6 O- and 4 O-rings). These migration processes are usually accompanied by an autoreduction process: this means that some silver cations reduce to Ag^0 atoms and, framework oxygen or water oxygen oxidate. When the activation temperature increases, this autoreduction is favored and an increase in the number of Ag^0 atoms can be expected. The main consequences would be: a) an increase of the N_2 and O_2 adsorbed volumes at moderated temperatures due to the migration of cations located in the mouth of the channels (8 O-rings), which favor the access of the N_2 and O_2 molecules into the cavities, and b) a decrease on the N_2 adsorbed volume at higher temperatures because the cations located in the 4 O-rings are less accessible for the gas molecules and also, due to a more important decrease on the number of Ag^+ cations associated to some reduction process. In this way, at higher temperatures we can also explain the observed increase on the O_2 adsorption volume, since silver atoms present more affinity for O_2 than N_2.[21] The increase of the number of Ag atoms at these higher activation temperatures justifies the dark color observed at 723 K (Table 1).

Although in the activation process positive charges are generated on the structural walls and silver aggregations (Ag_m^{n+}) are formed,[18] both with potential ability to interact selectively with N_2 respect to O_2 molecules, from our results, we think that the main responsible for the adsorption properties of these silver cation-exchanged A zeolite samples is the accessibility of the molecules to the Ag^+ species together with the presence of Ag atoms, since the increase of the number of positive defects on the walls and the bigger silver aggregations species (Ag_m^{n+}) formed by increasing the activation temperature cannot explain the decrease of the N_2/O_2 selectivity observed.

3.2.4. Conclusions

The main conclusion that we can extract from our work is that the N_2 and O_2 adsorption capacity of silver cation exchanged commercial A zeolite is greatly affected by the silver concentration on sample preparation and also by the conditions under which these samples are activated.

Thus, sample (Na/Ag(0.01M)-A) presents lower adsorption capacity than Na-A zeolite because during the sample activation process, silver metallic particles are formed, which partially hinder the entrance of the gas molecules to the cavities of the zeolite. On the other hand, the sample prepared using higher amounts of Ag^+ cations (Na/Ag(1M)-A) shows higher adsorption capacity than Na-A with a maximum N_2/O_2 selectivity at 623 K. This can be explained because the Ag^+ cations located in the 8 O-ring sites can migrate to more internal sites, and consequently the accessibility of the molecules to the cations is more favored. However, at higher activation temperatures, an increase of the O_2 adsorbed volume together with a decrease of the N_2 adsorbed volume was observed for this Na/Ag(1M)-A sample. In this case, besides the migration, some cations reduce to Ag^0 atoms. The presence of Ag^0 atoms, which have tendency to interact with O_2 molecules, and the loss of silver cations justify this behavior.

The results presented in this paper show the good N_2/O_2 separation properties of the fully exchanged commercial Ag-A zeolite when using the appropriated activation conditions.

3.2.5. Acknowledgements

The authors are grateful for the financial support of the Fundación Domingo Martínez and to the Generalitat de Catalunya (2002FI 00667).

3.2.6. References

[1] Barrer, R. M. *J. Soc. Chem. Ind.* **1945,** 64, 130.

[2] Yang, R. T. *Gas separation by adsorption process*; Butterworth: Boston, USA, 1987 reprinted by Imperial College Press, London and World Scientific Publishing Co.: River Edge, NJ, 1997.

[3] Choudary, V. N.; Jasra, R. V.; Bhat, T. S. G. *Ind. Eng. Chem. Res.* **1993**, 32, 548.

[4] Hutson, N. D.; Zajic, S. C.; Yang, R. T. *Ind. Eng. Chem. Res.* **2000**, 39, 1775.

[5] Coe, C. G. In Gas separation technology: proceedings of the International Symposium on Gas Separation Technology, Vasant, E. F.; Dewolfs, R. (Eds.), Elsevier, 1990, p. 149.

[6] Safarik, D. J.; Eldridge, R. B. *Ind. Eng. Chem. Res.* **1998**, 37, 2571.

[7] Huang, H. Y.; Padin, J.; Yang, R. T. *J. Phys. Chem.* **1999**, 103, 3206.

[8] Choi, E. Y.; Kim, S. Y.; Kim, Y.; Seff, K. *Micropor. Mesopor. Mater.* **2003,** 62, 201.

[9] Yang, R. T.; Chen, Y. D.; Peck, J. D.; Chen, N. *Ind. Eng. Chem. Res.* **1996**, 35, 3093.

[10] Hutson, N. D.; Reisner, B. A.; Yang, R. T.; Toby, B. H. *Chem. Mater.* **2000**, 12, 3020.

[11] Jacobs, P. A.; Uytterhoeven, J. B.; Beyer, H. K. *J. Chem. Soc.*, Faraday Trans. **1979**, 75, 56.

[12] Kim, Y.; Sep, K. *J. Am. Chem. Soc.* **1978**, 100, 175.

[13] Gellens, L. R.; Mortier, W. J.; Schoonheydt, R. A.; Uytterhoeven, J. B. *J. Phys. Chem.* **1981**, 85, 2783.

[14] Seifert, R.; Rytz, R.; Calzaferri, G. *J. Phys Chem. A* **2000**, 104, 7473.

[15] Miyanaga, T.; Hoshino, H.; Endo, H. *J. Synchrotron Rad.* **2001**, 8, 557.

[16] Calzaferri, G.; Leiggener, C.; Glaus, S.; Schürch, D.; Kuge, K. *Chem. Soc. Rev.* **2003**, 32, 29.

[17] Pavlovskaya, G. A.; Horton-Garcia, C. F.; Dybowski, C.; Corbin, D. R.; Meersmann, T. *J. Phys. Chem. B* **2004**, 108, 1584.

[18] Sebastián, J.; Jasra, R. V. *Chem. Comm.* **2003**, 268.

[19] Sebastián, J.; Jasra, R. V.; *UK Paten, GB 2386889*, 2003.

[20] Seifert, R.; Kunzmann, A.; Calzaferri, G. *Angew. Chem. Int. Ed.* 37 **1998,** 11, 1521.

[21] Pazzi, V. I.; Philipsen, P. H. T.; Baerends, E. J.; Tantardini, G. F. *Surf. Sci.* **1999**, 443 (1-2), 1.

Chapter 4

Styrene Oxide Isomerisation

After seeing that fluorine atoms in the mordenite structure have a positive effect on the N_2/O_2 adsorption selectivity in the previous chapter, we look into the possibility of using these modified-mordenite materials in their H-form for an acidic catalysed reaction. Inserting fluorine atoms, with high electronegative power, into the structure, may increase the strength acidity of Brönsted sites because they should better stabilize the negative charge on the oxygen atoms of the zeolite when the protons involved in the mechanism are lost (Scheme 5, chapter 1).

Isomerisation of styrene oxide to phenylacetaldehyde is an acid-catalysed reaction, as mentioned in the introduction. Mild acid zeolites in their acidic form have been found to be good catalysts for this reaction, since they can eliminate secondary reactions by shape control.

This reaction has been chosen not only because it can check the acidic properties of these modified mordenites, but also because it is important in the fragrances industry.

All the examples found in the bibliography use conventional heating. We thought of using microwaves, an emerging technique in recent years, as a novelty heating method for this isomerization reaction. Therefore, for purposes of comparison, we performed the reaction with two heating methods: microwave and conventional heating.

Microwave, or dielectric, heating is an alternative to conventional heating that uses the properties of liquids and solids to transform electromagnetic energy into heat. This "in situ" mode of energy conversion is very attractive for applications in chemistry and material processing, since microwaves can heat a reaction mixture rapidly, uniformly and directly, without the problems of heat transfer through the walls of the container. Since the first commercial microwave oven was developed by P. Spencer in 1952, numerous publications have appeared in organic synthesis and several reports have been made of catalytic reactions carried out under conditions of microwave irradiation. The main advantages of this technique are that reaction rates can be accelerated, yields can be improved, and reaction pathways can be selectively activated or suppressed. One of the important attributes of microwave heating is its ability to selectively heat one reaction component or, in the case that concerns us, some specific places inside zeolites.

4.1. Isomerisation of styrene oxide to phenylacetaldehyde by fluorinated mordenites using microwaves*

Abstract

In this paper, we studied the acidity of several mordenite samples, which were modified to have 1% (HM1F) and 10% (HM10F) in fluorine w/w, through their catalytic behaviour in the isomerisation of styrene oxide to phenylacetaldehyde in liquid phase. The catalytic experiments were performed by using microwaves as a new method and with a conventional heated batch reactor for comparison. We detect new stronger acid sites for sample HM1F by using NH_3 TPD and FTIR techniques, whereas for sample HM10F some dealumination, and therefore, loss of Brönsted acidity was observed by ^{29}Si, ^{27}Al NMR and X-ray fluorescence. Catalyst HMF1 is the most active at batch reaction conditions, but undergoes faster deactivation when using microwaves. Fluorination in low amounts gives to accessible stronger Brönsted acid sites due to the fluorine located in the external structure framework. This explains the higher activity in the batch reactor and the acceleration of condensation and coke products formation in microwaves experiments. When methanol is used as a solvent, the epoxide ring of styrene oxide opens catalysed by Lewis and Brönsted acid sites. In this case, the existence of high amounts of Lewis acid sites for sample HM10F explains its highest activity.

* Journal of Catalysis **2005**, 232 (1), 239-245.

4.1.1. Introduction

The isomerisation of styrene oxide to β-phenylacetaldehyde is used at industrial scale in fine chemistry for the production of fragrances (which give a narcissus-like smell in floral perfumes), pharmaceuticals, insecticides, fungicides and herbicides.[1]

Epoxides reactivity has been widely studied, because of their versatility as intermediates in organic chemistry.[2,3] In the isomerisation reaction, the use of conventional catalysts often results in the formation of a mixture of ketones and aldehydes, and also by-products such as aldol condensation products, diols and dioethers. The high-weight molecules formed by aldol condensation are the first step in the formation of 1,3,5-triphenylbenzene and coke, which causes a fast deactivation of the catalysts, limiting their lifetime.[1]

The rearrangement of different styrene oxides has been studied under gas and liquid conditions using several solid catalysts.[4,5] The main products of the styrene oxide isomerisation are the corresponding aldehyde and ketone depending on the properties of the catalyst.[6] This reaction can be catalysed by Brönsted acids (addition of a proton to the epoxide oxygen), by Lewis acids (coordination of the epoxide oxygen to a multivalent cation) as well as by bases,[7] although the first are much more active.[1] On the whole, by increasing acidity, the transformation of these oxides increases, and the formation of the aldehyde is favoured.[8]

Recently, the use of zeolites as catalysts for this reaction is of increasing interest because of their capacity to suppress the formation of by-products by stabilizing the α-carbocation intermedium, and by their shape selectivity which favours the selectivity to the aldehyde.[9] Zeolites have good acidic properties for their use as catalysts in isomerisation reactions. The synthesis of zeolites with very strong acid sites is one of the goals of catalysis at the moment.[10]

Mordenite is one of the zeolites catalogued as a strong acid zeolite.[11] Several studies, found in the literature, show the FTIR technique, among others, as an interesting tool for the study of the acidity of zeolites. Few of these studies made with mordenite report the existence of several types of Brönsted acid sites with different acidity strength located on different parts of its structure.[12,13]

The modification of zeolites and clay-type structures with fluorine has been intended by different authors as a way to modify their acidic properties.[14-18] Several authors reported changes in the structure of mordenite after activation under mild conditions (treatment with KF or NH_4F), or using more aggressive conditions like the treatment with HF or F_2. When using these fluorinated mordenites, changes on catalytic activity were observed in some reactions catalysed by acids, such as cumene cracking or transformation of alkylaromatics.[14,16] However, it has not been clearly demonstrated if these fluorine atoms are located in the framework or in the extraframework structure, generating Brönsted or Lewis acid sites, respectively.[16,18,19]

This work aims to study the acidity of different mordenite-type samples, which were modified by fluorination treatment under mild conditions, by testing them in the acidic catalysed transformation of styrene oxide to phenylacetaldehyde. Additionally, we also propose the use of microwaves as a new method to perform the catalytic experiments. The use of microwaves has been reported from 90's applied to the synthesis of materials.[20-22] The main advantages of using this technology are the faster preparation rate and the high yields and purity of the obtained products. However, until this moment, microwaves have not been practically used in catalysis.

4.1.2. Experimental Section

4.1.2.1. Starting materials

The starting material was a commercial Na-Mordenite (Si/Al = 6.5, CBV 10A Lot No. 1822-50), designated as NaM, which was supplied by Zeolist as hydrated powder with a SiO_2/Al_2O_3 mole ratio of 13 and a Na_2O weight % of 6.6. Ammonium chloride (NH_4Cl, 99% min, Prolabo) and ammonium fluoride (NH_4F, high purity, Probus) were used for samples preparation.

Styrene oxide (C_8H_8O, 97% min, Aldrich) and phenylacetaldehyde (C_8H_8O, 90% minimum, Aldrich) were used as reactants, whereas hexane (C_6H_{14}, 95% minimum, SDS) and methanol (CH_3OH, 99.5%, Prolabo) were used as solvents in the catalytic experiments.

4.1.2.2. Catalyst preparation

Commercial mordenite (NaM) was modified into its acidic form (HM) by completely cation exchange with a NH_4Cl 2.2 M solution and later calcination at 673 K for 12 h. Afterwards, HM was treated with different amounts of NH_4F in order to obtain 1% (HM1F) or 10% (HM10F) w/w of fluorine with respect to the amount of zeolite used. After fluorine treatment, samples were calcined again at 673 K for 12 h. Samples were kept all the time in a dissecator under dried conditions.

4.1.2.3. Characterization techniques

^{27}Al and ^{29}Si MAS-NM, NH_3 TPD, FTIR spectroscopy and X-ray fluorescence techniques were used in order to determine the location and the effect of fluorine for the modified samples.

TPD experiments were carried out on a TPD/R/O 1100 Thermo Finnigan equipment equipped with a temperature programmable oven and with a TCD and a PFEIFFER GSD 301 02 Mass Spectrometry detector. For the pre-treatment, samples were activated in situ by flowing Ar at 20 cm^3/min between room temperature until 673 K at 10 K/min. Afterwards, ammonia 3%/He was adsorbed at 313 K and desorbed by flowing He 20 cm^3/min from 373 K to 873K at 5 K/min. The desorbed ammonia was detected using both detectors.

^{27}Al and ^{29}Si, MAS NMR spectra were obtained at a frequency of 400 MHz by spinning at 5 kHz. The pulse duration was 2 μs and the delay time was 5 seconds. The chemical shift references for aluminum and silicium were high purity octahedral hexahydrated aluminum chloride $AlCl_3 \cdot 6H_2O$ and silicium nitrure Si_3N_4, respectively.

Infrared spectra were recorded using a Nicolet Magna 750 Fourier Transform instrument in the frequency range of 400 to 4000 cm^{-1} with a spectral resolution of 4 cm^{-1}. Acetonitrile was used to characterize the different samples. Pressed disks of pure zeolite powders were activated "in situ" the IR cell by outgassing at 773 K before the adsorption experiments. A conventional gas manipulation/outgassing ramp connected to the IR cell was used.

The acetonitrile adsorption/desorption process has been studied by transmission FT-IR. The adsorption procedure involves contact of the activated sample disk with vapors at room temperature at a pressure lower than 2.5 kPa. Desorption process at increasing temperatures was performed in vacuum at temperatures compressed in the range 298 K and 573 K.

X-ray fluorescence was used to determine the atoms distribution maps and the Si/Al ratio of the fluorinated and non-fluorinated samples. Experiments were performed on a scanning electron microscope, JEOL JSM6400, operating at accelerating voltage of 15 kV and work distances of 15 mm. All samples were covered with a graphite layer. Accumulating time for mapping experiments was around 120 s.

4.1.2.4. Determination of the catalytic activity

Isomerisation reactions were carried out in liquid phase at atmospheric pressure using batch reactors by conventional heating and microwaves. The microwaves experiments were performed in a Milestone ETHOS-TOUCH CONTROL equipped with a temperature controller.

The catalysts were first activated at 673 K. The solvents were dried with activated molecular sieves. In the case of n-hexane (95% purity), the solvent it was previously distilled with sodium. The catalytic experiments were performed using 0.04 g of catalyst, 25 ml of solvent (n-hexane or methanol) and 0.3 ml of reactant (styrene oxide or phenylacetaldehyde).

The reaction products were analysed by GC on a Shimadzu GC-2010 instrument equipped with a 30 m capillary column RTX-5 coated with phenylmethilsilicon and a FID detector. Conversion was defined by the following equations:

$$[[\text{area PA/area SO}]_{\text{after reaction}}-[\text{area PA/area SO}]_{\text{before reaction}}]\ g\ cat^{-1} \quad \text{(eq. 1)}$$

$$[[\text{area MPE/area SO}]_{\text{after reaction}}]\ g\ cat^{-1} \quad \text{(eq. 2)}$$

where PA means phenylacetaldehyde; SO, styrene oxide and MPE, 2-methoxy-2-phenylethanol.

For a more exhaustive characterization of some reaction products, Mass spectrometry, ^{1}H and ^{13}C NMR were used. Mass spectrometer results were obtained on a quadrupolar mass spectrometer Hewlett Packard 5989A equipped with a double injection font for electronic impact and chemical ionisation (EI/CI) and connected to a Gas chromatograph Hewlett Packard 5890. ^{1}H and ^{13}C NMR spectra were obtained on a Mercury 400 MHz equipment.

4.1.3. Results and Discussion

4.1.3.1. Samples characterization

Figures 1 and 2 show the ^{27}Al and ^{29}Si MAS NMR spectra, respectively, for several samples. ^{27}Al NMR spectra of the starting mordenite (NaM or HM) and the low fluorinated mordenite (HM1F) reveal that the aluminium is mainly tetrahedrally coordinated since only one peak at 50 ppm can be observed. However, for the highly fluorinated material (HM10F), besides this tetrahedral aluminium, a broad band around 0 ppm indicates the presence of some octahedral aluminium. Therefore, fluorination in mild conditions (using NH_4F) does not cause an appreciable dealumination of the structure when the amount of fluorine used is low (1 % w/w). This has also been suggested by Kowalak et al.[16] Otherwise, when the amount of fluorine is higher (10% w/w) part of the tetrahedral aluminium becomes octahedrally coordinated.

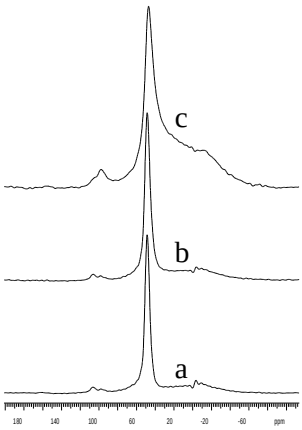

Figure 1. ^{27}Al MAS NMR spectra for (a) NaM, (b) NaMF1, (c) NaMF10 samples.

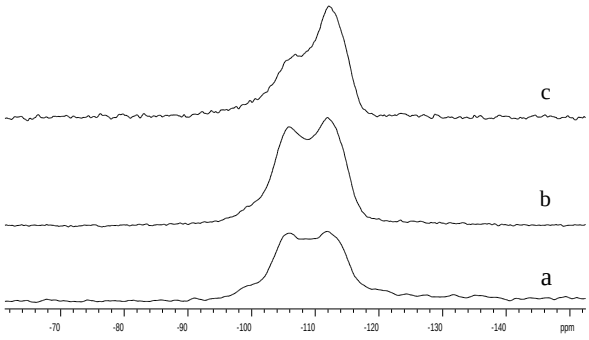

Figure 2. ^{29}Si MAS RMN of (a) NaM, (b)NaM1F and (c) NaM10F.

From the ^{29}Si NMR results (Figure 2), the non fluorinated mordenite (NaM and HM) and the low fluorinated mordenite (HM1F) show three bands at -115 ppm, –105 ppm, and –100 ppm (less intense) which correspond to the Si coordinated to 0 Al, 1 Al and 2 Al, respectively. The band at –105 ppm has slightly lower

intensity for the HM1F sample. This indicates a few dealumination not observed before by ^{27}Al NMR. For the HM10F sample also three bands were observed. In that case, the band at –105 ppm tends to disappear, increasing the band at –115 ppm. From these results, we can suggest that the dealumination observed in this sample is mainly produced by the initial attack of fluorine to the SiOHAl groups of its acidic form.

Table 1 shows the NH_3 TPD results obtained for all samples. Only one band was observed for NaM and HM samples at 475 K and 490 K, respectively. However, HM1F and HM10F show two bands with different relative intensities. Thus, for the HM1F sample, the first band at 513 K is much more intense than the second band at 770 K, whereas the sample HM10F shows the two bands with more similar intensity at 495 K and 775 K, respectively. The bands in the range 465-515 K can be assigned to the initial SiO(H)Al groups while the bands in the range 770-775 K, only observed for the fluorinated samples, should be associated to the presence of some new Lewis acid sites, according to the other characterisation results reported in this work.

Table 1. NH_3 TPD results for all samples.

Sample	NH_3 T_D (K) [a]	
NaM	475	-
HM	490	-
HM1F	513	770
HM10F	495	775

[a] T_D: Maxima of NH_3 desorption temperature peaks.

Referring to the first band, the highest NH_3 desorption temperature of sample HM1F involves the existence of very strong acid sites for this sample.

Meanwhile, the sample with higher amount of fluorine (HM10F) presents this band around the same temperature than the non-fluorinated acidic sample (HM). This could indicate that the stronger Brönsted acid sites observed for HM1F sample should be probably generated by the presence of fluorine atoms in the framework structure. The second desorption band has slightly higher desorption temperature and higher intensity for the most fluorinated sample. Therefore, HM10F presents higher amounts of Lewis sites than HM1F but with similar acidic strength.

In order to confirm this behaviour, the FTIR spectra of HM, HM1F and HM10F samples were also registered. Figure 3 shows the FTIR spectra in the region compressed between 3900 and 3000 cm^{-1}. Spectra have been normalised to the weight of zeolite used for the spectra collection. For the non-fluorinated sample (HM) two peaks are observed with the main maximum at 3743 and 3609 cm^{-1}, respectively. The first corresponds to SiOH terminal groups, and the second to SiOHAl groups.[23] After fluorination, some changes are observed in the FTIR spectra of that region, specially regarding the band at 3609 cm^{-1} since the band at 3743 cm^{-1} does not almost change for both fluorinated samples. The band intensity of that bridging silanol groups decreases when increasing the amount of fluorine introduced, confirming the attack of fluorine ions to the starting mordenite structure. For HM10F, we observe the appearance of new bands, with absorption wavenumbers between 3650 and 3750 cm^{-1}, which correspond to some new species, whose nature can be related to different extraframework aluminium formed as a consequence of the dealumination detected by ^{27}Al RMN for this sample. This agrees with the data found in the literature.[16]

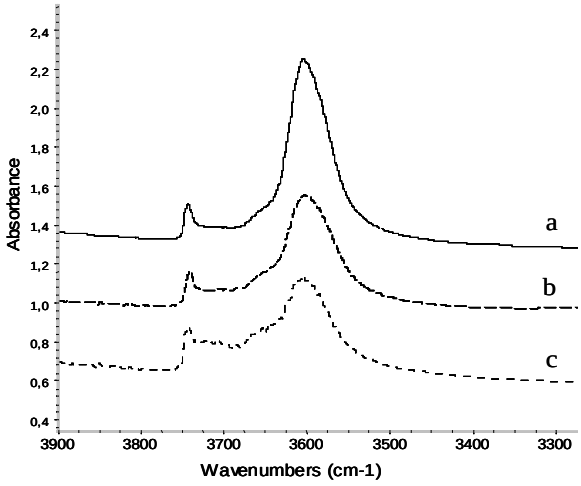

Figure 3. FTIR spectra of (a) HM, (b) HM1F and (c) HM10F samples.

In order to evaluate the acidity of these bridged SiOHAl groups, the so called *hydrogen-bond method* was used, in which the acid strength measure is based on the red shift that the OH stretching modes undergo as a result of interaction with bases, like acetonitrile.

Figure 4 shows the spectra for all acidic mordenite samples in the presence of acetonitrile at room temperature, which show an appropriated behaviour for acidic-mordenite like samples.[12] The so called A, B, C bands with maxima around 2800, 2450 and 1670 cm^{-1} are the result of the bridged OH groups interacting with acetonitrile molecules. Additionally, a component at 3400 cm^{-1} can also be observed corresponding to the result of silanol terminal groups interacting with acetonitrile. The OHs bands shift observed when interacting with acetonitrile respect to the OHs bands observed on HMOR (3743 and 3609 cm^{-1}) confirm that bridging OHs groups are strong Brönsted acid sites, while terminal SiOH groups are weak Brönsted acid sites. The position of the minimum between A and B components, which corresponds to the first

overtone of the in-plane bending band of the hydrogen-bonded OHs, allows us to evaluate the strength of interaction between the OH groups with acetonitrile, which can easily be related to the different strength acidity.[13] Thus, from Figure 4 we observe that HM1F sample shows the frequency of that minimum at the lowest frequency ($\Delta\nu$ = 13 cm^{-1} respect to HM sample), indicating the existence of the strongest Brönsted acid sites for this sample. However, HM10F sample shows this minimum also at lower frequencies than HM sample ($\Delta\nu$ = 6 cm^{-1}), so the still remaining acidic groups after fluorination (Figure 3) have slightly higher acidity than HM sample.

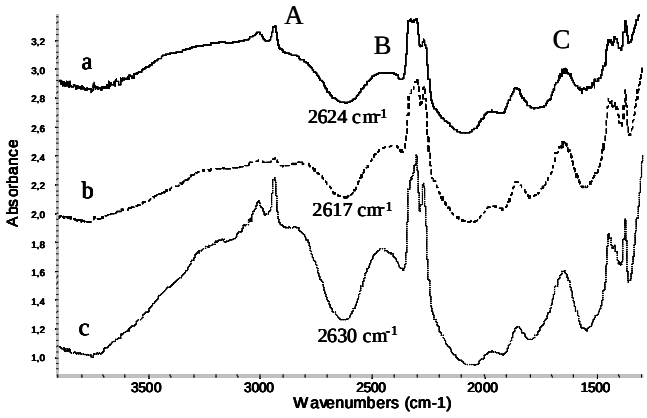

Figure 4. FTIR spectra of acetonitrile interacting with HM (a), HM1F (b) and HM10F (c) at room temperature.

Moreover, the shift in the position for symmetric and asymmetric TO_4 tetrahedral bands in the mid-IR region (see Table 2), is almost the same for the non-fluorinated (HM) and the low fluorinated (HM1F) structures, but shifting towards higher frequencies for the highly fluorinated sample (HM10F), confirming the dealumination of the structure.

Table 2. IR Frequencies of fluorinated Mordenites and Si/Al ratio determined by X-ray fluorescence

Sample	IR frequencies (cm^{-1})		Si/Al ratio
	ν_{as} (T-O)	ν_{s} (T-O)	
HM	1064	630	7.0
HMF1	1065	629	7.4
HMF10	1072	637	8.2

Finally, to complete the characterization of these samples, element maps distribution (not shown here) of Si, Al and Na were also performed and Si/Al ratio was determined by X-ray fluorescence for the modified mordenites (Table 2). Si, Al and Na maps distribution showed a homogeneous atomic distribution in all cases. Quantification results, expressed as Si/total Al (framework + extraframework) ratio, show that there is an initial loss of aluminium during the fluorination treatment, which is higher when a higher amount of NH_4F is used, confirming what was observed by other techniques.

4.1.3.2. Catalytic results.

Figures 5 and 6 show the catalytic activity results in the isomerisation of styrene oxide, with hexane as a solvent, for the four samples using microwaves and conventional heating, respectively. Conversion results are expressed as commented in the Experimental section.

From the results obtained by using microwaves at 353 K at different reaction times (Figure 5), we observe a very low activity for the NaM sample at all reaction times. Modified mordenites present higher activity than the NaM

sample, but their catalytic behaviour with time is different. Thus, HM and HM10F show a similar behaviour, which is an increase of the conversion as reaction time increases for all conditions tested, but HM10F sample has lower catalytic activity than sample HM, probably associated to the loss of some Brönsted acid sites in the fluorination process. This is in agreement with the characterisation results and with the fact that Lewis acid sites, present in higher amounts in sample HM10F, are less active for this isomerisation reaction.[1] Additionally, a slight deactivation of catalyst HM10F cannot be discarded, as we will see below for the HM1F sample, since HM10F contains also some strong acid sites, as observed by FTIR. Surprisingly, HM1F, for which larger conversions would be expected according to the presence of stronger Brönsted acid sites, shows a very different behaviour with an increase of the conversion at the beginning of reaction, which then decreases and maintains practically constant after 30 min. For the modified mordenites (HM, HM1F, HM10F) a blackish colour was observed after reaction, which could be related to the formation of coke on the surface of the catalyst. We think that these facts could be ascribed to a typical behaviour of very strong acid catalysts: first, the formation of condensation products, which deposit on the catalytic surface and, consecutively, the coke formation is favoured provoking a fast deactivation of the catalyst.[1] Thus, the catalyst with the strongest Brönsted acid sites (HM1F) shows the fastest deactivation (Figure 5).

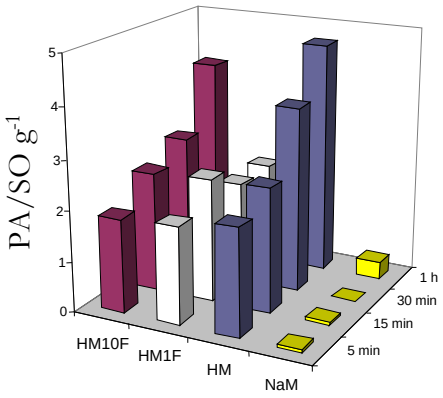

Figure 5. Catalytic results in a microwave heated batch reactor at 353 K using hexane as a solvent.

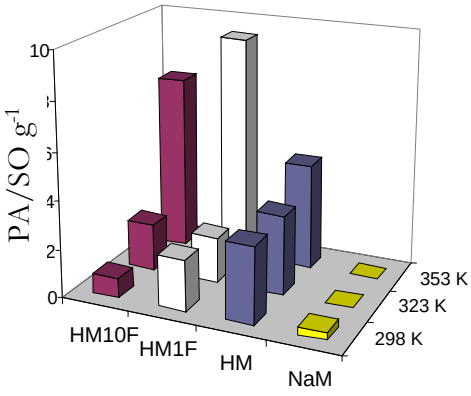

Figure 6. Catalytic results in a conventional heated batch reactor at atmospheric pressure at different temperatures using hexane as a solvent

Additional experiments were carried out in order to try to avoid the formation of deactivation products by varying the amount of catalyst in HM and HM1F samples, at 353 K for 1h using ¼, ½ and 2 times the catalyst amount tested in the previous catalytic experiments. Samples became also blackish after reaction. The results indicate that, for both catalysts, it was not possible to avoid the formation of condensation products by varying the catalyst amount. Although an increase on the activity was observed when using higher amounts of catalyst, also a few increase of deactivation was observed, especially for HM1F, which corroborates the stronger acidity observed for this catalyst.

In order to compare the influence of using microwaves in this reaction, catalytic experiments using batch reactors were also performed at different temperatures (298 K, 323 K and 353 K) for 1 h. From the results shown in Figure 6, we

observe at 353 K an increase on the activity respect to the microwave conditions for all samples except for NaM, as expected, since this sample almost does not contain acidic groups which are necessary to catalyse this reaction, as commented above. Catalyst HM1F shows the best conversion but now, the catalytic activity of sample HM10F is higher than that of sample HM, contrarily to the results obtained with microwaves. This can be probably associated to the presence of strong acid sites in both fluorinated samples, which are present in lower amounts in sample HM10F. We can conclude that the use of microwaves accelerates the catalyst deactivation, especially for the fluorinated samples, although in less extension for sample HM10F. This confirms again that these samples contain very strong acid sites, which favour the formation of condensation products that impede the interaction of the styrene oxide molecules with the Brönsted acidic centres, deactivating the catalyst. When lower temperatures were used (298 and 323 K) in batch reactor experiments, lower activities were observed for the HM, HM1F and HM10F catalysts, meanwhile for NaM, the activity was practically null.

In order to see the influence of the solvent in this catalytic reaction, a more polar solvent, methanol, was chosen since it has already been used for this reaction.[24] The experiments were performed using the microwaves at 333 K for 1 h. From the results shown in Figure 7 some differences were observed. In this case, a new major product was obtained besides the aldehyde. This new product, identified by ^{1}H and ^{13}C NMR, corresponds to the formula 2-methoxy-2-phenylethanol (MPE) showing signals (400 MHz, CD_3OD) at 3.25 (s, 3H,OCH_3), 3.6 (m, 2H, CH_2OH), 4.20 (dd, 1H, Ar-CH), 4.91 (s, 1H, OH), 7.20 (m, 5H, Ar) for ^{1}H NMR, and (100.6 MHz, CD_3OD) at 57.24 (s, 1C, OCH_3), 67.82 (s,1C, CH_2OH), 86.36 (s, 1C, Ar-CH), 129.10, 129.26, 129.58 and 140.32 (4s, 6C, Ar) for ^{13}C NMR. The identification of this product was also confirmed by mass spectrometry.

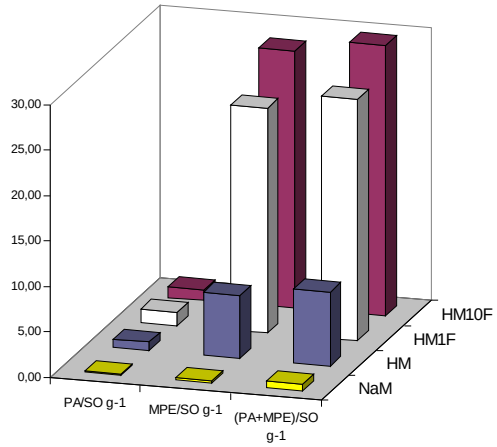

Figure 7. Catalytic results in a microwave heated batch reactor at 333 K using methanol as a solvent.

In order to check the origin of that product, whether it comes from the reactant (styrene oxide) whether from the isomerisation product (phenylacetaldehyde), additional catalytic experiments were carried out using phenylacetaldehyde as the starting reactant but maintaining the same reaction conditions. The reaction products were also identified by GC, ^{1}H NMR, ^{13}C NMR, and Mass Spectrometry techniques. Phenylacetaldehyde dimethyl acetal was the main product, and also small amounts of condensation products were observable by ^{1}H and ^{13}C NMR techniques. This let us to think that the formation of 2-methoxy-2-phenyletanol comes from the aperture of the oxide ring in styrene oxide and not from the aldehyde.

The catalytic activity, expressed as the sum of eq. 1 and eq. 2 ((PA+MPE)/SO g^{-1}), and the conversion to MPE (MPE/SO g^{-1}) increase when the percentage of fluorine increases (Figure 7). This indicates that the formation of 2-methoxy-2-phenylethanol is a reaction catalysed by both Brönsted and Lewis acid sites. However, the conversion to the isomerisation product (PA/SO g^{-1}) follows the same tendency than that observed when hexane was used (Figure 6), but in this

case the conversions are lower, because the opening of the oxide ring is the most favoured reaction.

4.1.4. Conclusions

The introduction of fluorine in the mordenite structure framework is found to have a remarkable effect on its acidic properties as demonstrated in this study. Introducing low amounts of fluorine, the Brönsted acidity of the catalyst increases as concluded from the catalyst characterization and also from the comparison of the catalytic results obtained on the microwaves and batch reactors under the same reaction conditions. The results confirm that the use of microwaves accelerate the condensation and coke products formation, which are responsible for the catalyst deactivation. Thus makes evident the importance of using microwaves as a radiation font for catalytic reactions, especially those showing low yields and/or low reaction rates.

Besides, this fluorine must be mainly located on the more external structure positions, and therefore, without the shape restriction expected in a zeolite. This explains the higher and faster catalyst deactivation observed in the microwave reactor when mordenite is modified using low amounts of NH_4F (HM1F catalyst). Consequently, only the more accessible positions are fluorinated and materials are easily deactivated during the styrene oxide isomerisation reaction.

Otherwise when methanol is used as a solvent, the styrene oxide ring breaks easily to give 2-methoxy-2-phenylethanol. This reaction is favoured by the presence of Brönsted and Lewis acid sites, and the conversion increases as the % of fluorine introduced increases.

4.1.5. Acknowledgements

The authors are grateful for the financial support of the Ministerio de Ciencia y Tecnología and FEDER funds (REN2002-04464-C02-02) and to the Generalitat de Catalunya (2002FI 00667).

4.1.6. References

[1] Hölderich, W. H.; Barsnick, U. In *Fine Chemicals through Heterogeneous Catalysis,* Sheldon, S. A.; van Bekkum, H. Eds.; Wiley-VCH: Weinheim, 2001, p 217.

[2] Ruiz-Hitzky, E.; Casal, B.; *J. Catal.* **1985,** 92, 291.

[3] Neri, C.; Buonomo, F.; US Patent, US 4609765, 1986.

[4] Hölderich, W. H.; US Patent, US 4990684, 1989.

[5] Taramasso, M.; Pergo, G.; Notari, B. US Patent, US 4410501, 1983.

[6] Arata, K.; Tanabe, K. *Catal. Rev. Sci. Eng.* **1983**, 25, 365.

[7] Kochkar, H.; Clacens, J. M.; Figueras, F. *Catal. Lett.* **2002**, 78, 91.

[8] Molnár, A.; Bucsi, I.; Bartók, M.; Resofski, G.; Gáti, G. *J. Catal.* **1991**, 129, 303.

[9] Neri, C.; Buonomo, F.; US Patent, US 4495371, 1985.

[10] Corma, A. *J. Catal.* **2003**, 216, 298.

[11] Van Bokhoven, J. A.; Tromp, M.; Koningsberger, D. C.; Miller, J. T.; Pieterse, J. A. Z.; Lercher, J. A.; Williams, B. A.; Kung, H. H. *J. Catal.* **2001**, 202, 129.

[12] Bevilacqua, M.; Busca, G. *Catal. Commun.* **2002**, 3, 497.

[13] Bevilacqua, M.; Gutièrrez Alejandre, A.; Resini, C.; Casagrande, M.; Ramírez, J.; Busca, G. *Phys. Chem. Chem. Phys.* **2002**, 4, 4575.

[14] Panov, A. G.; Gruver, V.; Fripiat, J. *J. Catal.* **1997**, 168, 321.

[15] Belzunce, M. J., Mendioroz, S.; Haber, J. *Clay. Clay. Miner.* **1998**, 46, 603.

[16] Kowalak, S.; Khodakov, A. Y.; Kustov, L. M.; Kazanky, V. B. *J. Chem. Soc. Faraday Trans.* **1995**, 91, 385.

[17] Sánchez, N. A.; Saniger, J. M.; d'Epinose de la Caillerie, J. B.; Blumenfeld, A. L.; Fripiat, J. *J. Catal.* **2001**, 201, 80.

[18] Becker, K. A.; Kowalak, S. *J. Chem.Soc., Faraday Trans I* **1985**, 81, 1161.

[19] Breck, D. W.; Skeels, G. W. in *Proc. 6th Int. Congr. Catal.*, The Chemical Society: London, 1977, vol 2, p. 645.

[20] Cumming, S. *Green Chem.* **1999**, 1, G94.

[21] Rao, K.J.; Vaidhyanathan, B.; Ganguli, M.; Ramakrishnan, P.A. *Chem. Mater.* **1999**, 11, 882.

[22] Elander, N.; Jones, J. R.; Lu, S. Y. *Chem. Soc. Rev.* **2000**, 4, 239.

[23] Jentys, A.; Lercher, J.A. Tecniques of zeolite characterization. In *Introduction to zeolite science and practice;* van Bekkum, H.; Flanigen, E. M.; Jacobs, P. A.; Jansen J. C. Eds.; Elsevier: Amsterdam, 2001, p. 345.

[24] Neri, C.; Buonomo, F. US Patent, US 4609765, 1986.

Chapter 5

FT-IR Characterization

IR spectroscopy is a technique that is commonly used to characterize materials. Of the different modalities, transmission-absorption, diffuse reflectance and attenuated total reflection are the most frequent.

The IR spectroscopic study of surface active centers is based on the observation that vibrational perturbation undergoes by probe-molecules when they adsorb on the surface.

The ideal probe molecule should have certain characteristics:

- The functional group or the atom through which the molecule is bonded to the surface should be well known.
- The probe molecules should form the same interaction complex for similar adsorbents.
- Adsorption complexes should be stable enough to allow characterization.
- The probe molecules should have spectral parameters that are sensitive to the state of the sites on which they are adsorbed.
- The informative absorption bands of the complexes should be in regions in which the sample is transparent.
- The extinction coefficients of the informative bands must be high.
- The probe molecule should not cause any chemical modification to the surface.

- The probe molecule should be small enough to avoid steric hindrance of the adsorption.

Because we were studying cations or Brönsted acid type centres, we used nitriles of different sizes and electronic properties, and CO to characterize the zeolite samples.

Nitriles are relatively weak bases and coordinate via the nitrogen of the nitrile group to the acid sites. Upon interaction, the band of the CN stretching vibration is shifted to higher wavenumbers. Coordination to aprotic sites via the nitrogen lone-pair electrons results in blue shifts of approximately 30 to 60 cm^{-1}. Coordination to a hydroxyl group, on the other hand, results in shifts of approximately 10 to 30 cm^{-1}.

Carbon monoxide is a weak base molecule and interactions with most solid acids are weak. Thus, low temperature adsorption experiments are necessary for more quantitative studies. Under these conditions, CO is unreactive for all practical purposes, and Brönsted and Lewis sites can be qualitatively and quantitatively determined. The smallness of CO makes it possible to probe nearly all acid sites. CO usually interacts by bonding via the carbon atom to the acid sites and shifts the adsorption maximum of the CO stretching vibration band to higher wavenumbers. However, it can also interact by bonding via the oxygen atom to form isocarbonyls, and the result is that the complexes are less stable than the carbon bonded CO. In this case the CO stretching frequency shifts to lower frequencies. In addition, other complexes for example, with CO in bridging position, CO bonded via both ends or species like $M^{n+}(CO)_x$, can also be found.

In our work, adsorption experiments were first performed on Na-Mordenite (chapter 5.1) in order to characterize its active sites, and a new interaction was found with either nitriles or CO adsorption. Therefore, in order to go more

deeply into this interaction, these probe molecules were adsorbed into several alkali-mordenites (chapter 5.2) and on two sodium faujasites (chapter 5.3).

5.1. An FT-IR study of the adsorption of CO and nitriles on Na- Mordenite: evidence of a new interaction*

Abstract

The low-temperature adsorption of CO and the room temperature adsorption of acetonitrile, propionitrile, isobutironitrile, pivalonitrile, benzonitrile and orthotoluonitrile on Na-mordenite have been investigated by FT-IR spectroscopy. The results have been compared with analogous experiments performed on H-mordenite, Na-X zeolite and Na-silica-alumina. The Na distribution in Na MOR has also been investigated by XRD and Far-IR spectroscopy. The conclusions are that Na ions distribution is essentially random and that together with the well known interaction of the probes with Na ions in the side pockets and the main channels, a stronger additional interaction occurs in all cases. This new interactions is likely multiple, involving either more Na ions or Na and oxygen species. This interaction is more pronounced with the hindered nitriles, whose access at the cavities is likely forbidden. This suggests that this interaction, which is also observed on Na-X zeolites but not with Na-silica-alumina, occurs at the mouths of the mordenite channels.

* Journal of Physical Chemistry B **2005**, 109 (2), 915-922.

5.1.1. Introduction

Zeolites in their protonic forms are largely used as environmentally friendly catalysts for proton catalyzed reactions.[1] In particular, H-mordenite finds application for catalyzing efficiently the skeletal isomerizations of light alkanes such as butane and pentane.[2] Partially Na-exchanged MOR (Na-H-MOR) has been studied for application in xylenes isomerization.[3] However, usually light alkali metal exchanged zeolites (like e.g. Na-X and Na-Y) act as quite mild basic catalysts.[4-6] Whereas, heavy- alkali metal zeolites (like Cs-Y) are reported to be strong bases. In parallel, Na-zeolites show a mild Lewis acid behavior associated to the activity of highly unsaturated alkali cations which can adsorb electron rich molecules so allowing their separation.[7] Several studies have been reported recently concerning Na-Mordenites. In particular, the effect of localization of Na cations and of hydrations have been studied by dielectric relaxation spectroscopy,[8] by thermally stimulated current measurement[9] and by modelling.[10] The adsorption isotherms of small molecules such as N_2, H_2 and O_2 have been studied on Na mordenite[11,12] and modified Na mordenites.[13]

The low temperature adsorption of CO is today perhaps the most popular technique for characterizing adsorption sites of zeolites by IR spectroscopy. It actually allows a very detailed analysis of the surface sites as they appear at low temperature without strong perturbations of the surface, having also free access to any cavity and avoiding steric hindrances.[14, 15] This is a good opportunity to evaluate "pure acidity" without any steric constraint,[16] and has been applied to both H-MOR and Na-MOR.[17, 18] On the contrary, the adsorption of a set of differently hindered nitriles allowed to investigate the accessibility and the multiplicity of the protonic sites on H- mordenite[19, 20] and of Cobalt-exchanged mordenite.[21]

In this paper we describe the results of an IR study of the adsorption of different hindered nitriles on Na-mordenite. The results will be compared with those of low temperature CO adsorption measurements. The aim is to have indications on the locations and accessibility of the adsorption sites of Na Mordenite.

5.1.2. Experimental

5.1.2.1. Sample preparation

Mordenite has been used as the main object of study of this work.

Na-MOR (Si/Al = 6.5, CBV 10A Lot No. 1822-50) was supplied by Zeolyst as hydrated powder. The chemical composition was SiO_2/Al_2O_3 mole ratio 13 and a Na_2O weight % of 6.6. H-MOR was prepared by cation exchanging the starting form, Na-MOR, with a NH_4Cl 2.2 M solution and later calcining at 673 K for 12 hours.

Other materials (NaX and Na-Silica-alumina) have also been used in other to clarify some results obtained with mordenite for comparison. NaX zeolite was supplied by Rhône Poulenc. Na-Silica-alumina was prepared by impregnation of a commercial silica–alumina from STREM with a Na_2CO_3 solution. The impregnation was carried out in order to achieve that the moles of Na^+ ions introduced were equal to the moles of aluminium atoms in the commercial silica-alumina.

5.1.2.2. Characterization techniques

Mordenite samples were characterized using the following techniques:

Powder X-ray diffraction patterns of the samples were obtained with a Siemens D5000 diffractometer (Bragg-Brentano parafocusing geometry and vertical θ-θ goniometer) fitted with a curved graphite diffracted-beam monochromator, incident and diffracted-beam Soller slits, a 0.006º receiving slit and scintillation counter as a detector. The angular 2θ diffraction range was between 5º to 70º. The data were collected with an angular step of 0.05º at 3s per step and sample rotation. $Cu_{K\alpha}$ (1.542 Å) radiation was obtained from a copper X-ray tub operated at 40kV and 30mA. The cell parameters and cell volume values were calculated using a matching profile with TOPAS 2.0 software (Bruker AXS).

Skeletal MIR (KBr pressed disks) and FIR (pure powder on polyethylene supports) spectra were recorded on a Nicolet Magna 750 Fourier Transform instrument (resolution 4 cm^{-1}). Additionally, both samples were characterized (on MIR range) by adsorbing several probe molecules. Different nitriles like acetonitrile (AN), propionitrile (PrN), isobutilonitrile (IBN), pivalonitile (PN), benzonitrile (BN) and o-toluonitrile (o-TN) were used to characterize mordenite samples, and furthermore CO at low temperature was also used. The pressed disks of pure zeolite powders were activated "in situ" the IR cell by outgassing at 773 K before the adsorption experiments. A conventional gas manipulation/outgassing ramp connected to the IR cell was used.

The adsorption/desorption process has been studied by transmission FT-IR. For nitriles, the adsorption procedure involves contact of the activated sample disk with vapors at room temperature at a pressure not higher than 2,5 kPa. The desorption process at increasing temperatures was performed in vacuum at temperatures compressed in the range 273 K and 573 K. On the other hand, CO adsorption was performed at 130 K by the introduction of a well-known

dose of the gas inside the low temperature infrared cell containing the previously activated wafers. IR spectra were collected evacuating at increasing temperatures between 130 and 273 K. Additionally, the co-adsorption of acetonitrile and CO was performed in the way that first acetonitrile was adsorbed at room temperature and posterior evacuated at 373 K. Consecutively the cell temperature was decreased until 130 K and a well-known dose of CO was introduced, which was posterior evacuated at temperatures between 130 K and 273 K.

5.1.3. Results and Discussion

5.1.3.1. Skeletal MIR and FIR spectra

Figure 1 shows the X-ray Diffraction patterns obtained for NaMOR and HMOR samples, which agree to the respective Mordenite JCPDS file. The calculated cell parameters and cell volume for both samples are also reported in Table 1. Both samples present similar cristallinity, and no significant differences on the peak width and on the peak intensity are appreciable from X-ray patterns in Figure 1. However, the cell parameters values indicate an increase on the cell dimensions from HMOR to NaMOR, which can be assigned to the effect of the different dimensions of H^+ and Na^+ cations in the cavities and to a certain dealumination during HMOR preparation. In both NaMOR and HMOR X-ray patterns only hkl peaks assigned to the Mordenite framework can be observed. Consequently, the absence of hkl peaks associated to a cation match on structure, suggest that cations may be randomly distributed on mordenite.

Table 1. Cell parameters of HMOR and NaMOR samples calculated by XRD.

Sample	a (Å)	b (Å)	c (Å)	cell vol. (Å^3)
HMOR	18.098(4)	20.447(3)	7.510(1)	2279
NaMOR	18.180(4)	20.315(3)	7.484(1)	2764

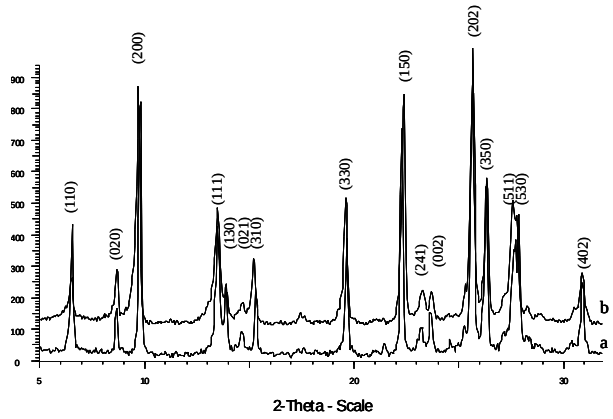

Figure 1. X-ray Diffraction patterns of NaMOR (a) and HMOR (b) samples.

In Figure 2, the skeletal IR spectra (KBr pressed disks) for HMOR and NaMOR are reported. The spectra compare well with those reported in the literature. The substitution of Na^+ cations for H^+ causes a slight shift to higher frequencies of the main maximum in the massive asymmetric mode probably related to some dealumination in the preparation process[22]. Also in FIR spectra no differences associated to the cation type present can be distinguished in both samples. In particular no bands are observed in the region below 450 cm^{-1}, where Na-oxygen stretching modes are expected and found e.g. in the case of

NaX zeolite.[22] This fact agrees with a random distribution of Na^+ cations in the structure.

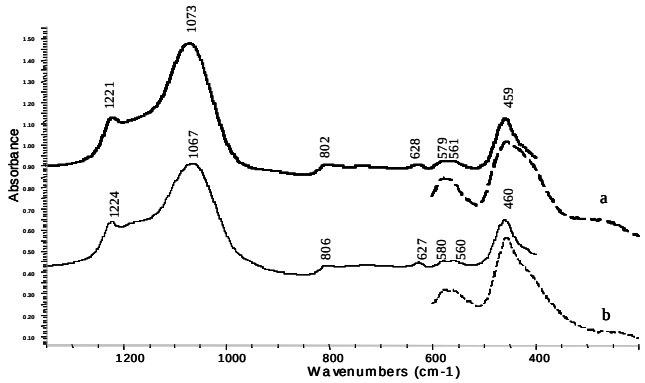

Figure 2. Skeletal MIR (continuous line) and FIR (discontinuous line) of HMOR (a) and NaMOR (b) samples.

5.1.3.2. Spectra of the surface hydroxy groups

The overall spectrum of activated Na-MOR sample (pure powder pressed disks) in the 4000-900 cm^{-1} range is compared to the spectrum of H-MOR sample in Figure 3. In the OH stretching region for HMOR sample, two bands can be observed: the first at 3744 cm^{-1} associated to the terminal silanol groups, and the second one (very strong and complex) with the main maximum at 3605 cm^{-1}, assigned to the bridging Si-OH-Al groups. According to Bevilacqua et al. such OH groups are exclusively located on the inner surface and possess a strong Brønsted acidity.[19,20] The asymmetry of this band indicates the presence of different components. At least three components were previously identified by Bevilacqua et al.[19,20] and later confirmed by Marie et al.[17] An additional weak component can be observed for HMOR sample at 3655 cm^{-1}, which can be

associated to small amounts of extraframework aluminum species formed during the activation by heating *in vacuo*. Meanwhile for Na-MOR, only one small peak at 3745 cm^{-1} was observed. The absence of the band centred at 3605 cm^{-1} indicates that all the possible cationic positions are occupied by Na^+ cations in the Na-MOR sample. In contrast, the band corresponding to terminal silanol groups has roughly the same intensity and position in both samples, suggesting that external silanols are not affected by cation exchange.

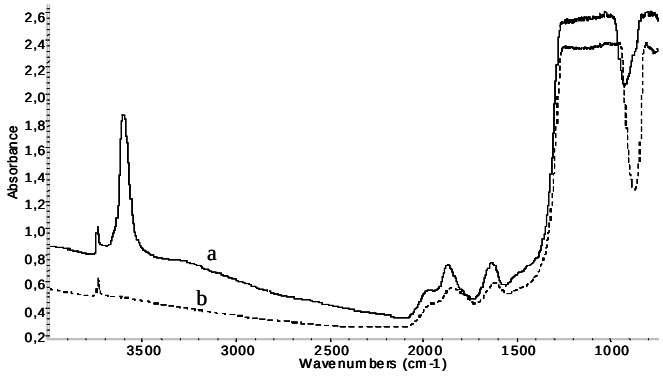

Figure 3. FT-IR spectra of activated HMOR (a) and NaMOR (b) samples at 773 K in vacuum conditions.

In the 2100-1500 cm^{-1} region, three typical skeletal overtones are found like on any silica-based material, while in the region between 1300 and 1000 cm^{-1} a cut-off is observed due to the Si-O-Si(Al) asymmetric stretching skeletal mode. In agreement with the shift observed for the main maximum near 1070 cm^{-1} in the skeletal spectrum (KBr disks), also in the pure powder pressed disks spectrum, both overtones and fundamental skeletal bands are slightly shifted to lower frequencies for NaMOR respect to HMOR.

5.1.3.3. Low temperature adsorption of CO on NaMOR and HMOR

Adsorption of CO at low temperature has been carried out on both zeolites (Figures 4, 5 and 6). Figure 4 shows the IR bands of adsorbed CO on NaMOR. At 133 K (real adsorption temperature as measured on the sample when liquid nitrogen is in the external cooling jacket) two main bands are observed on the CO stretching range: the first one, more intense, has the main maximum at 2164 cm^{-1} and a shoulder at 2175 cm^{-1} and the second one, less intense, located at 2138 cm^{-1}. By progressively increasing temperature upon outgassing, the higher frequency band together with its shoulder parallelly decrease their intensity. In the same way, the lower frequency band decreases on intensity, but much slower, when temperature increases. However, this band, which is initially weaker than the higher frequency band, has finally a similar intensity at 213 K and 233 K. In the OH vibration range (not shown here), the band at 3745 cm^{-1} is not perturbed indicating that terminal silanol groups do not interact with CO molecules in these conditions.

The band at 2164 cm^{-1} with its shoulder at 2175 cm^{-1} have been previously identified by other authors. Marie et al. have found them at 2163 and 2174 cm^{-1} for a NaMOR (Si/Al ratio 10).[17] Bordiga et al. reported the frequency of those bands at 2159 and 2177 cm^{-1} for a NaMOR (Si/Al of 5).[18] In both papers, taking into account the respective polarizing properties of cations depending on the location in the zeolitic structure, the component at lower frequency has been assigned to the C-bonded CO interacting with Na^+ cations located on the side pockets, while the component at higher frequency has been associated to the CO interacting with those located on the main channels.

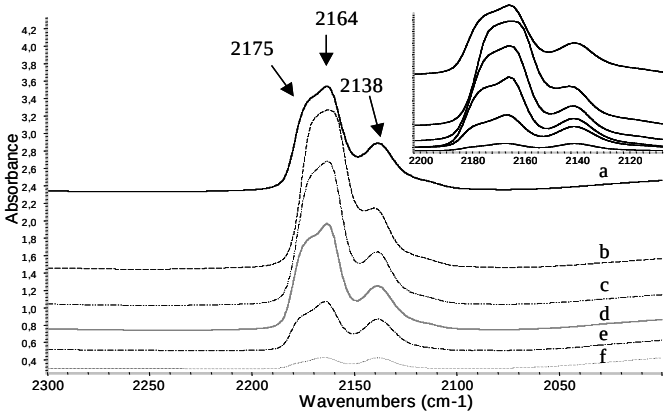

Figure 4. FT-IR spectra of NaMOR in the presence of CO gas at 133 K (a), and under evacuation at 143 K (b), 173 K (c), 193 K (d), 213 K (e), 233 K (f) on the CO stretching range.

The band at 2138 cm^{-1} (wavenumber value which is very near to that of liquid CO) can be attributed to pseudo-liquid physisorbed CO inside the zeolite pores with hindered rotation[15,17,18], which should desorb or evaporate quite fast. However, from our spectra, the intensity of this band decreases slower than that expected for pseudo-liquid physisorbed CO, even slower than those two higher frequency bands. Therefore, this disagrees with the assignment of this band to liquid-like CO only. In our opinion two superposed bands are present. The initial decrease of the band could be due to an evacuation of pseudo-liquid CO, which should be responsible for only part of this band, but the posterior so slow decrease on the intensity can evidence the existence of an additional stronger interaction-like involving Na^+ cations. This interaction cannot be apparently attributed to O-bonded CO species ($Na^+\cdots OC$) since this interaction has been reported to absorb at lower frequencies (between 2220 and 2212 cm^{-1}).[15,23] The possibility of the formation of CO species interacting with two Na^+ ions will be discussed below.

The adsorption of CO on HMOR gives rise, on the CO stretching range, again to two bands: one, the first formed and last disappeared during outgassing, centred at 2173 cm^{-1} with a tail towards lower frequencies, and the other one, again at 2138 cm^{-1} (Figure 5). In that case, contrarily to that observed for NaMOR, we are unable to single out two components for CO stretching band of C-bonded CO interacting with H^+ located on the main channels and side pockets. In that case, the band at 2138 cm^{-1} disappears progressively upon outgassing and can consequently be assigned, with confidence, to the pseudo-liquid CO. This further supports the idea that part of the band at 2138 cm^{-1} on NaMOR is something associated to interactions of CO molecules with Na^+ cations.

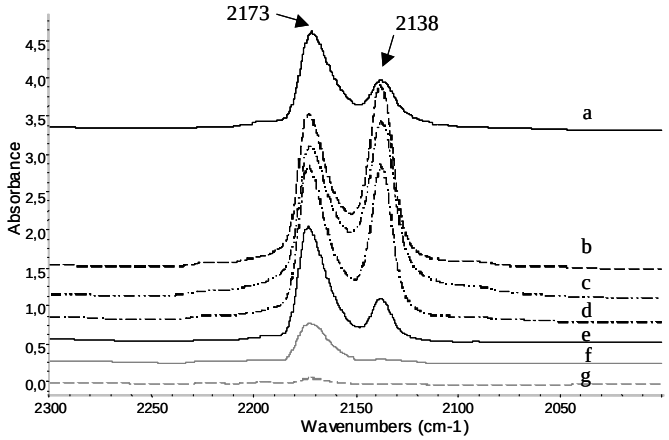

Figure 5. FT-IR spectra of HMOR in the presence of CO gas taken immediately at 133 K (a) and after 2 min (b), and under evacuation at 133 K (c), 143 K (d), 173 K (e), 193 (f) and 213K (g) on the CO stretching range.

Figure 6 shows the effects of the CO adsorption on HMOR in the OH vibration range. The band at 3745 cm^{-1} is not perturbed as for the NaMOR sample. Otherwise, just after contacting surface with CO (Figure 6a) only part

of the bridging OH band at 3605 cm^{-1} shifts to near 3300 cm^{-1}, and a residual band is still present at 3590 cm^{-1}. After more prolonged contact, this component at 3590 cm^{-1} disappears and the band of the OH, interacting with CO, seems to present an additional component at higher frequencies (around 3400 cm^{-1}). By evacuating, the situation seems to be exactly reversed, since, in first place, the component near 3590 cm^{-1} is restored, when the absorption near 3400 cm^{-1} disappears, while the band at 3605 cm^{-1} is restored later. Our conclusion is that CO adsorbs first on OHs in the main channels and later, more slowly, diffuses into the side pockets. The OHs located in the side pockets, responsible for the 3590 cm^{-1} band, are less perturbed than those in the main channels upon interaction with CO. This may be due to a higher acidity of OHs in the main channels or to some hindering of the interaction occurring in the side pockets in agreement with Hadjiivanov et al.[15] and Maache et al.[24]

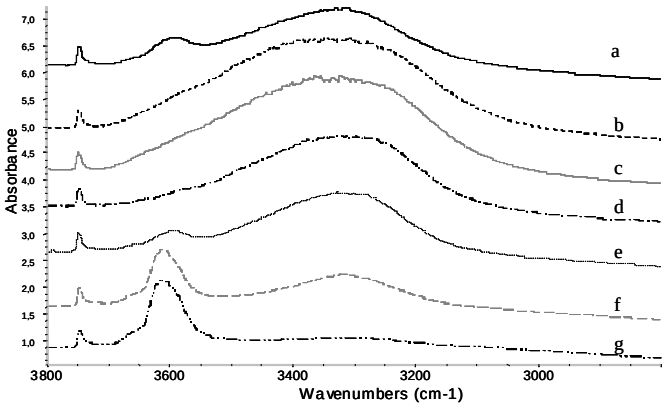

Figure 6. FT-IR spectra of HMOR in the presence of CO gas taken immediately at 133 K (a) and after 2 minutes (b), and under evacuation at 133 K (c), 143 K (d), 173 K (e), 193 (f) and 213K (g) on the OH vibration range.

5.1.3.4. IR study of the adsorption of acetonitrile and propionitrile

Acetonitrile (AN) adsorption has been used for characterizing the different hydroxy groups of H-zeolites including HMOR, since they can access to all protonic sites on HMOR.[19,25] The AN adsorption has also been investigated on NaY and NaX.[26, 27]

The spectra of AN adsorbed on NaMOR sample, and after outgassing at different temperatures are shown in Figure 7. The activated sample spectrum as well as the gas phase spectrum have been subtracted to all spectra. The same procedure has been applied to all adsorption experiments reported in this work. The nitrile spectrum on CCl_4 solution, used as a reference, is also shown.

From the substracted spectra obtained in contact with AN vapour and evacuated at room temperature (Figure 7b-7c) two bands at 2268 cm^{-1} and 2299 cm^{-1} can be observed on the CN stretching region. It is well known that the AN CN stretching mode gives place to two bands due to the Fermi Resonance between the fundamental stretching CN with a δCH_3 + $\nu C\text{-}C$ combination. Both bands are slightly asymmetric with a tail towards lower frequencies. By evacuating, the bands become narrower since the tail at lower frequencies seems to disappear. On the desorption process, by increasing temperature under vacuum, the intensity of these bands on the CN region decreases, and additionally, when outgassing at 373 K and 473 K (Figure 7d-7e) a new band at 2248 cm^{-1} is also observed, possibly with a further Fermi Resonance component near 2270 cm^{-1}. The position of the main CN Fermi Resonance bands (2268 and 2299 cm^{-1}) of adsorbed AN is, as usual, shifted to higher frequencies than those observed in CCl_4 diluted solution. In contrast, the doubled still present after outgassing at 473 K is observed at slightly lower frequencies than in CCl_4 solution.

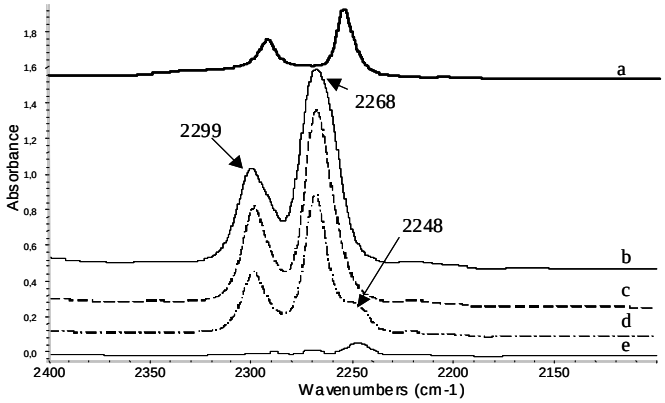

Figure 7. FT-IR spectra of AN in CCl_4 solution (a), NaMOR in the presence of AN vapors (b) and after evacuation at room temperature (c), 373 K (d) and 473 K(e).

The subtracted spectra of PrN adsorbed on NaMOR sample and after outgassing at different temperatures are shown in Figure 8. For propionitrile adsorption on NaMOR, one asymmetric band with a maximum at 2267 cm^{-1} can be observed on the CN stretching in the presence of PrN vapors. The tail observed towards lower frequencies starts to disappear upon evacuation at room temperature (Figure 8b-8c). By increasing temperature, the band intensity decreases and a new component at 2241 cm^{-1} appears at 373 K (Figure 8d-8e). Again the main band is at definitely higher frequency than that observed for the nitrile in CCl_4 solution whereas the band appeared after evacuation at 473 K is at lower frequencies.

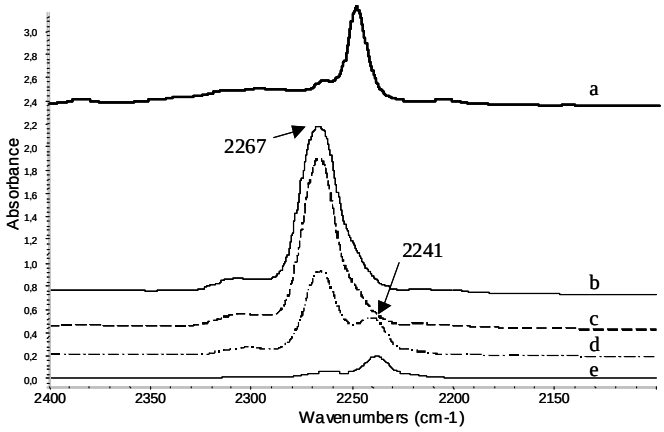

Figure 8. FT-IR spectra of PrN in CCl_4 solution (a), NaMOR in the presence of PrN vapors (b) and after evacuation at room temperature (c), 373 K (d) and 473 K (e).

The main bands at 2268 and 2299 cm^{-1} observed for AN adsorbed on NaMOR can be assigned to the same interaction of CN group with Na^+cations observed for AN adsorbed on NaY (2293 and 2263 cm^{-1})[26] and on NaX (2296 and 2267 cm^{-1})[27] and also for the $Na(CH_3CN)_3^+$ complex in solution (2302 and 2270 cm^{-1}).[27] Moreover, the lower frequency tails observed could be attributed to the CN group interaction with terminal silanol groups since on the OHs region (not shown here) it is clear that the terminal silanol groups are perturbed on contact with nitrile vapors, since the OHs band at 3745 cm^{-1} disappears, and a broad new band centered around 3450 cm^{-1} is observed. The easy recovery of the silanol band by outgassing at room temperature together with the CN stretching tails disappearance indicates the weakness of that interaction.

A parallel situation is found for PrN. The main band at 2267 cm^{-1}, shifted well above the band in CCl_4 solution, is assigned to the interaction with Na^+, while the tail at lower frequencies is assigned to the interaction with external silanols.

The nature of the species responsible for the bands at 2270 and 2248 cm^{-1} for AN and at 2241 cm^{-1} for PrN adsorption experiment, is not straightforward. To our knowledge, there is no case in the literature in which an interaction between nitriles and zeolitic sites gives rise to an IR absorption band at lower frequencies than the corresponding band observed for the liquid (Figures 7a and 8a).

Interestingly, this seems to parallel what happens with CO on NaMOR, which also gives rise to a quite strongly adsorbed species characterized by absorbing at slightly lower frequencies than that observed for free CO.

Trying to clarify this phenomenon we studied the adsorption of more hindered nitrile probe molecules.

5.1.3.5. IR study of the isobutironitrile and pivalonitrile adsorption

Isobutironitrile (IBN) and pivalonitrile (PN) have been previously used for the different hydroxy groups characterization on HMOR samples.[19,20] It has been shown that because of the higher steric hindrance of the nitrile alkilic group they do not access all the OH groups on HMOR, in particular IBN does not seem to access the side pockets and PN only interacts with OHs pointing to the centre of the main channels.

The subtracted adsorption/desorption spectra obtained for NaMOR sample using isobutironitrile (IBN) and pivalonitrile (PN) vapors as probe molecules are shown in Figures 9 and 10 respectively. The spectra of IBN on NaMOR after the adsorption and evacuation at increasing temperatures are shown in

Figure 9b-9e. In all cases at least two bands with the maximum at 2260 and 2245 cm^{-1} are observed. Intensity diminishes by increasing outgassing temperature, but interestingly, the band at lower frequencies does it slower. While the position of the band at higher frequencies keeps invariable, the band at lower frequencies furtherly shifts to lower frequencies (until 2235 cm^{-1}) when outgassing temperature increases. Another time, this component is at lower frequencies than that in CCl_4 solution, while the other component is at higher frequencies.

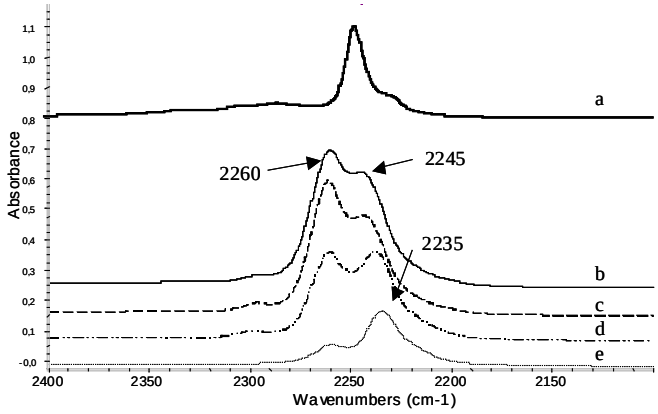

Figure 9. FT-IR spectra of IBN in CCl_4 solution (a), NaMOR in the presence of IBN vapor (b) and after evacuation at room temperature (c), 373 K (d) and 473 K (e).

Adsorption/desorption behaviour observed for PN on NaMOR is similar to that observed for IBN. The spectrum on the CN stretching region obtained at room temperature in the presence of PN vapors shows two bands with the maxima at 2253 cm^{-1} and 2233 cm^{-1} (Figure 10b). Again, when temperature increases the bands resolution improves and a decrease on the intensity is also observed. During the desorption process at increasing temperatures (Figure 10c and 10d), as it has been reported above for IBN, a shift is observed for the

lower frequency band, down to 2221 cm^{-1} at 373 K. Also in that case, that band at lower frequencies shows a higher resistance to the desorption process, since its intensity at 373 K is much more higher than that found for the previously used probe molecules.

In both cases, when NaMOR contacts with nitrile vapours, the band corresponding to the terminal silanol groups (at 3745 cm^{-1}) disappears and the previously commented band at 3450 cm^{-1} is formed. As it was previously commented, silanol-nitrile interaction is weak, since the corresponding OHs band is restored by evacuating at room temperature.

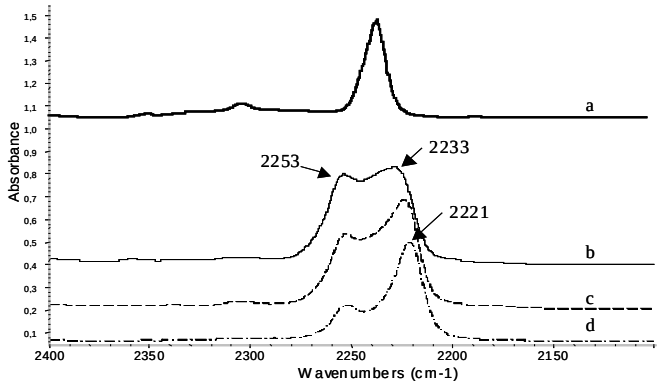

Figure 10. FT-IR spectra of PN in CCl_4 solution (a), NaMOR after evacuation at room (b), at 373 K (c) and 473 K (d).

Interestingly, the highest intensity ratio between the lower and the higher frequency bands was obtained for PN among all the nitriles tested so far. Therefore, in the case of PN, whose access to the channels is highly hindered, the CN stretching band shifted to lower frequencies than the liquid appears to be much stronger than in the case of nitriles with less restricted access to the channels like AN, PrN and IBN.

Due to the fact that the more hindered nitriles give rise to a stronger interaction, additional adsorption studies with other kind of hindered nitriles, as aromatic nitriles, have been performed.

5.1.3.6. IR study of the adsorption of benzonitrile and ortoluonitrile

Subtracted spectra of benzonitrile (BN) and orthotoluonitrile (oTN) adsorbed on NaMOR and after evacuation at increasing temperatures are shown in Figure 11 and in Figure 12, respectively. The spectra of the nitriles molecules on NaMOR show in the CN stretching region two peaks, whose main maxima are centred at 2254 cm $^{-1}$ and 2221 cm^{-1} for BN and at 2246 and 2216 cm^{-1} for oTN. In both cases, at room temperature, the intensity of the bands at higher frequency is higher than those at lower frequency, but during the desorption process, the intensity of the first ones decreases faster, until they have similar intensity.

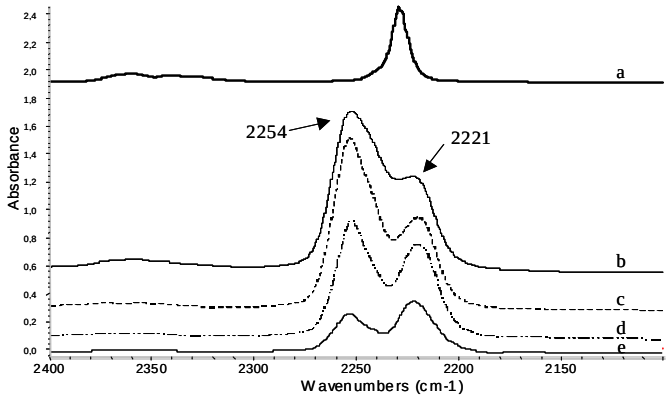

Figure 11. FT-IR spectra of liquid BN (a), NaMOR in the presence of BN vapor (b) and after evacuation at room temperature (c), 373 K (d) and 473 K (e).

Comparing those frequencies with that of the nitrile spectra in CCl_4 solution (Figure 11a for BN and Figure 12a for oTN), we observe again that one band is located at higher and the other band at lower frequencies. However, in these samples the intensity ratio between the lower and the higher frequency bands is lower than for PN and IBN, but higher than for AN and PrN. Thus, although the hindering influence has been corroborated, additional factors should be involved.

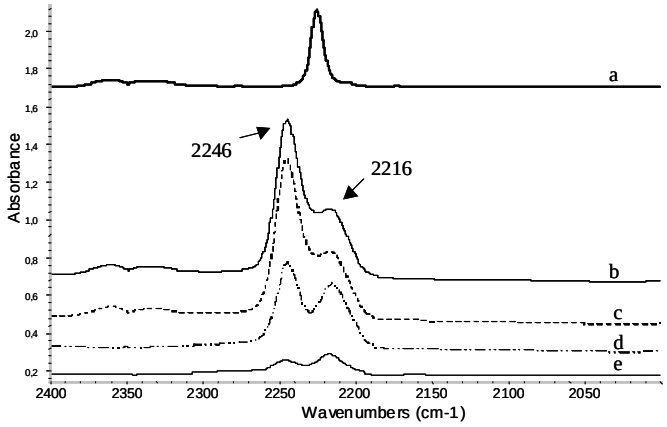

Figure 12. FT-IR spectra of liquid oTN (a), in the presence of oTN (b) and after evacaution at room (c) at 473 K (d) and 573 K (e).

Therefore, for all nitriles tested, a new band due to species more resistant to outgassing, whose CN stretching frequency is shifted to lower frequencies, is formed. This band is more intense for the more hindered nitriles (that do not access the cavities) than for smaller molecules. This indicates that the interaction takes place on the outer surface or on the mouth of the main channels. The interpretation that we can propose for these species is to

hypothesize a complex and probably multiple interaction of CN groups with Na^+ cations or Na^+ cations and framework oxygens.

Besides, the CN stretching band shifted download is more resistant to outgassing than the band shifted upwards for nitriles whose access even to the main channels is very highly hindered (PN, BN and oTN), whereas for the smaller molecules (AN, PrN and IBN) this band is relatively weaker. In order to explain the adsorption behaviour obtained for these nitriles, a comparative discussion is presented, for which aromatic nitriles have not been taken into account since the comparison becomes difficult due to their different nature. Table 2 shows the relation between peak areas obtained for aliphatic nitriles with respect to the acetonitrile one. Liquid phase nitrile spectra have been collected in diluted CCl_4 solution using quantitative conditions. Peak areas obtained for adsorbed nitriles spectra have been normalized to the disk weight. The data show that the absolute intensity of the CN stretching modes (in the case of AN both components of the Fermi Ressonance double have been considered) tends to increase in the order AN < PrN < IBN ≈ PN in CCl_4 solution (Table 2), while exactly the inverse tendency is found for nitriles adsorbed on NaMOR, where the amount of nitrile adsorbed follows the trend AN > PrN>> IBN > PN. This can be easily understood considering that AN and PrN have free access to the main channels and side pockets, while for IBN and PN the access to the side pockets is likely forbidden. Taking into account the dimensions of the main channels (6.7 Å x 7.0 Å) and the ionic radius of the Na^+ cations (0.95 Å), as well as, the critical diameter of the isopropil group (5 Å) and terbutil group (6 Å), i. e. alkil groups of IBN and PN respectively, it is easy to conclude that the access of PN to the main channels is likefully forbidden, but even that for IBN is probably highly hindered. Therefore, the spectrum observed for adsorbed AN is essentially the result of the sum of the spectra of AN in the side pockets, in the main channels and in the outer surface. In contrast, the spectra of adsorbed PN are only due to the interaction

occurring on the outer surface and on the channel mounths. The cases of PrN and IBN are somehow intermediate.

Table 2. Peak area relation for aliphatic nitriles respect to the AN one, in CCl_4 solution (L) and adsorbed on NaMOR (A).

	L (in solution)	A (adsorbed)	A/L
AN	1	1	1
PrN	1.14	0.90	0.79
IBN	1.65	0.45	0.27
PN	1.56	0.32	0.20

The adsorption of a hindered nitrile, PN, has been investigated also on a commercial Na-X zeolite and on a Silica-alumina highly impregnated with Na^+ cations for comparison,. The spectra of PN adsorbed on NaX zeolite are reported in Fig. 13a - 13c, where the CN stretching band of adsorbed PN is found, quite broad, after outgassing at room temperature at 2240 cm^{-1}. By outgassing at progressively higher temperatures, the intensity band decreases and the main maximum shifts to higher frequency up to 2250 cm^{-1}, showing some heterogeneity of the adsorption sites. The maximum rises to a similar position (but a little shifted downwards) that found for Na-MOR. However, also in this case upon outgassing at 473 K a component appears at lower frequency, namely at 2223 cm^{-1}, near the same position as observed for Na-MOR in the same conditions.

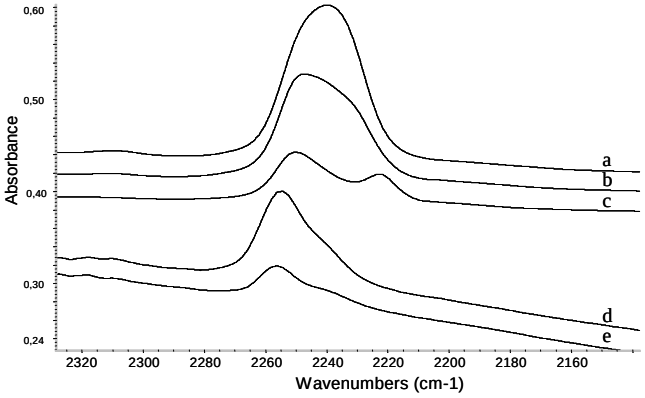

Figure 13. FT-IR of adsorbed PN on NaX evacuated at room temperature (a), at 373 K (b) and 473 K (c), and on NaSilicaAlumina evacuated at room temperature (d), and at 373 K (e).

In the case of PN adsorption on Na-Silica-alumina (Figure 13d–13e), the main band is again observed well shifted upwards, at even higher frequencies (2257 cm^{-1}), with a shoulder centered near 2238 cm^{-1}, but in this case, the lower frequency component does not appear. This supports the idea that the complex interaction responsible for the lower frequency band occurs at the mouths of the channels.

5.1.3.7. Coadsorption AN + CO

The co-adsorption of AN and CO has been performed as described on the experimental section. The obtained spectra are shown in Figure 14.

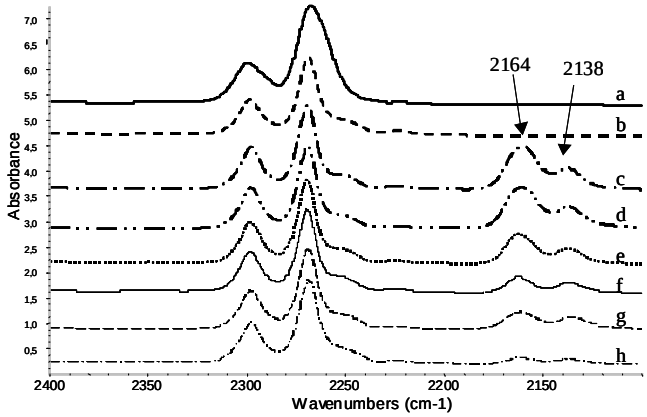

Figure 14. FT-IR of adsorbed AN on NaMOR at room temperature (a) evacuated at 373 K and cooled at 133 K (b) after CO adsorption at 133K (c), under evacuation at 143 K (d), 173 K (e), 193 K (f), 213 K (g), 233 K (h).

As we have previously described, the maxima of the bands of adsorbed AN on NaMOR slightly shift to higher frequencies upon outgassing at increasing temperatures. This shows the heterogeneity of the adsorption sites. After outgassing at 373 K the intensity of the band diminishes a factor of 0,3. This indicates that AN is desorbed from the weaker sites, while still interacts with the stronger ones, and by co-adsorbing CO in these conditions the spectra now show two bands at 2164 cm^{-1} and 2138 cm^{-1}. The shoulder at higher frequencies (2175 cm^{-1}), which is present when adsorbing only CO (Figure 4), is absent here. Therefore, CO is able to access the weakest sites, that have been freed by AN, while it cannot displace the AN adsorbed on the stronger sites. However, interestingly, the low frequency component at 2138 cm^{-1} is already formed just after contact with CO.

5.1.4. Conclusions

The data described and discussed above, may allow us to have deeper information on the NaMOR structure and its interaction with several adsorbates.

By comparing X-ray diffraction patterns and skeletal FIR spectra of NaMOR and HMOR, it is possible to conclude that Na^+ cations are randomly matched on the mordenite cavities.

Low temperature CO adsorption experiments show two different $Na^+ \cdots CO$ complexes characterized by different frequencies that are enhanced respect to the free molecule spectrum. These complexes can be assigned to single CO molecules interacting with single Na^+ cations in two different positions, main channels and side pockets. Parallel experiments performed on HMOR show quite clearly that CO first interacts with the Brönsted sites located on the main channels and later diffuses into those located in the side pockets. By outgassing, CO molecules first desorb from the sites located in the side pockets and later leave those of the main channels. This behaviour agrees with the stronger perturbation of the OHs located in the main channels showing in agreement with Maache et al. that the OHs in the main channels are likely more acidic, or in any case give a stronger interaction with CO, than those in the side pockets. Thus, in HMOR interaction with a so small molecule as CO, adsoption/desorption phenomena are mostly determined by adsorption strength more than by diffusion phenomena.

However, in the case of CO adsorption on NaMOR, a third, even stronger and perhaps activated, adsorption mode seems to occur. According to our results, the band observed at 2138 cm^{-1}, and previously assigned at liquid-like CO, contains an additional component that resists outgassing at 233 K. This quite stable species should be assigned to CO molecules involved in a multiple

perturbation that causes a slight decrease on the CO stretching frequency. Being these species not observed on HMOR, it seems likely that this interaction involves Na^+ cations.

Adsorption of nitriles characterized by differently hindered hydrocarbon entities, show in all cases the formation of complexes with Na^+ cations. The adsorption of AN shows a clear heterogeneity of the adsorption sites and shows that, as expected, the species characterized by the stronger perturbation are more resistant when outgassing. Also, in this case, consequently, adsorption/desorption phenomena seem to be mostly determined by adsorption strength more than by diffusion phenomena. In the case of PN, which was previously found to access, very slowly, only to the main channels of HMOR, the access to the cavities of NaMOR is like fully forbidden. Thus is also very likely the case of BN and oTN. However, although such big hydrocarbon entities cannot enter the cavities, the CN can do this by interacting with the Na^+ cations located either at the external surface or near the mouth of the channels.

For all nitriles, additionally to that band with a CN stretching frequency located at higher frequencies than the liquid value (CN shift 15-20 cm^{-1}), a new band is formed at frequencies near or slightly below than the liquid value, whose stability seems to be higher than the usual ones. The behaviour observed for all nitriles, at 300-500 K seems to parallel that observed for CO at 150-250 K. A new band associated to more resistant species is observed, with a CN stretching frequency shifted lower than the liquid value. The interpretation that we propose for these species is to hypothesize multiple interactions where CN groups interact with Na^+ cations or Na^+ cations and framework oxygen atoms (Scheme 1 for possible structures). The fact that this interaction is more important for highly hindered molecules together with that it does not appear

on Na-Silica-alumina, where zeolitic pores do not exist, suggests that the interaction takes place on the mouth of the main channels.

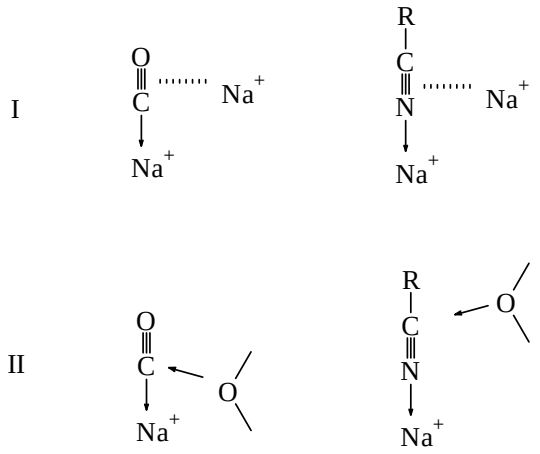

Scheme 1. Tentative structures for the strongest interactions of CO and nitriles on NaMOR. I: interactions with two Na^+ ions. II: Interaction with Na^+ and $O^=$ ions.

5.1.5. References

[1] Guisnet, M.; Gilson, J.P., eds., *Zeolites for cleaner technologies*, Imperial College Press: London, Catalytic Science Series, Vol 3, 2002, p. 209.

[2] van Bokhoven, J.A.; Tromp, M.; Koningsberger, D.C.; Miller, J.T.; Pieterse, J.A.Z.; Lercher, J.A.; Williams, B.A.; Kung, H.H. *J. Catal.* **2001**, 202, 129.

[3] Moreau, F.; Ayrault, P.; Gnep, N. S.; Lacombe, S.; Merlen, E.; Guisnet, M. *Micropor. Mesopor. Mat.* **2002**, 51, 211.

[4] Weitkamp, J.; Hunger, M.; Rymsa, U. *Micropor. Mesopor. Mat.* **2001**, 48, 255.

[5] Davis, R. J. *J. Catal.* **2003**, 216, 396.

[6] Martra, G.; Ocule, R.; Marchese, L.; Centi, G.; Coluccia, S. *Catal. Today* **2002**, 73, 83.

[7] Armaroli, T.; Finocchio, E.; Busca, G.; Rossini, S. *Vib. Spectrosc.* **1999**, 20, 85.

[8] Pamba, M.; Maurin, G.; Devautour, S.; Vandershueren, J.; Giuntini, J. C.; Di Renzo, F.; Hamidi, F. *Phys. Chem. Chem. Phys.* **2000**, 113, 4498.

[9] Devautour, S.; Abdoulaye, A.; Giuntini, J.C.; Henn, F. *J. Phys. Chem. B* **2001**, 105, 9297.

[10] Bell, R. G.; Devautour, S.; Henn, F.; Giuntini, J. C. *J. Phys. Chem. B* **2004**, 108, 3739.

[11] Webster, C. E.; Cottone, A.; Drago, R.S.; *J. Am. Chem. Soc.* **1999**, 121, 12127.

[12] Yuvaray, S.; Chang, T. H.; Yeh, C. T. *J. Phys. Chem. B* **2003**, 107, 4971.

[13] Salla, I.; Salagre, P.; Cesteros, Y.; Medina, F.; Sueiras, J. E. *J. Phys. Chem. B* **2004**, 108, 5359.

[14] Knözinger, H.; Huber, S. J. Chem. Soc., *Faraday Trans.* **1998**, 94 (15), 2047.

[15] Hadjiivanov, K. I.; Vayssilov, G. N. Characterization of oxide surfaces and zeolites by Carbon Monoxide as an IR Probe Molecule in *Advances in Catalysis*, Academic Press, 2002, Vol 47, p 307.

[16] Onida, B.; Monelli, B.; Borello, L.; Fiorilli, S.; Geobaldo, F.; Garrone, E. *J. Phys. Chem. B* **2002**, 106, 10518.

[17] Marie, O.; Massiani, P.; Thibault-Starzyk, F. *J. Phys. Chem. B* **2004**, 108, 5073.

[(18)] Bordiga, S.; Lamberti, C.; Geobaldo, F., Zecchina, A.; Turnes Palomino, G; Otero Areán, C. *Langmuir* **1995**, 11, 527.

[19] Bevilacqua M.; Gutiérrez-Alejandre A.; Resini C.; Casagrande M.; Ramírez J.; Busca G. *Phys. Chem. Chem. Phys.* **2002**, 4, 4575.

[20] Bevilacqua, M.; Busca, G. *Catal. Commun.* **2002**, 3, 497.

[21] Montanari, T.; Bevilacqua, M.; Resini, C.; Busca, G. *J. Phys. Chem. B* **2004**, 108, 2120.

[22] Busca G.; Resini, C. Vibrational spectroscopy for the analysis of geological and inorganic materials, in *Enciclopedia of Analytical Chemistry*, R.A. Meyers eds., Wiley, Chichester, 2000, p. 10984.

[23] Tsyganenko, A. A.; Escalona Platero, E.; Otero Areán, C.; Garrone, E.; Zecchina, A.; *Catal. Letters* **1999**, 61, 187.

[24] Maache, M.; Janin, A.; Lavalley, J. C.; Benazzi, E. *Zeolites* **1995**, 15, 507.

[25] Zecchina, A.; Geobaldo, F.; Spoto, G.; Bordiga, S.; Ricchiardi, G.;Buzzoni, R.; Petrini, G. *J. Phys. Chem.* **1996**, 100, 16584.

[26] Angell, C. L.; Howell, M. V. *J. Phys.Chem.* **1969**, 73, 2551.

[27] Armaroli, T.; Finocchio, E.; Busca, G. Rossini, S. *Vib. Spectrosc.* **1999**, 20, 85-94.

[28] Reedijk, J.; Zuur, A.P.; Groeneveld, W.L. *Recueil* **1967**, 86, 1127.

5.2. A reexamination of the adsorption of CO and nitriles on alkali-metal-mordenites: characterization of multiple interactions*

Abstract

Low temperature CO adsorption and room temperature propionitrile and ortho-toluonitrile adsorption on LiMOR, NaMOR, KMOR and CsMOR zeolites have been investigated by FT-IR spectroscopy. Two different CO species, probably located in the main channels coordinated to Na^+ at IV and VI sites, have been observed. These are associated to a shift of the CO stretching to higher frequencies, as usual. However, together, more strongly bonded species associated to a slight shift of the CO stretching to lower frequency are also observed. Similar species, with the CN stretching shifted upwards (weaker adsorption) and with the CN stretching shifted downwards (stronger adsorption) are also observed in the case of the interaction of propionitrile and ortho-toluonitrile. The data show that the species characterized by a stronger adsorption but a lower stretching frequency may form both in the main channels and at the external surface. Their formation is easier with the larger cations. These species are identified as "multiply bonded" species. The evidence for this new interaction, stronger than the usual one site–one molecule species, may change considerably the view of the adsorption chemistry of cationic zeolites, from localized simple sites to cooperative complex interactions.

* Physical Chemistry Chemical Physics **2005**, 7 (12), 2526-2533.

5.2.1. Introduction

Light alkali metal exchanged zeolites (like e.g. Na-A, Li-MOR, Na-X and Na-Y) act as selective regenerable adsorbants for purification of gaseous streams[1] or for the separation of industrial products (e.g. the xylenes separation[2] and the oxygen-nitrogen air separation[3] on alkali-metal X or Y) and as quite mild basic catalysts as well.[4,5] Whereas, heavy- alkali metal zeolites (like Cs-Y) are reported to be strong bases.

Mordenite is a medium pore zeolite, which finds, in its protonic (HMOR) or partially Na-exchanged (NaHMOR) forms, application in the industry for several hydrocarbon conversions.[6-8] Alkali-metal exchanged MOR have been the object of investigations in particular for their ability to adsorb nitrogen and for the possibility to substitute Na-FAU adsorbants used for the industrial separation of air's N_2 from O_2 in pressure swing adsorption processes.[9-11]

The orthorombic mordenite structure[12] is characterized by nearly straight "main" channels running along the [001] crystallographic direction, which are accessible through twelve-membered (elliptical) silicon-oxygen rings having 6.5 Å x 7.0 Å diameters. Additionally, 8-ring "side pockets" exist in the [010] direction having 3.4 Å x 4.8 Å diameter, which however do not allow flow of molecules being in fact interrupted by narrow-necked obstructions. The side pockets connect the twelve ring main channel to a distorted eight-ring channel also running parallel to the [001] direction, but having an elliptical compressed opening 5.7 Å x 2.6 Å wide. The localization of Na^+ in Na-MOR samples has been the object of several studies.[12-16] Assuming the idealized composition for dehydrated MOR $Na_8Si_{40}Al_8O_{96}$ (Si/Al = 5) it seems quite established that half of Na^+ ions are located just in the middle of the small compressed channels in the site called (I) or A. These Na ions do not move upon water adsorption and cannot bind adsorbed water. Location (I) or A is also fully occupied for MOR

samples with Si/Al = 11. It is usually supposed that only monoatomic species can enter the compressed channels of NaMOR and interact with cations in sites A. The other half Na^+ ions are distributed between site IV, also called D, near the opening of the side pocket in the main channel, and in position VI, also called E, which is well exposed in the main channel. The theoretical occupation degree of each site is 4,3,1 for A, D, E.[14]

The low temperature adsorption of CO is today perhaps the most popular technique for characterizing adsorption sites of zeolites in IR spectroscopy.[17-20] This technique has been applied to investigate the properties of alkali metal mordenite, showing the formation of two kinds of alkali ion carbonyl species associated to different cation locations either in the main channels or in the side pockets.[21-23] The polarizing effect of the cation was found to constitute the main factor influencing the CO stretching frequency although the polarity of the zeolite framework has also an effect.

In a more recent IR study on Na-MOR, the adsorption of different hindered nitriles together with CO were used for zeolitic sites characterization. Evidence has been provided for the formation of more complex interactions, where the adsorbate molecule interacts with more than one site, has been reported by us.[24] The formation of such species has later been shown also for nitriles adsorbed on NaX and NaY faujasites.[25]

To have more information on such new species and on the localization of the different adsorption sites, we re-investigated the alkali-metal zeolite systems by using both nitriles and CO as adsorption probes.

5.2.2. Experimental

Na-MOR (Si/Al = 6.5, CBV 10A Lot No. 1822-50) was supplied by Zeolyst as hydrated powder. The chemical composition was SiO_2/Al_2O_3 mole ratio 13 and a Na_2O weight % of 6.6. H-MOR was prepared by cation exchanging the starting form, Na-MOR, with a NH_4Cl 2.2 M solution and later calcining at 673 K. LiMOR, KMOR and CsMOR samples were obtained by cation exchanging three times the NaMOR zeolite with the corresponding cloride salt 2.2 M.

Powder X-ray diffraction patterns of the samples were obtained with a Siemens D5000 diffractometer (Bragg-Brentano parafocusing geometry and vertical θ-θ goniometer) fitted with a curved graphite diffracted-beam monochromator, incident and diffracted-beam Soller slits, a 0.006º receiving slit and scintillation counter as a detector. The angular 2θ diffraction range was between 5º to 70º. The data were collected with an angular step of 0.05º at 3s per step and sample rotation. CuKα (1.542 Å) radiation was obtained from a copper X-ray tub operated at 40kV and 30mA. The cell parameters and cell volume values were calculated using a matching profile with TOPAS 2.0 software (Bruker AXS).

Skeletal MIR (KBr pressed disks) and FIR (pure powder on polyethylene supports) spectra were recorded on a Nicolet Magna 750 Fourier Transform instrument (resolution 4 cm^{-1}). Additionally, both samples were characterized (on MIR range) by adsorbing several probe molecules. Different nitriles like propionitrile (PrN) and o-toluonitrile (o-TN) were used to characterize mordenite samples, and furthermore CO at low temperature was also used. The pressed disks of pure zeolite powders were activated "in situ" the IR cell by outgassing at 773 K before the adsorption experiments. A conventional gas manipulation/outgassing ramp connected to the IR cell was used. The adsorption/desorption process has been studied by transmission FT-IR. For nitriles, the adsorption procedure involves contact of the activated sample disk

with vapors at room temperature at a pressure not higher than 2.5 kPa. The desorption process at increasing temperatures was performed in vacuum at temperatures in the range between 273K and 573K. On the other hand, CO adsorption was performed a 130 K by the introduction of a well-known dose of the gas inside the low temperature infrared cell containing the previously activated wafers. IR spectra were collected evacuating at increasing temperatures between 130 and 273 K.

5.2.3. Results.

5.2.3.1. Skeletal MIR and FIR spectra

Figure 1 shows the X-ray Diffraction patterns obtained for the alkali- cation MOR samples. They agree to their respective Mordenite JCPDS files. The samples present similar cristallinity, and no significant differences on the peak width are appreciable from X-ray patterns. Only in the case of CsMOR, the peaks intensities are a bit different, in agreement with the data reported in the corresponding JCPDS file (01-083-1627 for CsMOR). No structural changes can be observed in all cases from the corresponding JCPDS file fit. Thus, these intensity changes are likely due to the effect of electronic parameters of Cs that are quite different from those of other cations. The calculated cell parameters and cell volume for all samples are also reported in Table 1. The variation of cell volume values observed could be related to the real hydrated cation size. The absence of hkl peaks associated to a cation match on structure, suggests that cations may be randomly distributed on our samples.

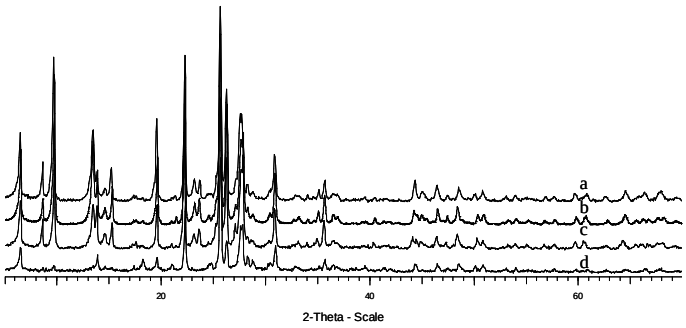

Figure 1. X-ray Diffraction patterns of LiMOR (a), NaMOR (b), KMOR (c) and CsMOR (d) samples.

Table 1. Cell parameters of HMOR and alkali-MOR samples calculated by XRD.

	a (Å)	b (Å)	c (Å)	cell vol. (Å^3)
HMOR	18.0979(41)	20.4470(31)	7.5109(10)	2779
LiMOR	18.1985(30)	20.4095(25)	7.4907(8)	2782
NaMOR	18.1063(16)	20.4533(13)	7.5143(4)	2783
KMOR	18.1142(37)	20.5163(28)	7.5159(8)	2793
CsMOR	18.2036(40)	20.4157(41)	7.4955(13)	2786

In Figure 2, the skeletal MIR/FIR spectra (KBr and polyethylene pressed disks, respectively) for HMOR and alkali metal MOR samples are reported. The spectra compare well with those reported in the literature[26]. Slight shifts (few cm^{-1}) of the main maxima are found, showing a slight effect of the hydrated cations on the vibrations of the framework.

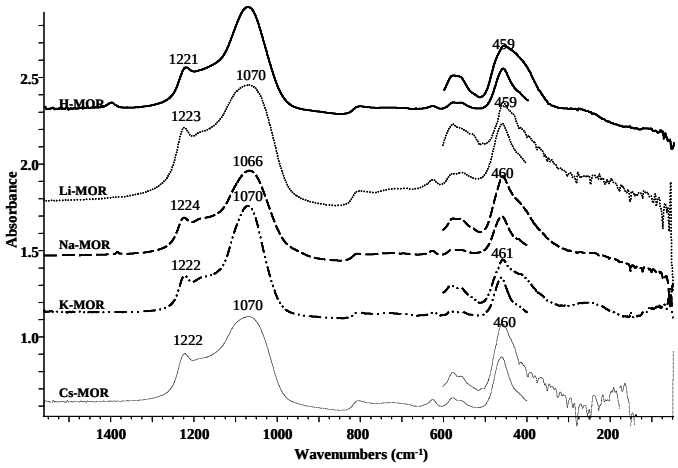

Figure 2. Skeletal MIR (1500-400 cm^{-1}) and FIR (600-50 cm^{-1}) of HMOR, LiMOR, NaMOR, KMOR and CsMOR.

The spectra of pressed disks of the pure MOR powders after activation in vacuum show in the region 2100-1600 cm^{-1} broad absorptions due to harmonics of the fundamental skeletal modes, as usually observed. These features are relevantly shifted down the more the heavier the cations, more than expected by looking at the corresponding fundamentals. The two main maxima are observed at 1636, 1862 cm^{-1} for LiMOR, 1626, 1860 cm^{-1} for NaMOR, at 1620, 1839 cm^{-1} for KMOR and at 1614, 1838 cm^{-1} for CsMOR. This suggests a stronger effect of the naked extraframework ions with respect to the hydrated ones on the mechanics of the framework.

5.2.3.2. Spectra of the surface hydroxy groups

The overall spectrum of activated alkali metal -MOR samples (pure powder pressed disks) in the 4000-3200 cm^{-1} range are compared to the spectrum of HMOR sample in Figure 3. In the OH stretching region for HMOR sample, two bands can be observed: the first at 3744 cm^{-1} associated to the terminal

silanol groups, and the second one (very strong and complex) with the main maximum at 3605 cm^{-1}, assigned to the bridging Si-OH-Al groups. According to Bevilacqua et al. such OH groups are exclusively located on the inner surface and possess a strong Brønsted acidity.[27,28] The asymmetry of this band indicates the presence of different components. At least three components were previously identified by Bevilacqua et al.[26,27] and later confirmed by Marie et al.[23] An additional weak component can be observed for HMOR sample at 3655 cm^{-1}, which can be associated to small amounts of extraframework aluminum species formed during the activation by heating in vacuo.

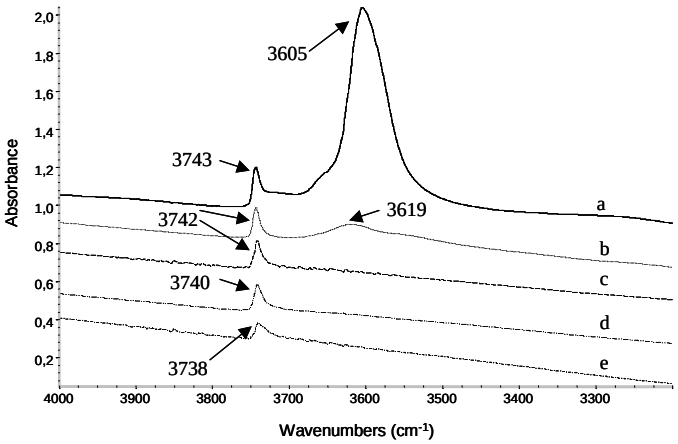

Figure 3. FT-IR spectra on the OHs region of HMOR (a), LiMOR (b), NaMOR (c), KMOR (d) and CsMOR (e) samples activated at 773 K in vacuum conditions.

In the case of Na-, K- and CsMOR the absence of the band centered at 3605 cm^{-1} indicates that all the possible internal positions are occupied by alkali cations. Only in the case of Li-MOR some absorption is present near 3610 cm^{-1}, as observed for a similar sample also by Geobaldo et al.,[29] who assigned this band to unexchanged proton sites. Thus, in our case these protonic sites could have been generated during NaMOR exchange with LiCl solution.

In all cases, a sharp band is present above 3700 cm^{-1}, suggesting that external silanols are present and not exchanged. In the case of LiMOR and NaMOR this band is just at 3744-5 cm^{-1}, so really unshifted with respect to H-MOR and all typical "unperturbed" silanol groups. However, in the case of KMOR and CsMOR this band is found at a lower frequency, down to 3738 cm^{-1}. This effect, not reported previously,[29] may be related to the overall effect of the exchanging cations on the mechanics of the framework, as shown above for skeletal vibrations, or to effect of some alkali cations outside the channels on the external surface where terminal silanols are located.

5.2.3.3. Low temperature adsorption of CO on Li-, Na-, K- and Cs-MOR

Figure 4 shows the IR bands of adsorbed CO on LiMOR under evacuation at low temperature. At 133 K, a single sharp band is observed in the CO stretching range, whith two weaker components at lower frequency. The first one, intense, quite narrow and asymmetric, with a tail towards lower frequencies shows the main maximum at 2185 cm^{-1}, the second band is centered at 2161 cm^{-1}, and the last band has a maximum centered at 2138 cm^{-1}. By progressively increasing temperature upon outgassing, the higher frequency band progressively decreases its intensity. In the same way, the bands at 2161 cm^{-1} and 2138 cm^{-1} also decrease in intensity, but they do it much faster up to their complete disappearance during evacuation at 193 K.

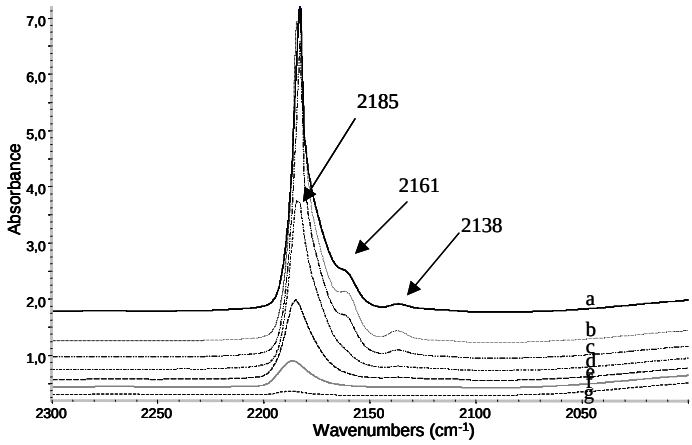

Figure 4. FT-IR spectra of LiMOR in the presence of CO under evacuation at 133 K (a), at 143 K (b), 173 K (c), 193 K (d), 203 K (e), 233 K (f) and 263 K on the CO stretching range.

In the case of CO adsorbed on NaMOR (Figure 5) two main bands were observed on the CO stretching range with the main maximum at 2164 cm^{-1} and a shoulder at 2175 cm^{-1} and the second band, less intense, located at 2138 cm^{-1}. By progressively increasing temperature upon outgassing, the higher frequency band together with its shoulder parallelly decrease their intensity. In the same way, the lower frequency band decreases in intensity, but much slower, when temperature increases. This band, which is initially weaker than the higher frequency band, has finally a similar intensity at 213 K and 233 K.

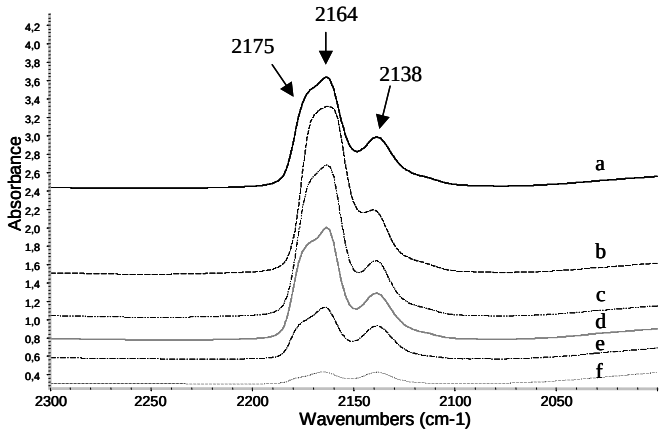

Figure 5. FT-IR spectra of NaMOR in the presence of CO gas at 133 K (a), and under evacuation at 143 K (b), 173 K (c), 193 K (d), 213 K (e), 233 K (f) on the CO stretching range.

The IR bands of adsorbed CO on KMOR under evacuation are shown in Figure 6. At 133 K at least four components are observed on the CO stretching, with the main maximum at 2161 cm^{-1} and shoulders of decresing intensities at 2150 cm^{-1}, 2134 cm^{-1} and 2117 cm^{-1}. By progressively increasing temperature upon outgassing, the two components at higher frequencies toghether with the band at 2117 cm^{-1} parallelly decrease their intensity. Otherwise the band at 2134 cm^{-1}, which also decreases its intensity under evacuation at increasing temperatures, does it much slower up to the point that at 223 K this band has higher intensity than the two bands at higher frequencies.

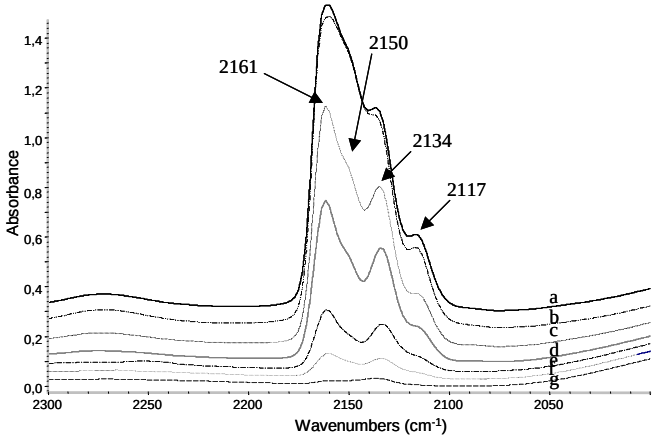

Figure 6. FT-IR spectra of KMOR in the presence of CO under evacuation at 133 K (a), at 153 K (b), 173 K (c), 183 K (d), 193 K (e), 203 K (f) and 223 K (g) on the CO stretching range.

Finally, for CsMOR, the IR bands of adsorbed CO under evacuation at different temperatures are shown in Figure 7. In all spectra three bands are observed on the CO stretching range at 2155 cm^{-1}, 2143 cm^{-1} and 2120 cm^{-1}. The band at 2143 cm^{-1} is the strongest in all spectra.

In the OH vibration range (not shown here), in all cases, the silanol band at around 3738-45 cm^{-1} is not perturbed when mordenite samples are contacted with CO molecules, indicating that terminal silanol groups do not interact significantly with CO molecules in these conditions.

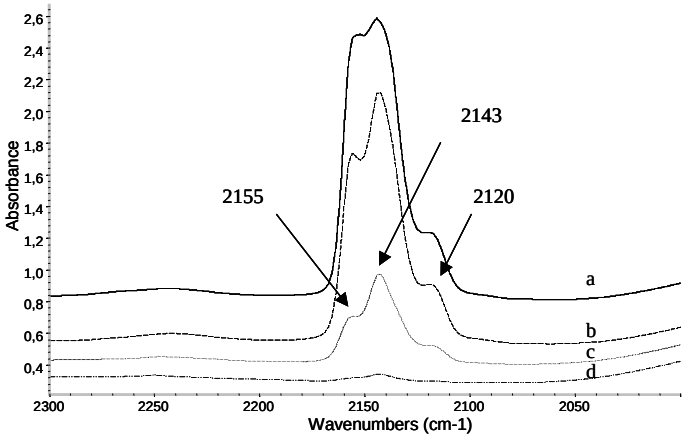

Figure 7. FT-IR spectra of CsMOR in the presence of CO under evacuation at 133 K (a), at 143 K (b), 153 K (c), 163 K (d), 173 K (e), 183 K (f) and 193 K (g) on the CO stretching range.

In all cases except LiMOR, a band at frequency lower or near that of "unperturbed" CO is observed, but is more resistant to outgassing than the higher frequency band. This behavior was examined by us previously in the case of NaMOR and this analysis, also supported by parallel experiments performed by using nitriles as adsorption probes, allowed us to reassign this band, previously attributed to liquid like CO,[22,23] to multiply bonded CO.[24] Only a multiple adsorption in fact can explain a stronger interaction with a lower CO stretching frequency. This assignment seems to be confirmed here. The bands observed at 2138 cm^{-1} on NaMOR, at 2134 cm^{-1} on KMOR and at 2143 cm^{-1} on CsMOR show this behavior and may consequently be assigned to "multiply bonded" species in all cases. However, in the case of LiMOR a similar species is not observed, since the band at 2138 cm^{-1} is atributed to physisorbed pseudo-liquid CO, because of its fast intensity decrease with increasing temperature.

In all spectra a weak band is also observed near 2120-2115 cm^{-1}, for which a likely assignment is to O-bonded carbonyl species, as discussed elsewhere previously.[29,30]

5.2.3.4. IR study of the adsorption of propionitrile on Li-, Na-, K- and Cs- MOR

Propionitrile (PrN) adsorption has been previously used to characterize the different cationic positions on H-MOR and Na-MOR, since it can access to all sites located in the main channels and side pockets.[24,26,27] As for the other nitrile molecules, the interaction of the N lone pair with electronwithdrawing centers causes a strengthening of the CN triple bond and a consequent shift upwards of the CN stretching frequency (2249 cm^{-1} in the liquid[32]). This has been shown e.g. as in the case of nitrile metal complexes where metal cations act as Lewis acid sites,[33] as well as on Co-containing zeolites including Co-MOR[34] and in the case of the H-bonding complex with phenol[35] and meta-cresol[36] or on the acidic OHs of protonic zeolites.[34]

The spectra of PrN adsorbed on the different mordenite samples, and after outgassing at different temperatures are shown in Figures 8 to 11. The activated sample spectrum as well as the gas phase spectrum have been subtracted to all spectra. The same procedure has been applied to all adsorption experiments reported in this work. The nitrile spectrum on CCl_4 solution, used as a reference, is also shown.

The subtracted spectra of PrN on LiMOR sample after outgassing at different temperatures are shown in Figure 8. At low temperatures (Figure 8b-c) we can observe a single but asymmetric CN stretching band shifted well above the position observed for the liquid (Figure 8a), whose maximum shifts from 2274 to 2278 cm^{-1} by increasing outgassing temperature. However in the spectrum

collected after evacuation at 573 K (Figure 8e) a low intensity band appears at almost the same frequency than that of the liquid propionitrile (2249 cm^{-1}).

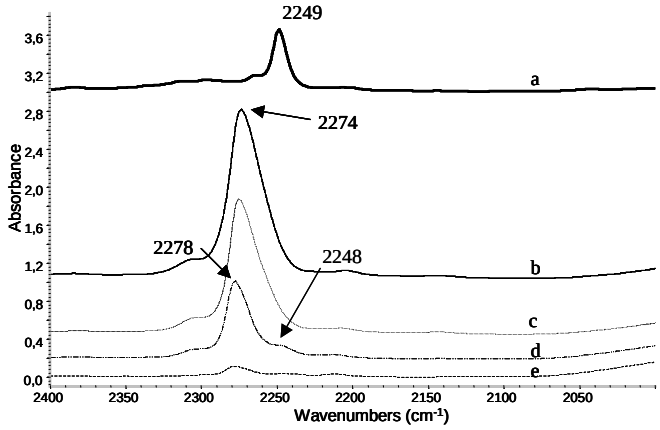

Figure 8. FT-IR spectra of liquid PrN (a), LiMOR in the presence of PrN after evacaution at room temperature (b) at 373 K (c), 473 K (d) and 573 K (e).

In the case of PrN adsorbed on NaMOR and after outgassing at different temperatures (Figure 9) an asymmetric band with a maximum at 2267 cm^{-1} can be observed on the CN stretching region. The tail observed towards lower frequencies starts to disappear upon evacuation at room temperature (Figure 9b-9c). By increasing the temperature, the band intensity decreases and a new component at 2241 cm^{-1} appears at 373 K. In that case this band is shifted well below the band of the liquid nitrile.

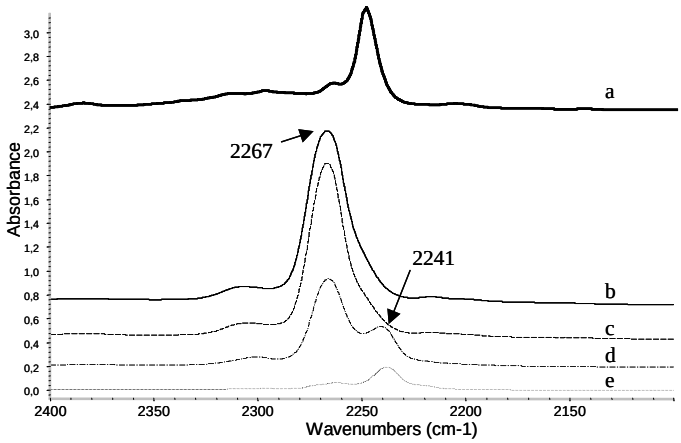

Figure 9. FT-IR spectra of PrN in CCl_4 solution (a), NaMOR in the presence of PrN vapors (b) and after evacuation at room temperature (c), 373 K (d) and 473 K (e).

The spectra of PrN adsorbed on KMOR are shown in Figure 10. In that case, the main band of adsorbed nitrile is centered at slightly lower frequency than that of the liquid nitrile. The position of this band is exactly at 2245 cm^{-1} but a well resolved shoulder is evident at higher frequencies (around 2258 cm^{-1}). In the spectrum collected after the evacuation at 473 K, the maximum of this band is shifted to lower frequencies down to 2241 cm^{-1}, while the shoulder is still much weaker.

Also in the case of propionitrile adsorption on CsMOR (Figure 11), one band at slightly lower frequencies than the liquid nitrile is observed (2246 cm^{-1}), which shifts to lower frequencies (down to 2242 cm^{-1}) during evacuation at increasing temperatures.

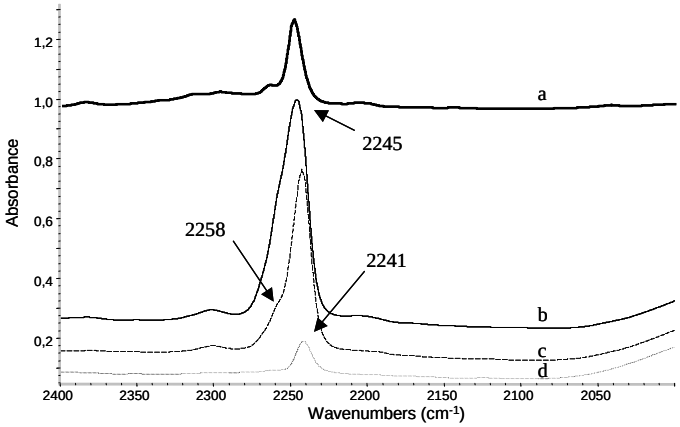

Figure 10. FT-IR spectra of liquid PrN (a), KMOR in the presence of PrN after evacaution at room temperature (b) at 373 K (c) and 473 K (d).

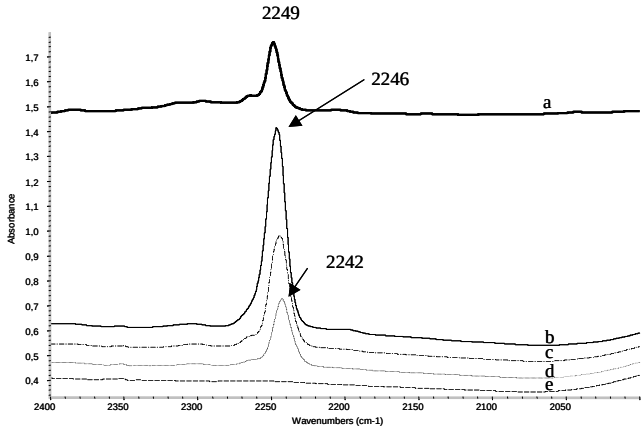

Figure 11. FT-IR spectra of liquid PrN (a), CsMOR in the presence of PrN after evacuation at room temperature (b) at 373 K (c), 473 K (d) and 573 K (e).

The formation of PrN adsorbed species characterized by a shift upwards of the CN stretching, as usual for molecules interacting with Lewis sites, is evident at least in the case of LiMOR (2274-2278 cm^{-1}), NaMOR (2267 cm^{-1}) and KMOR (2258 cm^{-1}). As expected and in parallel with what has been shown for adsorbed CO, the position of this band shifts upwards the more the smaller the cation size, confirming that these features are associated to N-bonded species on cationic sites. In all cases, however, a strongly adsorbed species characterized by the CN stretching at quite low frequency (2250-2240 cm^{-1}) is observed. This species has been previously identified by us, on NaMOR, as a "multiply bonded" species. The two bands are not resolved in the case of CsMOR at 2246 cm^{-1}.

In all cases, a sharp band is present above 3700 cm^{-1}, suggesting that external silanols are present and not exchanged. In the case of LiMOR and NaMOR this band is just at 3744-5 cm^{-1}, so really unshifted with respect to H-MOR and all typical "unperturbed" silanol groups. However, in the case of KMOR and CsMOR this band is found at a lower frequency, down to 3738 cm^{-1}. This effect, not reported previously,[29] may be related to the overall effect of the exchanging cations on the mechanics of the framework, as shown above for skeletal vibrations, or to effect of some alkali cations outside the channels on the external surface where terminal silanols are located.

5.2.3.5. IR study of the adsorption of orthotoluonitrile on Li-, Na-, K- and Cs- MOR

Orthotoluonitrile (oTN) adsorption has been used to characterize basically the external positions of several zeolites including H-MOR and Co-MOR,[34] since its access to medium- and small-pore zeolite channels is highly hindered. Like other aromatic nitriles, such as benzonitrile, ortho-toluonitrile produces complexes through the coordination of its N lone pair to metal cations in metal

complexes[37] and on the surface of metal oxides.[38] Its CN stretching band, observed at 2225 cm^{-1} in the case of the liquid[39] shifts upwards upon these interactions.

The spectra of oTN adsorbed on all the alkali-mordenite samples, and after outgassing at different temperatures are shown in Figures 12 to 15. Also in this case, the activated sample spectrum as well as the gas phase spectrum have been subtracted to the sample spectra. Ortho-toluonitrile spectrum in CCl_4 solution, used as a reference, is also shown.

Subtraction spectra of ortho-toluonitrile (oTN) adsorbed on LiMOR and after evacuation at increasing temperatures are shown in Figure 12. The CN stretching region shows two peaks, whose main maxima are centred at 2253 cm^{-1} and 2217 cm^{-1}. The frequency of the first band is higher than the frequency observed on the liquid nitrile spectrum (Figure 12a), as usual for species interacting with Lewis acid sites, whereas the second band is, unusually, at lower frequency than that of the liquid spectrum. At room temperature, the ratio between the peak area relating to"usual adsorbed species" and the peak area relating to "unusual low-frequency adsorbed species" decreases when temperature increases, showing that the "unusual low-frequency adsorbed species" is more strongly bonded.

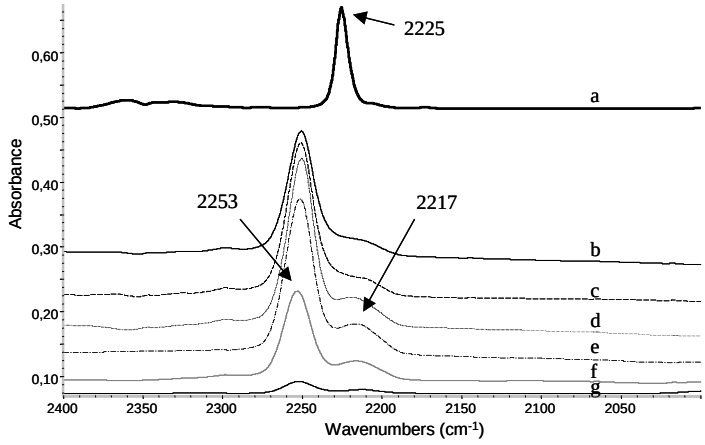

Figure 12. FT-IR spectra of liquid oTN (a), LiMOR in the presence of oTN (b) and after evacaution at room temperature(c) at 473 K (d), 573 K (e), 673 K (f) and 773 K (g).

The spectra of oTN on NaMOR show in the CN stretching region two peaks (Figure 13), whose main maxima are centred at 2246 and 2216 cm^{-1}. The band at higher frequency is more intense than that at lower frequency, but during the desorption process, the intensity of the first one decreases faster, until they have similar intensity. Comparing those frequencies with that of the nitrile spectrum in CCl_4 solution (Figure 13a) we observe again that one band is located at higher and the other band at lower frequencies.

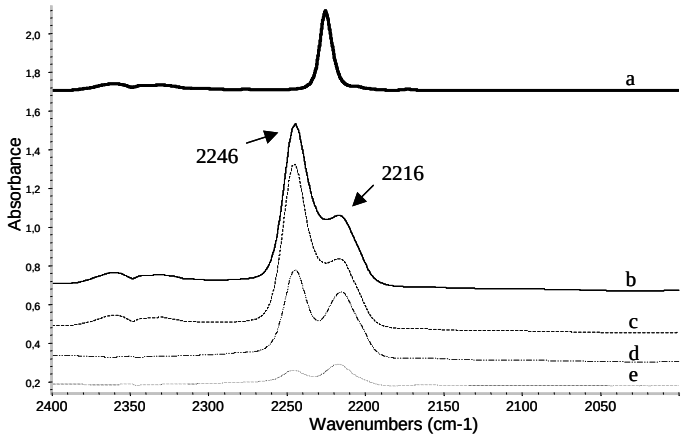

Figure 13. FT-IR spectra of liquid oTN (a), in the presence of oTN (b) and after evacaution at room (c) at 473 K (d) and 573 K (e).

In the case of KMOR (Figure 14), subtracted spectra of oTN adsorbed on this sample and after evacuation at increasing temperatures show, in the CN stretching region, two peaks, whose maxima are centred at 2238 cm^{-1} and 2224 cm^{-1}. As it was obserbed for LiMOR and NaMOR samples, the frequency of the first band is higher than the frequency observed for the liquid nitrile, whereas the second band is at slightly lower frequency than that of the liquid nitrile spectrum. While on the spectra taken at lower temperatures (Figure 14b-d) the higher frequency band is more intense, at temperatures higher than 573 K (Figure 14e-g) the situation is completely reversed: the band at lower frequency is more intense than that at higher frequencies, and at desorption temperatures of 673 K and 773 K, only the band at 2224 cm^{-1} is observed.

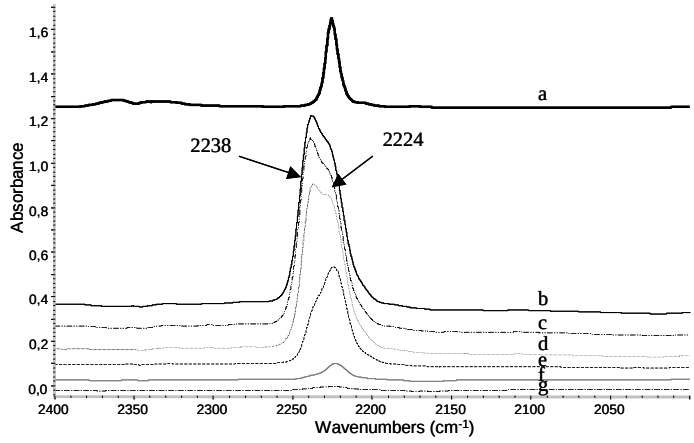

Figure 14. FT-IR spectra of liquid oTN (a), KMOR in the presence of oTN (b) and after evacaution at room temperature(c) at 473 K (d), at 573 K (e), at 673 K (f) and at 773 K (g).

Subtracted spectra of oTN adsorbed on CsMOR and after evacuation at increasing temperatures are shown in Figure 15. The spectra show in the CN stretching region one assymmetric band with the maximum at 2233 cm^{-1} and a tail to lower frequencies. The band intensity decreases by increasing temperature and the main maximum shifts to lower frequencies until at 773 K the maximum is centered at 2227 cm^{-1}.

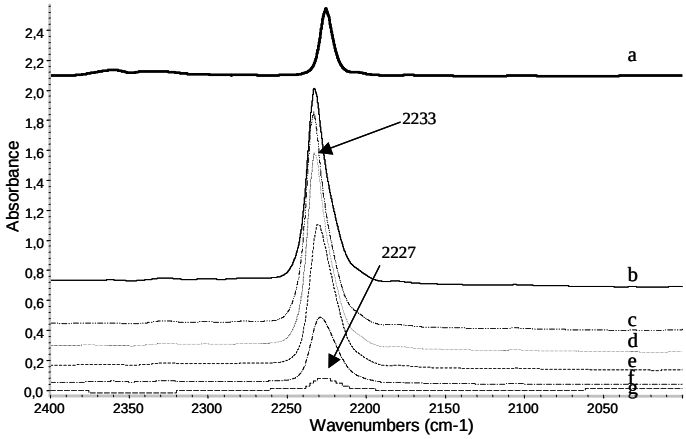

Figure 15. FT-IR spectra of liquid oTN (a), CsMOR in the presence of oTN (b) and after evacaution at room temperature(c) at 473 K (d), at 573 K (e), at 673 K (f) and at 773 K (g).

The higher frequency CN stretching component is found in all cases well above the liquid phase value while decreasing in the order LiMOR (2253 cm^{-1}) > NaMOR (2246 cm^{-1}) > KMOR (2238 cm^{-1}) > CsMOR (2233 cm^{-1}), in parallel with the decreasing acidity of the cations as already observed for adsorbed CO and PrN. This species may be identified as a "usual" species coordinated through the N lone pair to the different cations. However, due to the large size of oTN, this interaction should occur out of the porous structure of mordenite or just at the mouth of the main channels.

Like in the case of PrN adsorption on alkaly mordenites, the lower frequency component is also observed at least for LiMOR, NaMOR and KMOR and the CN stretching seems to follow the inverse trend: LiMOR (2217 cm^{-1}) ≈ NaMOR (2216 cm^{-1}) < KMOR (2224 cm^{-1}). In the case of CsMOR the two bands nearly coincide. These results well indicate that this interaction should also occur just at the mouth of the main channels or, alternatively, on the external zeolite surface. It has, anyway to be taken into account that such an

interaction was not observed with a non-zeolitic material such as Na-silica alumina.[24]

5.2.4. Discussion

The data summarized above allow to improve the knowledge on the adsorption mechanisms occurring in the case of adsorption of gases and vapours on cationic zeolites. The data concerning CO adsorption on alkali mordenites fully agree with those reported previously.[21-23] In all cases it is evident the formation of C-bonded CO species whose stretching frequency shift increases by increasing the acidity of the cation, i.e. by decreasing its ionic radius. In the case of Na-MOR and K-MOR a splitting of this band is also quite evident, likely associated to two different accessible locations for Na^+ and K^+ cations. According to previous studies, in fact, Na^+ ions in NaMOR occupy three different sites. The most populated one, called (I) or A, is just in the middle of the compressed channels and is considered to be not accessible. The others are site IV, also called D, near the opening of the side pocket in the main channel, and site VI, also called E, which is well exposed in the main channel. In the case of CsMOR the same sites are likely occupied by Cs^+ ions.[40,29] Actually, as also shown in the computer simulations of Geobaldo et al. concerning N_2 adsorption on NaMOR the molecules adsorbed to the two accessible cations, at sites IV and VI, lay well in the center of the main channel, no adsorbed molecules being actually located in the side pockets. This makes less evident the reasons for the assignments given previously of the two components of the high frequency band.[23] Actually, the cations in position IV (near the center of an eight oxygen ring) appear to be more shielded by oxygens that those at position VI (off center of a six ring), and this allows us to assign the higher

frequency component to CO C-bonded at position VI cations, the lower frequency one being assigned to CO C-bonded at position IV cations.

Similar species are also observed for propionitrile. N-bonded propionitrile molecules are well evident and, at least in the case of PrN adsorbed on LiMOR, the multiplicity of the CN stretching band, whose maximum shifts significantly upwards by decreasing coverage, may be an indication of the duplicity of the adsorbing ions (site VI and IV). This shift is less or not at all evident, in the case of PrN adsorbed on the other alkali-MOR samples, where the band at lower frequency with respect to the pure nitrile becomes more and more predominant.

The adsorption of oTN gives also rise to a CN stretching band shifted well above the value of the pure compound. The intensities of the bands of adsorbed oTN are well lower than those of the bands of adsorbed PrN, this agreeing with the fact that, due to its definitely higher size, the access of oTN in the MOR channels is highly, if not completely, hindered, so being essentially limited to the external surface and the pore mouths. Thus, the detection of the bands at 2240-2255 cm^{-1} for oTN adsorbed on LiMOR, NaMOR and KMOR strongly suggests that alkali cations are also located at the mouth of the channels or well at the outer mordenite surface, and interact via the usual N-coordination, with oTN. The location of alkali ions at the outer surface also somehow agrees with the shift of the position of the OH stretching band of the silanol groups, thought to be located at the external surface, with the heaviest alkali cations K^+ and Cs^+, both agreeing with a "perturbation" of the external mordenite surface by alkali cations.

In all cases, species characterized by CO and CN stretchings at lower frequency than the free molecule are also observed. In all cases these species appear to be more stable than the "usual" C-bonded (for CO) and N-bonded (for nitriles) species. This allows us to suppose that a different interaction occurs in this

case, and this interaction seems very likely to be "multiple". Only in the case of nitriles adsorption on CsMOR the two species (N-bonded and "multiply" bonded) are difficult to be distinguished or resolved. The relative intensity of the two components, due to "usual C- or N- bonded species and for "multiply" bonded species, seem to indicate that the amount of multiply bonded species grows (at least relatively to that of the usual C- or N- bonded species) with the following trends: LiMOR < NaMOR < KMOR < CsMOR and CO < PrN < oTN. These trends indicate that this interaction is easier to be formed with larger cations, with more basic molecules (nitrile > CO) and at the external versus the internal surface (oTN > PrN). These data, together with those reported elsewhere for NaMOR interacting with other nitriles[24] and for CO and nitriles adsorbed on Na-FAU samples,[25] suggest that the possibility to find two interaction sites (likely two alkali cations) at the correct distance is a key factor for establishing this interaction. Very tentative structures for double interactions with two cations are reported in the scheme I.

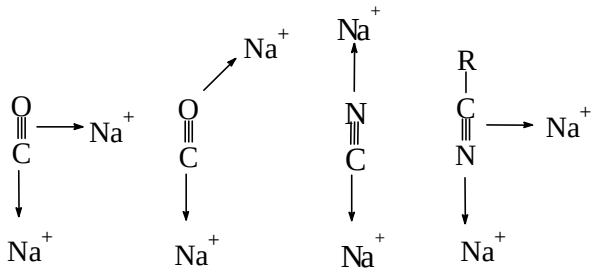

Scheme 1. Tentative structures for CO and nitriles interacting with two cations.

The possibility of the interaction of CO with two cations has been considered previously by Ugliengo et al.[41] These authors considered the interaction of CO with couples of naked cations at various distances, and found these complexes

unstable. However, they did not exclude the possibility of formation of species interacting with two cations in the channels of zeolites. In fact, the electric field in the channels of alkali–zeolites, in spite of the predominance of the field generated by the cations, is also strongly influenced by the oxygen atoms and by the zeolite framework. This limits the possibility of displacement of the cations and also their net charges, and also provides additional components to the electric field. Although the needed calculations on this subject seem to be lacking, it seems to us that the "multiply bonded species" should primarily involve two cations, just because in the zeolite channels the most basic oxygens are actually shielded by the cations and this should hinder their direct interactions with CO and the CN bonds of nitriles.

On the other hand, the evidence for the formation of this "multiply bonded species", that, when observed, are the most strongly adsorbed and the most resisting outgassing, tends to change the view of the chemistry of adsorption in zeolites. In fact, in previous studies only one site – one molecule or one site – two molecules interactions have been usually considered to occur and modeled in theoretical studies. In contrast, we show here that two sites – one molecule interactions may be very relevant. Adsorption on zeolites may appear as a cooperative action where the cavity plays a role not only as a host of the adsorption sites, but also as a unique environment where complex adsorption phenomena may occur.

5.2.5. Acknowledgements

The authors acknowledge the Generalitat of Catalunya for a grant (2002FI 00667).

5.2.5. References

[1] Rege, S. U.; Yang, R. T.; Qian, K.; Buzanowski, M. A.*Chem. Eng. Sci.* **2001**, 56, 2745.

[2] Méthivier, A. Separation of Paraxylene by Adsorption. In *Zeolites for cleaner technologies*; Guisnet, M.; Gilson, J. P.; Eds.; Imperial College Press: London, 2002, p. 209.

[3] Castle, W. F. *Int. J. Refrigeration* **2002**, 25, 158.

[4] Weitkamp, J.; Hunger, M.; Rymsa, U. *Micropor. Mesopor. Mat.* **2001**, 48, 255.

[5] Davis, R. J. *J. Catal.* **2003**, 216, 396.

[6] van Bokhoven, J. A.; Tromp, M.; Koningsberger, D. C.; Miller, J. T.; Pieterse, J. A. Z.; Lercher, J. A.; Williams, B. A.; Kung, H. H. *J. Catal.* **2001**, 202, 129.

[7] Guisnet, M.; Gilson, J.P., Eds., *Zeolites for cleaner technologies*, Imperial College Press: London, Catalytic Science Series, Vol 3, 2002.

[8] Moreau, F.; Ayrault, P.; Gnep, N. S.; Lacombe, S.; Merlen, E.; Guisnet, M. *Micropor. Mesopor. Mat.* **2002**, 51, 211.

[9] Webster, C. E.; Cottone, A.; Drago, R. S. *J. Am. Chem. Soc.* **1999**, 121, 12127.

[10] Yuvaray, S.; Chang, T. H.; Yeh, C. T.; *J. Phys. Chem. B* **2003**, 107, 4971.

[11] Salla, I.; Salagre, P.; Cesteros, Y.; Medina, F.; Sueiras, J. E. *J. Phys. Chem. B* **2004**, 108, 5359.

[12] Alberti, A.; Davoli, P.; Vezzalini, G.; *Z. Kristallogr.* **1986**, 175, 249.

[13] Macedonia, M. D.; Moore, D. D.; Maginn, E. J.; Olken, M. M. *Langmuir*, **2000**, 16, 3823.

[14] Devantour, S.; Abdoulaye, A.; Giuntini, J. C.; Henn, F. *J. Phys. Chem. B* **2001**, 105, 9297.

[15] Maurin, G.; Senet, P.; Devantour, S.; Henn, F.; Giuntini, J. C. *J. Non-Crist. Solids* **2002**, 307-310, 1050.

[16] Bell, R. G.; Devautour, S.; Henn, F.; Giuntini, J. C. *J. Phys. Chem. B* **2004**, 108, 3739.

[17] Zecchina, A.; Otero Areán, C. *Chem. Soc. Rev.* **1996**, *25,* 187.

[18] Knözinger, H.; Huber, S. *J. Chem. Soc., Faraday Trans.* **1998**, 94 (15), 2047.

[19] Hadjiivanov, K. I.; Vayssilov, G. N. *Adv. Catal.* **2002**, 47, 307.

[20] Onida, B.; Bonelli, B.; Borello, L.; Fiorilli, S.; Geobaldo, F.; Garrone, E. *J. Phys. Chem. B* **2002**, 106, 10518.

[21] Lamberti, C.; Bordiga, S.; Geobaldo, F.; Zecchina, A.; Otero Areán, C. *J. Chem. Phys.* **1995**, 103, 3158.

[22] Bordiga, S.; Lamberti, C.; Geobaldo, F.; Zecchina, A.; Turnes Palomino, G.; Otero Areán, C. *Langmuir* **1995**, 11, 527.

[23] Marie, O.; Massiani, P.; Thibault-Starzyk, F. *J. Phys. Chem. B* **2004**, 108, 5073.

[24] Salla, I.; Montanari, T.; Salagre, P.; Cesteros, Y.; Busca, G. *J. Phys. Chem. B* **2005**, 109, 915.

[25] Kozyra, P.; Salla , I.; Montanari, T.; Salagre, P.; Datka, J.; Busca, G. submitted paper

[26] Bevilacqua, M.; Gutiérrez-Alejandre, A.; Resini, C.; Casagrande, M.; Ramírez, J.; Busca, G. *Phys. Chem. Chem. Phys.* **2002**, 4, 4575.

[27] Bevilacqua, M.; Busca, G. *Catal. Commun.* **2002**, 3, 479.

[28] Flanigen, E. M. In *Zeolite Chemistry and Catalysis;* Rabo J. A.; Ed.; ACS: Washington, 1979, p. 80

[29] Geobaldo, F.; Lamberti, C.; Ricchiardi, G.; Bordiga, S.; Zecchina, A.; Turnes Palomino, G.; Otero Arean, C. *J. Phys. Chem* **1995**, 99, 11167.

[30] Tsyganenko, A. A.; Escalona Platero, E.; Otero Are**á**n, C.; Garrone, E.; Zecchina, A. *Catal. Lett.*, **1999***,* 61, 187.

[31] Martra, G.; Ocule, R.; Marchese, L.; Centi, G.; Coluccia, S. *Catal. Today* **2002**, 73, 83.

[32] Heise, H. M.; Winther, F.; Lutz, H. *J. Mol. Spectrosc.* **1981**, 90, 531.

[33] Szymańska-Buzar, T.; Gowiak, T.; Czeluśniak I. *J. Organomet. Chem.* **1999**, 585, 215.

[34] Montanari, T.; Bevilacqua, M.; Resini, C.; Busca, G. *J. Phys. Chem. B* **2004**, 108*,* 2120.

[35] Ng, J. C. F.; Park, Y. S.; Shurvell, H. F. *Spectrochim. Acta A* **1992**, 48, 1139.

[36] Quadri, S. M.; Shurvell, H. F. *Spectrochim. Acta A* **1995**, 51, 1355.

[37] Becker, J. J.; Van Orden, L. J.; White, P. S.; Gagne, M. R. *Org. Lett.* **2002**, 4, 727.

[38] Tretyakov, N. E.; Filimonov, V. N. *Kinet. Catal.* **1973**, 14, 803.

[39] Deady, L. W.; Harrison, P. M.; Topsom, R. D.*Spectrochim. Acta A* **1975**, 31, 1665.

[40] Chu, P. J.; Gerstein, B. C.; Nunan, J.; Klier, K. *J. Phys. Chem.* **1987**; 91; 3588.

[41] Ugliengo, P.; Garrone, E.; Ferrari, A. M.; Zecchina, A.; Otero Arean, C. *J. Phys. Chem. B* **1999**, 103, 4839.

5.3. FT-IR Study of the adsorption of carbon monoxide and of differently hindered nitriles on Na-Faujasites: a confirmation for the formation of complex interactions

Abstract

The low temperature adsorption of CO and the room temperature adsorption of acetonitrile (AN), propionitrile (PN), isobutyronitrile (IBN) and pivalonitrile (PN) has been investigated on NaX (Si/Al at. ratio =1.3) and NaY zeolite (Si/Al at. ratio =2.4). The bands of CO adsorbed species on NaY have been reassigned. The relevance of Na^+ ions at S_{III} or $S_{III'}$ positions also on NaY has been emphasized. Evidence is provided for the formation of complex interactions where nitrile molecules interact with more than one Na ions, like previously found on NaMOR.

5.3.1. Introduction

Sodium-Faujasites, in the form of either NaX or NaY, and other alkali-metal exchanged Faujasites are widely applied in the industry as selective adsorbants for gas mixture separation and gas purification, as well as catalysts, catalyst supports and catalyst components.[1]

Either in the form of powder packed beds or of membranes, alkali metal zeolites may allow the drying of air,[2] the separation of air's components (N_2/O_2) by pressure/vacuum swing adsorption procedures,[3] the separation of CO_2 from different gaseous streams,[4] the alkene/alkane,[5] the benzene/ cyclohexane[6] and the xylene isomer separations.[7] The faujasite structure is constituted by quite wide supercages accessed through 12-member silicate rings with diameter near 0.74 nm, much smaller sodalite cages accessed through 6-member silicate rings and hexagonal prisms connecting the sodalite cages. Cations are located in different positions in the cavities depending on hydration-dehydration states or upon adsorption of different molecules.[8,9] The significant medium Lewis acidity of the alkali and alkali earth cations, increased by the loss of ligands in dry zeolites, is the key feature for the use of these materials as regenerable adsorbants. According to Davis,[10] that reviewed recently the perspectives of their use as catalysts, alkali-exchanged zeolites are considered to be solid base catalysts but their active sites should be envisioned as a combination of a Lewis acid and a Lewis base sites.

The low temperature adsorption of CO is today perhaps the most popular technique for Lewis acidity characterization but is also used for characterizing Brønsted sites of protonic zeolites by applying the H-bonding method.[11-14] The position of νCO of adsorbed CO is shifted upwards on Lewis acidic d_0 cations and on protonic sites as the result of a σ-type donation of the lone pair at the carbon atom, or of a simple polarization of the molecule. However, it has been

shown that also the O lone pair can be involved in a very weak O-bond interaction which shifts down the CO stretching frequency.[15] CO as a probe actually allows a very detailed analysis of the surface sites as they appear at low temperature without strong perturbations of the surface, having also free access to any cavity and avoiding steric hindrances. This is a good opportunity to evaluate "pure acidity"[16] but, it is also a drawback, because it does not provide information on the location of the sites in or out the different cavities of microporous materials. On the contrary, the use of sets of differently hindered nitriles may allow to discriminate between adsorption sites located in differently hindered sites or at the external surface in protonic[17,18] and cationic zeolites.[19]
The interaction of basic molecules with the active sites in zeolites is generally modeled as being due to "one site-one molecule" interactions, or sometimes as "one site- two molecules" interactions. In the case of the adsorption of diatomic molecules on cationic zeolites, such as CO[20] and N_2[21,22] but also concerning the adsorption of nitriles, end-on σ-bonding interactions only are usually considered. In contrast, for olefins such as butenes[23,24] and pentenes[25] side-on π-bonding very likely occur.

Low temperature CO adsorption and hindered nitriles adsorption have been used recently to reexamine the adsorption sites of Na-Mordenite,[26] and in this case the formation of strongly adsorbed species interacting with more than one cation, possibly with a π-bonding additional to usual σ-bonding, or with a cation and an oxide ion has been proposed. The existence of complex interactions involving both cations and oxide species has also been proposed for ammonia adsorption on alkali-metal faujasites.[27]

Low temperature[28-33] and room temperature[34] IR studies of CO adsorption on alkali-metal faujasites have been published. In this paper we report on our re-examination of the CO- NaFAU system and on a new study on the adsorption

of hindered nitriles on NaX and NaY samples, in order to check if interactions similar to those observed on Na-MOR are detectable also on these systems.

5.3.2. Experimental

Zeolite NaY (Si/Al = 2.56) has been synthesized in the Institute of Industrial Chemistry of the Warsaw University while NaX zeolite (Si/Al = 1.31) has been synthesized in the Institute of Chemical Technology of the Jagellonian University in Krakow. CO cylinders were purchsed from SIAD while the nitriles acetonitrile (AN), propionitrile (PrN), isobutilonitrile (IBN), pivalonitile (PN), where pure products purchased from Aldrich.

Self-supporting pressed disks of pure zeolite powders were activated "in situ" in the IR cell by outgassing at 723 K before the adsorption experiments. The conventional gas manipulation/outgassing ramp was connected to a NaCl window- containing IR cell which allowed cooling by liquid nitrogen in an external jacket.

The adsorption/desorption process has been studied by transmission FT-IR. For nitriles, the adsorption procedure involves contact of the activated sample disk with vapors at room temperature at a pressure not higher than 2,5 kPa. The desorption process at increasing temperatures was performed in vacuum at temperatures compressed in the range 273 K and 573 K. CO adsorption was performed at 130 K (real sample temperature measured by a thermocouple) by the introduction of a known dose of CO gas. IR spectra were collected evacuating at increasing temperatures between 130 and 273 K.

5.3.3. Results

5.3.3.1. Low temperature CO adsorption on NaX and NaY

The overall spectra of activated NaX sample in the OH stretching region, a weak sharp band at 3684 cm^{-1} that does not correspond to the OH stretching of the bridging hydroxy groups of NaHX zeolite.[35] This weak feature, observed frequently on NaX samples[25] is likely associated to traces of residual water molecules.[37] In the case of the NaY, the spectrum shows only a sharp band at 3739 cm^{-1}. This band can be assigned to the OH stretching of terminal silanol Si-OH groups located at the external crystal surface or in structural defects. In both cases no evidence is found for bridging OH's (typically found in the range 3650-3550 cm^{-1} in proton-containing zeolites), showing that cation exchange is complete.

Figure 1 shows the IR bands of CO adsorbed at low temperature on NaX zeolite. At temperatures lower than 163 K mainly one asymmetric and very intense (maximum out of scale) band is observed on the CO stretching range. With outgassing at increasing temperatures, the intensity of this band diminishes its main maximum being found at 2165 cm^{-1} with a shoulder at 2176 cm^{-1}. Additionally, other two bands with very weak intensity, located at 2138 cm^{-1} and 2115 cm^{-1} are present. By progressively increasing temperature upon outgassing, the main band together with its shoulder (that at the lowest coverages shifts up to 2182 cm^{-1}) parallelly decrease their intensity, while the two lower frequency components disappear even earlier. Our spectra look very similar to those reported by Martra et al.[33] while they seem distinctly different from that reported by Hüber and Knözinger[31] at 0.1 hPa at 88 K on a NaX sample closely similar to our.

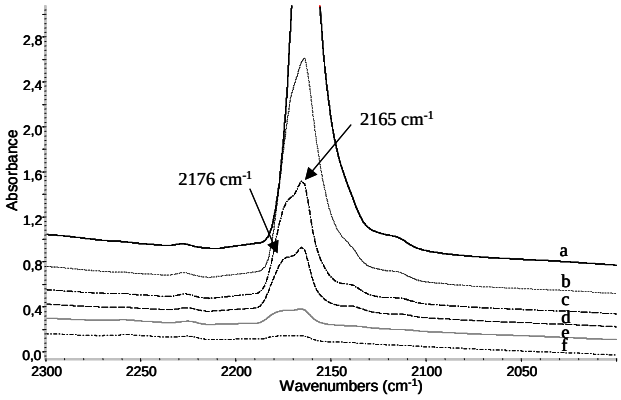

Figure 1. FT-IR spectra of activated NaX in the presence of CO gas under evacuation at 163K (a), 173K (b), 183 K (c), 193 K (d), 203 (e) and 213 K (f) in the CO stretching range.

As it is well known, four predominant locations have been found for Na^+ ions in the Faujasite framework. The S_I and $S_{I'}$ sites, that are in the center of the hexagonal prisms and near the six-fold mouth inside the sodalite cages, respectively, are considered to be not accessible to CO. The S_{II} site and SIII sites are near the walls of the supercage, at the center of six-fold and four-fold mouths, respectively. Martra et al.[30] assigned the main band they found at 2164-7 cm^{-1} to CO C-bonded to S_{II} site cations, while the shoulder they report at 2177-5 cm^{-1} has been assigned to CO C-bonded to S_{III} site cations. In contrast, Hüber and Knözinger[31] found the most intense band at 2166 cm^{-1}, they assigned to CO C-bonded to S_{III} site cations, with a shoulder at 2157 cm^{-1} assigned to CO C-bonded to S_{II} site cations.

The band at 2139 cm^{-1} disappears completely quite fast in vacuum and therefore can be attributed with confidence to pseudo-liquid physisorbed CO inside the zeolite pores. The band at 2115 cm^{-1} can be attributed to O-bonded

CO species ($Na^+ \cdots OC$) although, as noted by Martra et al.[33] C-bonded ^{13}CO and a component of sodium-dicarbonyl species may participate to it.

The spectra of the IR bands of adsorbed CO on NaY zeolite are shown in Figure 2.

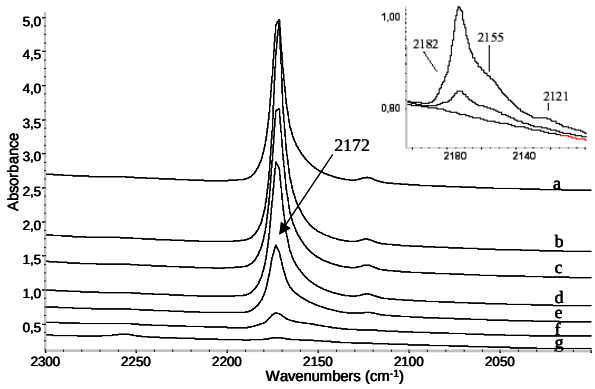

Figure 2. FT-IR spectra of activated NaY in the presence of CO gas under evacuation at 133K (a), 143K (b), 153 K (c), 163 K (d), 173 (e), 193 K (f) and 203 (g) in the CO stretching range.

We observe an intense and asymmetric band with the main maximum at 2172 cm^{-1} and a weak band at 2123 cm^{-1}. Only by expanding the weak spectra recorded after outgassing at 193 and 203 K (look at the inset in Figure 2) become evident two additional components, one at lower frequency the other at higher frequency, in the main peak namely at 2182 and near 2155 cm^{-1}. Hüber and Knözinger[29] found a similar spectrum with four components and attributed them to CO C-bonded on S_{II} sites near six-fold ring having one, two (meta), two (para) and three Al ions. The approach of Hüber and Knözinger,[31]

which also based on the Na and Al distribution between the different sites as deduced from NMR and XRD data, seems questionable to us, due to the exceeding intensity of the band at 2172 cm^{-1}. This band is in fact attributed to CO C-bonded to Na ions on S_{II} sites near two Al-containing six-fold rings, but this species should not be so more likely than the others. Also in this case, the band at 2123 cm^{-1} can be attributed to very weakly bonded CO possibly like $Na^+ \cdots OC$.

Therefore, neither on NaX nor on NaY we have been able to find low-frequency but strongly adsorbed CO species. We can conclude that multiply-bonded CO like that formed on Na-MOR[26] cannot be found on Na-FAU, possibly because of the larger dimensions of the supercages of the FAU structure, which prevents the cations responsible for the "multiple interaction" to be near enough to establish this interaction.

5.3.3.2. *Adsorption of acetonitrile and propionitrile on NaX and NaY*

Acetonitrile (AN) and propionitrile (PrN) adsorption can be used for characterizing adsorbing sites in zeolites. Both molecules do not have relevant steric hindrance and can interact with all adsorption sites in the case of mordenite samples.[18,26] The adsorption of AN on NaX and NaY has already been reported.[25,37] It is well known that the AN C≡N triple bond stretching mode gives rise to two bands due to the Fermi Resonance between the fundamental stretching CN with a δCH_3 + $\nu C\text{-}C$ combination. Both components shift upwards the more the stronger in the electronwithdrawing power of the cations to which the nitrile coordinates. The Fermi Resonance doublet for AN in CCl_4 solution is observed at 2292, 2255 cm^{-1} (Figure 3a.). On both NaX (Figure 3b-d, left) and NaY (Figure 3e-g, right) the bands tend to

shift further upwards by increasing outgassing temperature, i.e. by decreasing coverage. The final position is found at slightly higher wavenumbers for NaY (2300, 2270 cm^{-1}) than for NaX (2297, 2268 cm^{-1}) and this could be associated to a slightly higher Lewis acidity, i.e. a slightly lower electron density, for the most acidic Na^+ ions on NaY with respect to NaX. In both cases, however, upon outgassing a further band appears at lower frequencies that apparently are due to a species that resists outgassing more. These bands are found at 2237 cm^{-1} on NaX and at 2246 cm^{-1} on NaY, and resemble that found at 2238 cm^{-1} on Na-MOR,[26] assigned to "multiply bonded" species.

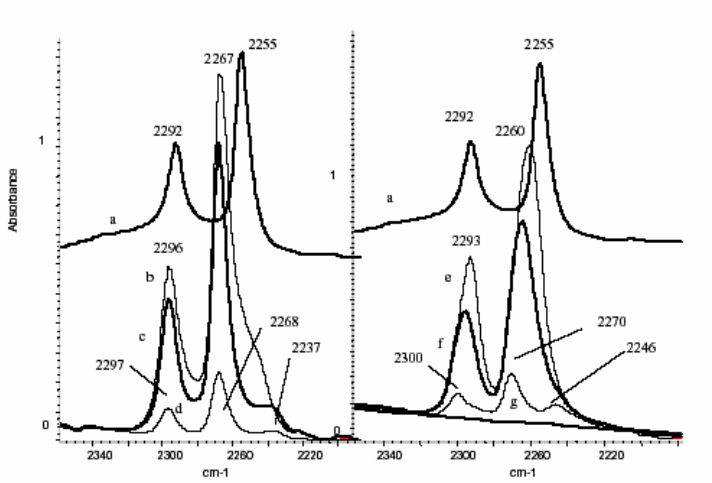

Figure 3. FT-IR spectra of AN in CCl_4 solution (a), NaX in the presence of AN vapors after evacuation at 373 K (b), 423 K(c) and 473 K (d), NaY in the presence of AN vapors after evacuation at 300 K (e), 373 K (f) and 423 K(g).

The spectra of PrN adsorbed on NaX and NaY samples, and after outgassing at different temperatures, are shown in Figures 4 and 5, respectively. The nitrile spectrum on CCl_4 solution, used as a reference, is also shown. From the subtracted spectra of PrN adsorbed on NaX after evacuation at room

temperature (Figure 4b) a broad band is observed at 2250 cm^{-1} on the CN stretching region. By heating at 373 K under vacuum, this band starts to resolve into two with maxima at 2256 and 2246 cm^{-1}. Finally, after the desorption process at 423 K and 473 K (Figure 4d-e), two bands are observed with the maxima at 2262 and 2228 cm^{-1}. The main band at the lowest coverages is found at similar wavenumbers than on Na-MOR[26] but is indicative of the PrN interaction with Na ions through the N lone pair. The lower frequency band, instead, is similar but at a definitely lower wavenumber with respect to that found on Na-MOR [26], and assigned to a "multiply bonded" species.

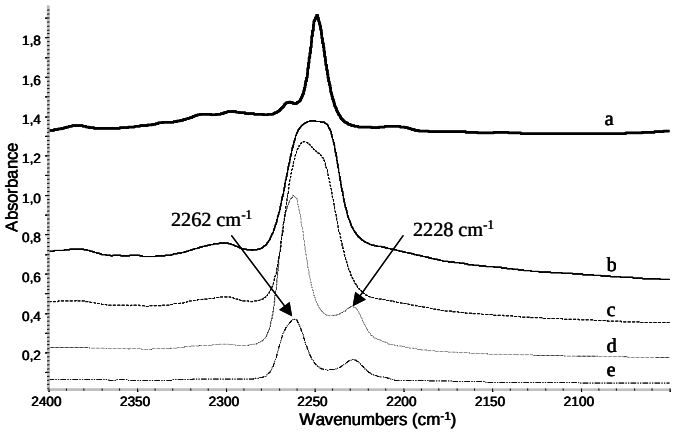

Figure 4. FT-IR spectra of PrN in CCl_4 solution (a), NaX in the presence of PrN vapors after evacuation at room temperature (b), at 373 K (c), 423 K(d) and 473 K (e).

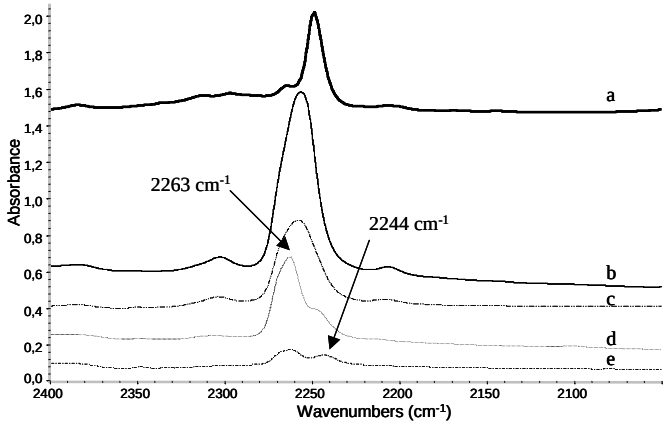

Figure 5. FT-IR spectra of PrN in CCl_4 solution (a), NaY in the presence of PrN vapors after evacuation at room temperature (b), at 373 K (c), 423 K(d) and 473 K (e).

A more detailed analysis of the CN stretching region can be made by analyzing the spectra obtained by subtracting from the band obtained in every step the spectrum of the step before (Figure 6). This shows that the main band shifted upwards with respect to that of the same compound in solution actually contains at the lowest coverages at least two components (2269, 2263 cm^{-1}) but that the main feature still present after outgassing at 373 K is still located near 2247 cm^{-1} with a fourth component near 2252 cm^{-1}. Interestingly, upon outgassing at 373 K the absorption at 2245-2253 cm^{-1} decreases in intensity while that at 2263 and 2269 cm^{-1} increases in intensity. In practice it seems clear that some propionitrile molecules displace from weaker to stronger adsorption sites, and that the two families (weaker and stronger sites, possibly due to Na^+ ions at S_{II} and S_{III} or $S_{III'}$ respectively) are both double (i.e. composed by two different species).

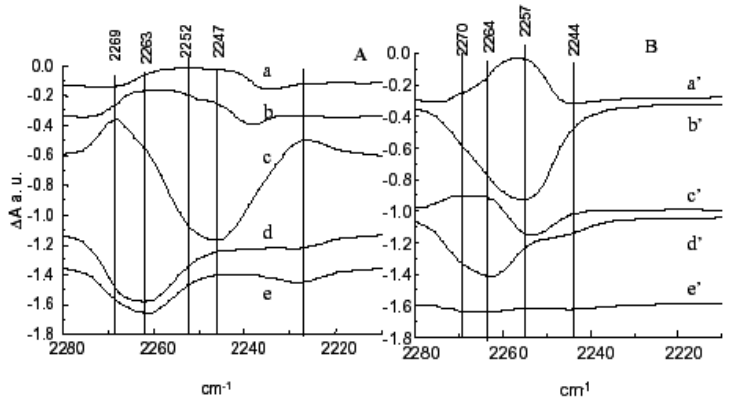

Figure 6A and B. Substraction spectra from Figure 4 and Figure 5, a and a': evac. at r. t. – in the prenence of the vapour, b and b': evac. at 373K- evac at r.t., c and c' evac. at 423K- evac 373 K, d and d': evac. at 473 K- evac. at 423K, e and e': evac. 523K – evac. 473 K.

A parallel situation is found for PrN on NaY (Figure 5). From the subtracted spectra of PrN adsorbed on NaY after evacuation at room temperature and at 373 K (Figure 5b-c) a broad band with the main maximum at 2258 cm^{-1} is observed on the CN stretching region. By heating at 423 and 473 K under vacuum (Figure 5d-e), also in that case a new band at lower frequencies appears. Thus two bands at 2263 and 2244 cm^{-1} are observed again. On NaY, however, the lower frequency band is relatively less shifted down than on NaX.

The analysis of the subtraction spectra (Figure 6B) shows that at the lowest coverages the bands on NaY and on NaX are very similar, for both position and relative intensity. Otherwise, at higher coverages, the main band on NaY is at higher frequencies than on NaX (2255 cm^{-1} with respect to 2245-2253 cm^{-1}). All features are actually shifted a little bit upwards on NaY than on NaX. This parallelism supports the assignment of the two features to the nitrile adsorbed on Na^+ ions at S_{II} and S_{III} or $S_{III'}$ respectively. If this is true, the existence and

activity of well defined Na^+ sites at S_{III} or $S_{III'}$ also in the case of NaY should be confirmed.

5.3.3.3. Adsorption of isobutyronitrile and pivalonitrile on NaX and NaY

Isobutironitrile (IBN) and pivalonitrile (PN) are more hindered nitriles, whose access to the mordenite "side pockets" was found to be partially forbidden.[18, 26] They have been used here to check if hindering of the access to Na ions in Faujasites can be found.

The subtracted spectra obtained for NaX sample using isobutironitrile (IBN) and pivalonitrile (PN) vapors as probe molecules are shown in Figures 7 and 8, respectively. On the spectra of IBN adsorbed on NaX and evacuated at room temperature a broad band centered at 2247 cm^{-1} can be observed (Figure 7b). When increasing the outgassing temperature to 373 K, this band becomes narrower with the maximum at 2253 cm^{-1} and a shoulder at 2244 cm^{-1} (Figure 7c). By still increasing temperature the intensity of the band diminishes and two bands are observed at 2259 and 2228 cm^{-1} (Figure 7d-e).

The behaviour observed for the spectra of PN adsorbed on NaX is similar to that observed for IBN on the same zeolite. After PN adsorption on NaX since a broad band centered at 2239 cm^{-1} is observed when evacuating at room temperature (Figure 8b). When increasing the outgassing temperature to 373K, a shoulder at 2234 cm^{-1} starts to appear (Figure 8c), and finally, at the desorption temperature of 473 K, the spectrum shows two bands with the maxima at 2250 and 2223 cm^{-1} (Figure 8d). Thus, after both IBN and PN adsorption/desorption on NaX, a band at frequencies lower than the frequency of the corresponding solution nitrile spectra is observed (Figures 7a and 8a), and these bands show a higher resistance to the desorption process.

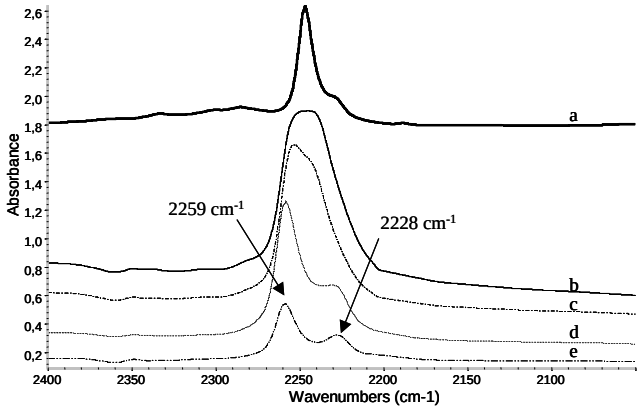

Figure 7. FT-IR spectra of IBN in CCl_4 solution (a), NaX in the presence of IBN vapors after evacuation at room temperature (b), at 373 K (c), 423 K(d) and 473 K (e).

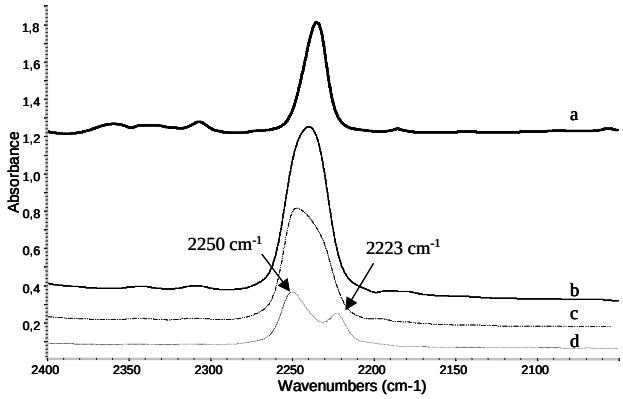

Figure 8. FT-IR spectra of PN in CCl_4 solution (a), NaX in the presence of PN vapors after evacuation at room temperature (b), at 373 K (c), and 473 K (d).

The subtracted spectra obtained for NaY sample using isobutironitrile (IBN) and pivalonitrile (PN) vapors as probe molecules are shown in Figures 9 and 10, respectively. In both cases the spectra obtained are similar, one asymmetric band with a tail to lower frequencies is observed, well shifted above than the band for the free nitrile. In the case of IBN this band is centered at 2258 cm^{-1}

and in the case of PN this band is centered at 2251 cm^{-1}. These bands decrease in intensity and become narrower when temperature increases on evacuation. So, in the case of IBN and PN adsorption on NaY we have not observed the band at lower frequencies than the liquid nitrile spectrum.

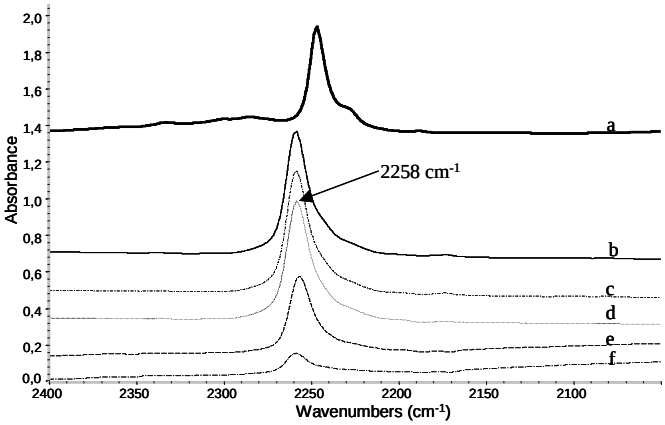

Figure 9. FT-IR spectra of IBN in CCl_4 solution (a), NaY in the presence of IBN vapors after evacuation at room temperature (b), at 373 K (c), 423 K(d), 473 K (e) and 523 (f).

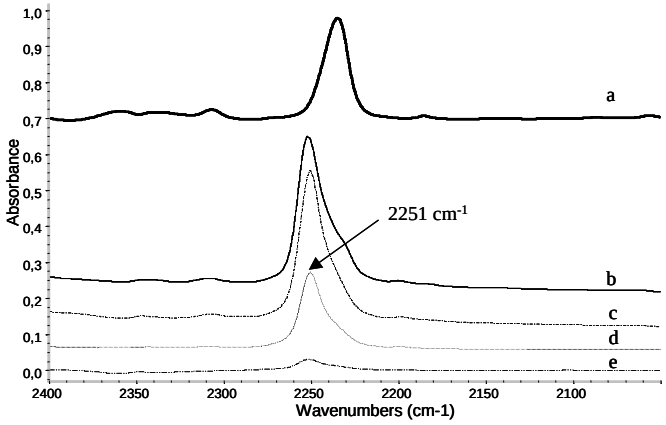

Figure 10. FT-IR spectra of PN in CCl_4 solution (a), NaY in the presence of PN vapors after evacuation at room temperature (b), at 373 K (c), 423 K(d) and 473 K (e).

An analysis of the subtraction spectra relative to the adsorption of the most hindered nitrile PN on NaX and NaY (Figure 11) can give some further information on the multiplicity and distribution of Na^+ sites. It seems that this hindered nitrile gives rise to less resolved bands but the maximum shifts more continuously from near 2240 to 2250 cm^{-1} on NaX and that the position is nearly the same also on NaY.

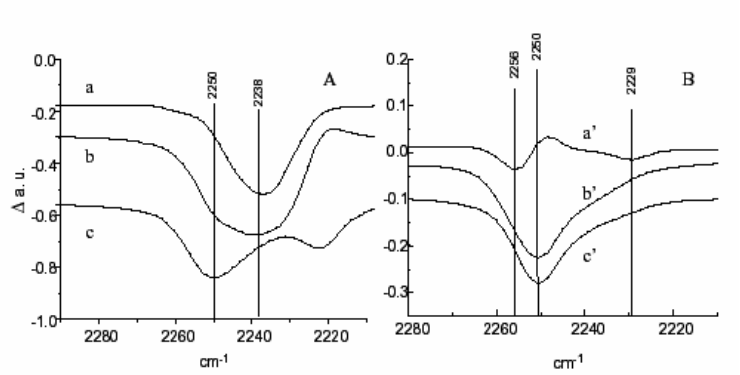

Figure 11A and B. Substraction spectra from Figure 8 and Figure 10, a and a': evac. at r. t. – in the prenence of the vapour, b and b': evac. at 373K- evac at r.t., c and c' evac. at 423K- evac 373 K,

5.3.4. Discussion.

5.3.4.1. Adsorption sites and σ-bonded CO adsorbed species

The sodium distribution in anhydrous NaX and NaY has been the object of several studies.[8,9,38,39] Although other possible locations have been considered by different authors, an idealized (and slightly simplified) model for NaX

Faujasite with a Si/Al ratio of 1, having for the unit cell the formula $Na_{96}Si_{96}Al_{96}O_{384}$, implies a 100 % occupation of the 32 so-called $S_{I'}$ sites which are located inside the sodalite cage in front of the 6-ring window connected to the haxagonal prism, the 100 % occupation of the 32 S_{II} sites which are located in the middle of the 6-ring window connecting the supercage and the sodalite cage, and the 66 % occupation of the 48 S_{III} sites, which are a little displaced towards inside the supercage, near the middle of the 4-rings separating them from the sodalite cage.[9] Other authors[8] consider the presence of 32 Na^+ ions in one third of the $S_{III'}$ sites (instead of the S_{III} sites), located in the 12-ring windows of the supercage. By decreasing the Al and the sodium contents[9] (so shifting from NaX to NaY) the occupancy of sites $S_{I'}$ and S_{III} decreses while sites I (located just in the middle of the hexagonal prisms) become populated. For a Si/Al of 3 (i.e with a formula $Na_{48}Si_{144}Al_{48}O_{384}$), sites S_I and S_{II} are fully populated, while $S_{I'}$ and S_{III} are empty.

According to most authors, sites I and I', which are inside the sodalite cage and of the hexagonl prisms, respectively, should be inaccessible to adsorbates. So adsorption is expected to occur only in the supercage. Every supercage may contain up to 8 Na ions: four cations at S_{II} and four cations at S_{III} (or $S_{III'}$) for Si/Al = 1, while only the four cations at SII for Si/Al = 3. In the case of our samples, characterized by Si/Al ratios of 1.31 and 2.56, the Na cation distribution should be not very different from those considered for the ratios Si/Al = 1 and 3, respectively.

In NaX Na^+ ions in S_{III} sites are expected to present a higher positive charge than those at SII, so the Lewis acidity of cations at S_{III} is expected to be the greatest.[29] Also cations located in $S_{III'}$ sites,[8] if any, should be more Lewis acidic than those in S_{II}. In agreement with this, and with previous authors, we assign the bands at 2176 and 2165 cm^{-1} observed after low temperature CO adsorption on NaX to carbonyls on Na^+ S_{III} (or $S_{III'}$) and S_{II} cations,

respectively. This also agrees with the relative intensity of the observed bands where the band attributed to carbonyls on S_{III} ions is less intense at saturation than that attributed to carbonyls on SII, in agreement with a S_{III}/S_{II} well lower than 1 in our sample whose composition is near $Na_{55}Si_{137}Al_{55}O_{384}$.

As for the assignment of the bands associated to CO adsorbed on NaY, the main band observed at 2172 cm^{-1} is quite easily attributed to carbonyls on Na^+ ions located in site S_{II}, which is expected to be largely predominant. The shift to higher frequency of this species on NaY with respect to NaX (for sites at S_{II}) should indicate that oxygen species in the six-ring windows near S_{II} are a little less basic on NaY than on NaX, according to the lower Al content in the framework. The expansion of the spectra recorded at very low coverages allows to evidence two other components here, but very weak, at 2182 and at 2155 cm^{-1}. In their previous work, Marra et al.[29] found only the main band. Hüber and Knözinger[31] and Vayssiliov et al. [30] instead, found, besides the main one at 2172 cm^{-1}, three other at 2182, 2165, 2155 cm^{-1}. They assigned those four bands to Na^+-carbonyls on four different S_{II} sites associated to different Al contents and positions. This assignment has also been given by Tsyganenko et al.[32] This assignment seems however to be inconsistent, in our opinion, with the exceedingly strongest intensity of the component at 2172 cm^{-1} observed at saturation. On the other hand, the composition of our sample (which is actually the same of that of the sample used in references 30 and 31) that corresponds to a formula near $Na_{55}Si_{137}Al_{55}O_{384}$, is such that occupancy of site III should be still not nil. So, the band at 2182 cm^{-1} can reasonably be due to Na^+ carbonyls on residual S_{III} sites. Consequently, the band assigned to CO on S_{II} cations should be almost insensitive to the number of Al ions in the 6- rings. As for the feature observed at 2155 cm^{-1}, it seems evident that it is due to a species which are in very small amounts but more strongly bonded than that characterized by the band at 2172 cm^{-1}. In fact, outgassing tend to cause the disappearance of the band at 2172 cm^{-1} but leaves more evident the band at 2155 cm^{-1}. Here we

found a species that apperas to be less shifted upwards but less resistant to outgassing than the usual Na^+ carbonyls. This may be due either to diffusional effects (the desorption is hindered in some way) or to the existence of a different interaction. From these consideration, we can prpose two different assignments for this species, either to terminal carbonyls on Na^+ ions located in the interior of the sodalite cage or of the hexagonal prisms, whose desorption could be hindered by the small dimensions of the cavity windows, or, alternatively, to multiply bonded species on the supercage. However, the lack of detection of this species on NaX (in whose supercage much more Na^+ ions are present) allows us to rule out this second possibility. It seems to us possible that few CO molecules, whose van der Waals radius is not far from the half of the diameter of six ring windows, could find the way to enter the sodalite cavities (perhaps through defective sites) and to produce carbonlys on Na^+ located at $S_{I'}$ sites.

5.3.4.2. " Usual" σ-bonded nitrile adsorbed species

As shown in Table 1 and in Figures 3-11, the adsorption of all nitriles gives rise to bands located well above the frequency of the free molecule, that may be assigned to " usual" σ-bonded nitrile adsorbed species on Na^+ ions. The analysis of the behaviour of these bands allows us actually to observe several components that are certainly related to a remarkable heterogenity of the available Na^+ ions. If the exact position of the components for adsorbed AN is difficult, due to the presence of the Fermi Resonance doublet, for PrN, IBN and PN three or four different adsorbesd species may be observed. The comparison allows to suggest that the bands at higher frequencies can be assigned to nitrile molecules adsorbed on the most electron poor Na^+ cations located at S_{III} or $S_{III'}$ sites, while the less perturbed nitrile species should be due to the more abundant Na^+ cations located at S_{II} sites. This means that the

existence and relative importance of Na^+ cations located at S_{III} or $S_{III'}$ sites should be not negligible, in agreement with the more recent data concerning the distribution of Na ions in Na Y zeolite.

Table 1. Position of the IR bands (cm^{-1}) of adsorbed nitriles and CO on Na-MOR, NaY and NaX.

Adsorbed molecule	Na-MOR	NaX	NaY	Free molecule
CO			2182	
	2175	2176	2172	
	2164	2165	2155	
	2138	--	--	2143 (gas)
AN	2299	2297	2293-2300	2292
	2268	2268	2260-2270	2255
	2248	2237	2246	
PrN	2267	2269-2263	2270-2264	
		2252-2247	2255-2253	2249
	2241	2228	2244	
IBN	2260	2265-2245	2265-2252	2247
	2235	2228	--	
PN	2253	2250-2237	2256-2250	2235
	2221	2223	--	

A rough evaluation of the amount of adsorbed nitriles on NaX and NaY shows that adsorbed species are definitely more abundant on NaX than on NaY, while that there is not much difference between the different nitriles adsorbed in the same solid. So the amount of adsorbed species depends on the amount of Na^+ ions in the supercage, while steric hindrance is not so important, due to the sufficiently large size of this cage.

5.3.4.3. "Unusual" low frequency nitrile adsorbed species

The data reported here may be discussed in parallel with those have been published recently concerning the adsorption of CO and several nitriles on Na-MOR zeolite in the same conditions.[26] Over NaMOR we found for both CO and the nitriles the unusual formation of bands at lower frequencies with respect to the free molecule but resisting outgassing more than the "usual" species characterized by bands at higher frequencies than the free molecules. This behavior was interpreted assuming that these "unusual" species are involved in multiple or complex interactions, involving either more than one cation or one cation and one oxygen atom.

The possibility of the formation of these strongly bonded species also on NaX and NaY is determined here and, finally, this confirms that this is a newly discovered but potentially very relevant kind of interaction. The spectroscopic evidence of the formation of such species actually gives a new light to the chemistry of cationic zeolites, where the formation of "two-sites – one molecule" adsorbate – adsorbant interaction (usually taken into account) must be considered possibly as the more determinant one.

In reference 26 the low frequency, strong interaction species were supposed to be due either to interaction with more than one cation or to a complex interaction involving one cation and one basic oxygen. In the case of NaX samples with Si/Al = 1, every supercage, which is near a sphere with 13 Å diameter, contains 8 Na^+ ions, four at S_{II} and four at S_{III} or $S_{III'}$ the data of Buttefey et al.[39] indicate that most Na ions should actually be displaced from the S_{III} crystallographic position significantly (~ 1 Å), and that some of them are displaced very much until the $S_{III'}$ crystallographic position. The distance between two S_{II} sites is 7.69 Å[40] while the distance between a S_{II} and a S_{III} or $S_{III'}$ crystallographic site may be as low as 4.5-5.5 Å.[41]

The possibility of forming species where interaction involves both the Na cation and the oxygen to which the same ion is also bonded, like proposed to occur with ammonia on NaX, seems unlikely for the much larger nitrile molecules. On the other hand, the possibility of weak interactions of the C-H bonds of nitriles with other oxygen atoms exposed in the cavity, like proposed to occur for hydrocholorocarbons in Na-Faujasites[42] should not cause a decrease in the CN stretching frequency. Taking into account that the cations may displace a little bit upon adsorption of different molecules, the possibility of the formation of adsorbed species where two different cations interact with the N lone pair and with a π-type orbital seems to be possible on NaX. The more difficult detection of such species on NaY, where we can find it for the unhindered nitriles AN and PrN, unlike the hindered nitriles IBN and PN, is logical due to the much lower occupancy of $S_{III'}$ and/or S_{III} sites in this case, and to the less easy accommodation of the hindered and rigid nitrile molecules PN and IBN, with respect to AN and PrN.

Another interesting feature is that the shift down of the CN stretching frequency is definitely stronger on NaX (~ 20 cm^{-1}) than on NaY and Na-MOR (~ 5-12 cm^{-1}) for AN, PrN and IBN, while it is similar on NaX and Na-MOR for PN. (~ 13 cm^{-1}). Due to the lower Al and sodium contents on NaMOR (Si/Al 6.5) and NaY than on NaX, we may conclude that the predominant Na-Na distance of the nearest cations is definitely larger on NaMOR (and NaY) than on NaX, so in the last solid this interaction may be stronger at least for the less sterically demanding nitriles.

The abundance of this "unusual" interaction may be measured by using the ratio (R) of the bands of "unusual strongly bonded species" / "usual σ-bonded species". This ratio is definitely larger on NaMOR when hindered nitriles are considered (like PN, or also benzonitrile and orthotoluonitrile) than when unhindered nitriles (like AN and PrN) are taken into account, just in contrast to

what happens on NaY. Consequently, it seems very likely that these interactions mostly occur in or at the mouth of the main channels in the case of NaMOR, where the more hindered nitrile should not penetrate. The above defined ratio (R) is definitely larger for NaMOR[26] than for NaX at least for PN and IBN, and this may be related to the larger size of the Faujasite supercage windows with respect to the Mordenite main channels. Thus this interaction should be limited at the external surface for NaMOR but should occur in the supercages for NaFAU, where the "usual" interactions also occur and are very abundant.

This "unusual" interaction is observed on NaX and NaY for nitriles but not for CO. This may be associated to the exceeding weakness of the basicity of CO with repect to that of the nitrile molecules (proton affinity 598 versus 783 kJ/mol, for acetonitrile). Alternatively, it may be due to the quadrupolar nature of CO (where the oxygen is formally positively charged) with respect to the polar nature of the C≡N triple bond, which finally results in a lower availability of π-type orbitals of CO to interact to a further No ion with respect to nitriles.

In any case this result evidences one of the limits in the use of CO as a probe molecule for zeolite adsorption sites, as discussed elsewhere.[43] Also in this case CO, due to its weakness as a base and its very low dimension fails in giving information on effects which are more or less cooperative and spatially demanding.

5.3.5. Conclusions

The study of CO adsorbed at low temperature and of a set of differently hindered nitriles adsorbed on NaX and NaY zeolites allows to obtain some new information on the sites available for these materials which are relevant in

industrial adsorption and catalysis processes. In particular we modified the assignments given in the literature to the features of CO adsorbed on NaY zeolite.

Our data show that two types of adsorbed species are well evident: i) simply coordinated species via a Lewis acid-base interaction. ii) multuiply bonded species.

The typical single coordination of CO through the C atom lone pair to Na^+ cations is well evident and has been the object of several previous investigations. However, the data reported here allow to modify significantly the previous assignments for CO adsorbed on NaY. Our data in fact indicate that the existence and the role of Na^+ cations at S_{III} or $S_{III'}$ sites is not negligible on NaY, even if they have lower population than on NaX, as shown by diffraction and model studies. We found here features that are assigned to CO and nitriles adsorbed on such ions. These species are the most strongly bonded and, consequently, they may be the more relevant from the points of view of catalysis and adsorption. So, although the S_{III} or $S_{III'}$ positions are expected to be empty for NaY having Si/Al atomic ration of 3, they are populated for samples whose Si/Al atomic ratios lower than 3, and they could become the more relevant in this case. Nitrile adsorbed species allow us to conclude that both families of sites, at S_{II} andf at S_{III} or $S_{III'}$ positions, are actually heterogeneous possibly due to the different number of Al ions present in the neighbors.

O-bonded adsorbed CO species are also observed, like emphasized in previous studies. They give rise to very weakly adsorbed species that should not be very relevant in practice just because of their weakness.

On the other hand, nitrile adsorption allows to show the formation on NaX and NaY, like on NaMOR, of multiply bonded species. These species are the most strongly bonded, so in principle they could be the most relevant in

adsorption and catalysis. They are formed with nitriles but not with CO on NaX and NaY, possibly due to the less basic character of CO with respect to nitriles. The detection of such species with nitriles unlike CO shows one of the limits of the use of CO as a probe for surface characterization.

The multiply bonded species are observed on NaY only when the less hindered nitriles are used. This may be due to a greater difficulty to find the right geometry to build up this interaction when the amount of Na cations is small (as for NaY) and the nitrile is hindered. This agrees with the observation, made on NaMOR but likely correct also for Na-FAU, that the formation of this interaction is activated (i.e. it needs a slight warming).

5.3.6. Acknowledgements

P.K., J.D. and G.B. acknowledge the grant from exchange research program of Italian and Polish Ministries of Education, I.S. acknowledges the Generalitat of Catalunya (2002FI 00667).

5.3.7. References

[1] Guisnet, M.; Gilson J. P.; eds., *Zeolites for cleaner technologies* Imperial College Press: London, Catalytic Science Series, Vol 3, 2002.

[2] Rege, S. U.; Yang, R. T.; Qian, K.; Buzanowski, M. A.; *Chem. Eng. Sci.* **2001**, 56, 2745.

[3] Castle, W .F. *Int. J. Refrigeration* **2002,** 25, 158.

[4] Hasegawa, Y.; Watanabe, K.; Kusakabe K.; Morooka, S. *Separ. Purif. Technol.* **2001,** 22-23, 319.

[5] Giannakopoulos I. G.; Nikolakis, V.; *Ind. Eng. Chem. Res*. **2005**, 44, 226.

[6] Kobayashi, Y.; Takami, S.; Kubo M.; Miyamoto, A. *Desalination*, **2002**, 147, 339.

[7] Finnouche, F.; Boucheffa, Y.; Boumaza, R.; Labed, A.; Magnoux, P. *Ind. Eng. Chem. Res,* **2004**, 43, 6708.

[8] Vitale G.; Mellot, C. F.; Bull, L. M.; Cheetam, A. K.; *J. Phys. Chem. B* **1997**, 101, 43559.

[9] Beauvais, C.; Guerrault, X.; Coudert, F. X.; Boutin, A.; Fuchs, A. H. *J. Phys. Chem. B* **2004**, 108, 399

[10] Davis, R. J. *J. Catal.* **2003**, 216, 396.

[11] Zecchina, A.; Otero Areán, C. *Chem. Soc. Rev*. **1996,** 25, 187.

[12] Knözinger, H.; Huber, S. *J. Chem. Soc., Faraday Trans*. **1998**, 94, 2047.

[13] Hadjiivanov K. I.; Vayssilov, G. N. *Advan. Catal.* **2002**, 47, 307.

[14] Datka, J.; Gil, B.; Kawalek, M.; Staudte B. *J. Mol. Struct.* **1999***,* 511-512, 133.

[15] Otero Areán, C.; Rodríguez Delgado, M.; Manoilova, O. V.; Turnes Palomino, G.; Tsyganenko A. A.; Garrone E. *Chem. Phys. Lett,* **2002**, 362, 109.

[16] Onida, B.; Monelli, B.; Borello, L.; Fiorilli, S.; Geobaldo, F.; Garrone, E. *J. Phys. Chem. B* **2002**, 106, 10518.

[17] Bevilacqua M.; Gutiérrez-Alejandre A.; Resini C.; Casagrande M.; Ramírez J.; Busca, G. *Phys. Chem. Chem. Phys.* **2002**, 4, 4575.

[18] Bevilacqua, M.; Busca, G. *Catal. Commun.* **2002**, 3, 497.

[19] Montanari, T.; Bevilacqua, M.; Resini, C.; Busca, G. *J. Phys. Chem. B* **2004,** 108, 2120.

[20] Lamberti, C.; Bordiga, S.; Geobaldo, F.; Zecchina A.; Otero-Arean, C.; *J. Chem. Phys.* **1995,** 103, 3158.

[21] Salla, I.; Salagre, P.; Cesteros, Y.; Medina, F.; Sueiras, J. E.; *J. Phys. Chem. B.* **2004**, 108*, 5359*.

[22] Maurin, G.; Llewellyn, Ph.; Poyet Th.; Kuchka, B. *J. Phys. Chem. B.* **2005**, 109, 125.

[23] Busca, G.; Ramis, G.; Lorenzelli, V.; Janin, A.; Lavalley*, J.C. Spectrochim. Acta A* **1987,** 43, 489.

[24] Tielens, F.; Denayer, J. F. M.; Daems, I.; Baron, G. V.; Mortier,W. J.; Geerlings, P. *J. Phys. Chem. B* **2003**, 107, 11065.

[25] Armaroli, T.; Finocchio, E.; Busca, G. Rossini, S. *Vib. Spectrosc.* **1999**, 20, 85.

[26] Salla, I.; Montanari, T.; Salagre, P.; Cesteros, Y.; Busca, G.; *J. Phys. Chem. B* **2005**, 109, 915.

[27] Gilles, F.; Blin, J. L; Toufar, H.; Briend, M.; Su, B. L.; *Colloids Surf. A Physicochem. Eng. Aspects,* **2004,** 241, 245.

[28] Bordiga, S.; Scarano, D.; Spoto, G.; Zecchina, A.; Lamberti, C.; Otero Areán, C.; *Vibrational Spectroscopy* **1993,** 5, 69.

[29] Marra, G. L.; Fitch, A. N.; Zecchina, A.; Ricchiardi, G.; Salvalaggio, M.; Bordiga, S.; Lamberti, C. *J. Phys. Chem. B* **1997**; 101, 10653.

[30] Vayssilov, G. N.; Staufer, M.; Belling, T.; Neyman, K. M.; Knozinger, H.; Rosch, N. *J. Phys. Chem. B* **1999**; 103*;* 7920.

[31] Hüber, S.; Knözinger, H. *Appl. Catal. A: Gen.* **1999**, 181, 239.

[32] Tsyganenko, A. A.; Escalona Blatero, E.; Otero Are**á**n, C.; Garrone, E.; Zecchina, A. *Catal. Lett.* **1999**, 61**,** 187.

[33] Martra, G.; Ocule, R.; Marchese, L.; Centi, G.; Coluccia, S. *Catal. Today* **2002**, 73, 83.

[34] Shete, B. S.; Kamble, V. S.; Gupta, N. M.; Kartha V. B.; *J. Phys. Chem. B* **1998**, 102, 5581.

[35] Datka, J.; Boczar, M.; Gil B.; *Colloids Surf. A: Physicoche. Eng. Aspects* **1995**, 105, 1.

[36] Rege, S. U.; Yang, R.T.; *Chem. Eng. Sci,* **2001,** 56, 3781.

[37] Angell, C. L.; Howell, M. V. *J. Phys. Chem.* **1969**, 73, 2551.

[38] Jaramillo, E.; Auerbach, S. M.; *J. Phys. Chem. B.* **1999**, 103, 9589.

[39] Lim, K. H.; Grey, C. P. *J. Am. Chem. Soc.* **2000**, 122, 9768.

[40] Buttefey, S.; Boutin, A.; Mellot Draznieks, C.; Fuchs, A. H. *J. Phys. Chem. B* **2001**, 105, 9569.

[41] Mellot, C. F.; Cheetham, A. K.; *C. R. Acad. Sci. Paris*, **1998**, Série II c, 737.

[42] Jaramillo, E.; Grey, C. P.; Auerbach, S. M.; *J. Phys. Chem. B* **2001**, 105, 12319.

[43] Busca, G.; In Metal Oxides: Chemistry and Applications, Fierro, J. L. G.; Ed.; Marcel Dekker Inc Pub., 2005, in press.

Chapter 6

Conclusions

The modifications made to the zeolites studied have improved the adsorption and catalytic properties in the following ways:

- Mordenite can adsorb slightly higher volumes of N_2 maintaining a good N_2/O_2 adsorption selectivity, even though its Si/Al ratio is higher than the normally used faujasite-type zeolites. The results are so good because the porous structure of the zeolite based in channels makes the cations more accessible. Therefore, this natural zeolite is a good alternative to the synthetic zeolite X for the N_2/O_2 separation process.
- In mordenites prepared by cationic exchange, the N_2 adsorbed volume increases in the way $Li^+ > Ag^+ > Na^+$ and the N_2/O_2 adsorption selectivity in the way $Ag^+ > Li^+ > Na^+$. Therefore, in the mordenite structure, the combination of different cations enabled equilibrium to be reached between the adsorbed volume and the interaction strength.
- The introduction of small amounts of fluorine into the mordenite framework was found to have a positive effect on the N_2/O_2 adsorption selectivity. The presence of the fluorine atoms means that the framework structure shields the cations less and, therefore, increases the electrostatic interaction between cations and the quadrupolar moment of N_2 molecules. This leads to an increase in the N_2/O_2 adsorption selectivity at lower pressures. On the other hand, the introduction of higher amounts of

fluorine causes some dealumination in the structure and decreases adsorption properties.

- Although Ag_m^{n+} clusters did not form inside the mordenite structure, probably due to the high Si/Al ratio of mordenite, they did on zeolite A. The N_2 and O_2 adsorption properties of these Ag_m^{n+} samples were studied and the results indicate that the sample prepared with high concentrations of Ag cations, (Na/Ag(1M)-A), has a higher adsorption capacity than Na-A when the activation conditions were suitable. Nevertheless, when the sample was prepared with a low concentration of silver cations (Na/Ag(0.01M)-A), silver metallic particles were formed during the sample activation process, which partially hindered the entrance of the gas molecules to the cavities of the zeolite, and therefore lower adsorption capacity than the Na-A zeolite was obtained.

- In the styrene oxide isomerisation, commercial mordenite (NaM), unlike the acidic mordenites, showed hardly any activity. The introduction of fluorine into the mordenite structure framework had a notable effect on its acidic properties. When a low amount of fluorine was introduced (HM1F sample), the Brönsted acidity was greater than that of the HM sample and the structure was not affected. This stronger acidity increased the isomeration reaction when conventional heating was used but the deactivation was fast when microwave heating was used. On the other hand, when higher amounts of fluorine were introduced (HM10F sample) some dealumination and the appearance of Lewis acid sites are observed, and this meant that the isomeration activity did not increase as much as in the HM1F sample.

- The use of microwaves as a heating source in the styrene oxide isomeration reaction accelerated the reaction rates and also the formation of

condensation and coke products. These products are responsible for a faster catalyst deactivation, especially in the most acidic catalyst HM1F.

- The reaction products depend on the solvent used. When hexane is used, the main product of the reaction is phenylacetaldehyde, but when methanol is used, the styrene oxide ring breaks to give 2-methoxy-2-phenylethanol. While the first reaction is mainly favoured by the presence of Brönsted acid sites, the second reaction is favoured by the presence of Brönsted and Lewis acid sites.

Some of the systems used were characterized in depth by means of FTIR spectroscopy adsorbing different probe molecules. The main conclusions that can be drawn are:

- Low temperature CO and room temperature nitrile adsorption experiments on the various zeolite samples form $M^+ \cdots$ CO and $M^+ \cdots$NC-R complexes ("usual" species) characterized by higher IR frequencies than the free or liquid molecule.
- However at lower frequencies than in the free molecule, a third, new interaction ("unusual" species) was observed in some of the zeolites tested. This interaction is more stable to outgassing processes than the "usual" species and the frequency observed for these species on the alkaly mordenites follows the tendency LiMOR ≈ NaMOR < KMOR< CsMOR.
- We propose that a stronger interaction whose stretching frequency is lower than that of free CO can only be explained by a multiple interaction. These species probably involve two cations, or one cation and one framework oxygen. The former should be more favored in zeolites because the most basic oxygens are most hindered by cations, which should impede some interaction with probe molecules.

- The relative intensity between the "unusual" and the "usual" species grows in the sense CO < less hindered nitriles < more hindered nitriles, and LiMOR<NaMOR<KMOR<CsMOR. This, therefore, indicates that the interaction takes place on the outer surface or on the mouths of the main channels.
- The distance between cations also seems to play an important role in the formation of the "unusual species". On NaX and NaY zeolites, the formation of these species is not as favored as in mordenite samples, possibly because of the larger dimensions of the supercages.

Table of contents